Cerebellar degeneration and prevention of symptom progression in a mouse model of spinocerebellar ataxia type 7.

Stephanie A. Furrer

A dissertation

submitted in partial fulfillment of the

requirements for the degree of

Doctor of Philosophy

University of Washington

2012

Reading Committee:

Gwenn A. Garden, Chair

Leo J. Pallanck

Farrel R. Robinson

Program Authorized to Offer Degree:

Neurobiology and Behavior

University of Washington

Abstract

Cerebellar degeneration and prevention of symptom progression
in a mouse model of spinocerebellar ataxia type 7.

Stephanie A. Furrer

Chair of the Supervisory Committee:
Professor Gwenn A. Garden
Department of Neurology

Spinocerebellar ataxia type 7 (SCA7) is a dominantly inherited disorder characterized by progressive cerebellar, brainstem, and retinal degeneration. SCA7 is caused by a CAG/polyglutamine (polyQ) repeat expansion in the ataxin-7 gene. Ataxin-7 is widely expressed, but certain neural populations, including cerebellar Purkinje cells (PCs), are selectively vulnerable to the mutation. Previous SCA7 mouse models have demonstrated multiple cell types must express mutant ataxin-7 to cause ataxia and non-cell autonomous PC degeneration. To further define specific cellular roles in SCA7 pathogenesis, we generated a novel SCA7 mouse model that expresses a loxP-flanked ataxin-7-92Q cDNA under the control of the murine prion protein (PrP) promoter in a bacterial artificial chromosome (BAC). To inactivate polyQ-ataxin-7 expression in specific cerebellar cell types, we crossed *PrP-floxed-SCA7-92Q BAC* mice with *Gfa2-Cre* mice (to direct Cre to Bergmann glia (BG)) or *Pcp2-Cre* mice (to direct Cre to PCs and inferior olive (IO)). Excision of ataxin-7 from BG partially rescued behavioral abnormalities, but did not prevent BG process loss or molecular layer thinning. Excision of ataxin-7 from PCs and IO provided significantly greater rescue and prevented both pathological changes, revealing a non-cell autonomous basis for BG

pathology. Prevention of mutant ataxin-7 expression in BG, PCs, and IO delayed symptom onset by half the lifespan (20 weeks) of *PrP-floxed-SCA7-92Q BAC* mice. Thus, cerebellar PCs and BG, and IO neurons in the brainstem, are the major cellular contributors to SCA7 pathogenesis. To determine whether neurological dysfunction is reversible during the progressive phase of SCA7 disease, we crossed the *PrP-floxed-SCA7-92Q BAC* mouse line to transgenic mice that ubiquitously express tamoxifen-inducible Cre recombinase. Administration of tamoxifen citrate four weeks after symptom onset globally inactivated mutant ataxin-7 expression, which prevented further symptom progression and restored some motor function. Tamoxifen treatment did not significantly alter molecular layer thinning and BG process loss, but it prevented the redistribution of climbing fiber terminals and reduced the number of PC nuclei containing ataxin-7 aggregates. Our results demonstrate that suppression of polyQ-ataxin-7 gene expression prevents further symptom progression, even when initiated after symptom onset and at a time when some histopathological changes cannot be reversed.

TABLE OF CONTENTS

LIST OF FIGURES

LIST OF TABLES

GLOSSARY

ALS	amyotrophic lateral sclerosis
AMPA	α-amino-3-hydroxy-5-methyl-4-isoxazolepropionate
B6	C57BL/6J (mouse strain)
BAC	bacterial artificial chromosome
BDNF	brain derived neurotrophic factor
BG	Bergmann glia
CF	climbing fiber
CNS	central nervous system
DNER	Delta/Notch-like EGF-related receptor
DRPLA	dentatorubral pallidoluysian atrophy
EAAT4	excitatory amino acid transporter 4
ECoG	electrocorticography
EGFP	enhanced green fluorescent protein
ER	estrogen receptor
FACS	fluorescent activated cell sorting
FcR	Fc receptor
GCN	granule cell neuron
GDNF	glial derived neurotrophic factor
Gfa2	glial fibrillary acidic protein promoter, human fragment
GFAP	glial fibrillary acidic protein
GFP	green fluorescent protein
GLAST	glutamate-aspartate transporter
GLT-1	glutamate transporter 1
GluRδ2	glutamate receptor subunit δ2
HAT	histone acetyl transferase
HD	Huntington's disease
IGF-1	insulin-like growth factor 1
IO	inferior olive
LCM	laser capture microdissection
NI	nuclear inclusion
Non-Tg	non-transgenic
PC	Purkinje cell
Pcp2	Purkinje cell protein 2
PDGF-β	platelet derived growth factor β
PF	parallel fiber
polyQ	polyglutamine
PrP	prion protein
SBMA	spinobulbar muscular atrophy
SCA	spinocerebellar ataxia
SCA7	spinocerebellar ataxia type 7
SOD1	superoxide dismutase 1
Tamox	tamoxifen citrate
TBP	TATA-box binding protein
VGLUT2	vesicular glutamate transporter 2

Acknowledgments

I have much gratitude for all of the people, inside *and* outside of the lab, who helped me along during my time in graduate school. First and foremost, I thank my mentors, Albert La Spada and Gwenn Garden for their patience, wisdom, and guidance. I shall never forget your contribution to my development as a scientist and as a person. Future successes I may enjoy will not have been possible without your tutelage.

Thanks to past and present members of the La Spada lab for technical help and moral support: Vince Damian, Netta Smith, Stephan Guyenet, Randell Libby, Travis Ashe, Scott Greenwald, Greg Cary, Jessica Young, Victor Pineda, Jing Huang, and Dan Possin. Special thanks to Sara Custer, my first mentor at the bench. Thanks to the past and present members of the Garden lab for providing aid with the day-to-day tasks in the lab and a soundboard for ideas: Chris Chang, John Song, Bryce Sopher, KT Nguyen, Richard Holman, Lisa Baldwin, Min Spencer, and Jeremiah Eng. Thank you especially to Travis Baughan for being a terrific benchmate for the past 3 years. I will miss your stories and our random rants about the current state of social affairs.

A very heartfelt "thank you" goes out to my dedicated undergraduates Sarah Waldherr and Mathini Mohanachandran. Not only did they contribute to almost all of my experiments, they also helped me grow into a mentor. Thanks for teaching me how much I truly value the opportunity to support someone in their academic pursuits; your lessons are some of the most important ones I have learned thus far.

Thank you to Rick Morrison, Sean Murphy, Jon Weinstein, and Weiqing Li for continually challenging my critical thinking skills. Sumie Jayadev, Amanda Case, and Stephanie Hopkins, thank you for pulling me back into the real world and allowing me to vent my scientific frustrations from time to time; you have helped me turn some of my most difficult times into fits of laughter.

Thanks to my committee members: Leo Pallanck, Ric Robinson, and Richard Gardner. Your genuine curiosity and warm encouragement helped propel me along the rough road that is graduate school.

The Neurobiology and Behavior program, and especially Ann Wilkinson and Lucia Wisdom, have been a wonderful source of continued support.

Thank you to the Seattle chapter of the ARCS foundation, especially for matching me with the Barbo family. Words cannot fully describe the friendship, the opportunities, and the support that the Barbo family has selflessly shared with me. I shall be eternally grateful for all you have done for me.

To all of the wonderful friends I have made during my journey: Melissa Caras, Adrienne Mueller, James Lawton, Charlie Hass, Grant Storey, Helen Gerns, Hiro Watari, Mike Famulare, Brennan and Kristen McQuerry, and Anna Sczaniecka. You have truly enriched my life in more ways than can be imagined. I can only hope to return the favor.

I would also like to thank my family for their continued love and support to do whatever it is that I was meant to do, especially Anton and Bonnie Wosick and Dean, Deanna, Craig, and Sara Furrer. I would not have gotten this far without you!

Finally, I wish to extend my gratitude and love to my fiancé, Geoff Bucks. He has continued to be my rock and has helped me weather the tumultuous storms of experimental failures. His belief in my abilities has always magnified my own self-confidence. I am truly fortunate to have such a supportive partner, and I very much look forward to our life together.

Dedication

This work is dedicated to my parents, Dean L. Furrer and Deanna M. Furrer, and to my grandparents, Anton G. Wosick and Bonnie R. Wosick. I would not have developed into the person I am today without their continued loving support and their encouragement to make my own destiny.

Chapter I

Introduction

Spinocerebellar ataxia type 7 (SCA7) is a dominantly inherited genetic disorder that results in the progressive degeneration of structures primarily in the cerebellum, brainstem, and retina. Consequently, patients develop ataxia (i.e., loss of motor coordination) and blindness (Garden and La Spada, 2008). SCA7 is caused by the expansion of a CAG/polyglutamine (polyQ) trinucleotide repeat within the ataxin-7 gene, making this disorder one of nine known polyQ expansion diseases (Orr and Zoghbi, 2007). Although the normal function of ataxin-7 is yet to be fully understood, one of its roles is as a transcriptional regulator (McMahon et al., 2005; Palhan et al., 2005; Strom et al., 2005; Helmlinger et al., 2006). Ataxin-7 is expressed widely throughout tissues within, and outside of, the central nervous system (CNS). However, only specific subpopulations of neural cells degenerate in patients with SCA7. The progressive nature of this degeneration causes patients to suffer with symptoms that worsen over years or even decades (Orr and Zoghbi, 2007). Mouse models have been developed to investigate the mechanisms of SCA7 neurodegeneration, including which cellular events lead to cell type-specific death and how polyQ-expanded, or mutant, ataxin-7 is influencing these events (Ingram et al., 2012).

Symptoms and neuropathology

The severity of symptoms in SCA7 patients ranges broadly from infantile onset with early mortality to elderly presentations of slowly progressive ataxia (Garden and La Spada,

2008). SCA7 patients develop ataxia that eventually results in difficulties with walking, speaking, and manual dexterity. Ataxia often is the first symptom reported, although a subset of patients with earlier disease onset may first present with vision deficiencies (Giunti et al., 1999). As the disease progresses, more severe symptoms include dysarthria, dysphagia, hypoacusis, and eye movement abnormalities that can progress to ophthalmoplegia. Involvement of the corticospinal tracts and extrapyramidal motor system may also be present (David et al., 1998; Giunti et al., 1999). The first sign of SCA7 retinal degeneration is dyschromatopsia (color blindness; Gouw et al., 1994). Central vision is then lost, followed by peripheral vision loss, and often patients become completely blind (Hamilton et al., 1990; Enevoldson et al., 1994).

Neuroimaging of SCA7 patients reveals atrophy of the cerebellum and pons (Bang et al., 2003). Autopsy studies confirm degeneration of the cerebellar cortex, dentate nucleus, inferior olive, subthalamic nucleus, and olivocerebellar, spinocerebellar, and pyramidal tracts (Martin et al., 1994; Michalik et al., 2004). Cerebellar Purkinje cells (PCs) are almost entirely lost and marked neuronal loss and gliosis occurs in the inferior olive (Michalik et al., 2004). Only minor changes are found in the cerebellar granule cell layer. Neuronal loss in brainstem cranial nerve motor nuclei, spinal motor neurons, and regions of the basal ganglia such as the substantia nigra, has also been observed (Martin et al., 1999). SCA7 patients demonstrate loss of cone receptor function prior to rod abnormalities and macular degeneration in late-stage disease (To et al., 1993). SCA7 retinal degeneration is thus classified as a cone-rod dystrophy.

The polyglutamine expansion and ataxin-7

The SCA7 causative gene was initially mapped to chromosome 3p12-p21.1 (Benomar et al., 1995; Holmberg et al., 1995). Further investigation revealed that a CAG trinucleotide expansion mutation occurred in a then unknown gene, named ataxin-7. Upon this discovery, SCA7 became a member of the polyglutamine expansion family of neurodegenerative disorders that today includes the nine disorders listed in Table 1 (Zoghbi and Orr, 2000; Orr and Zoghbi, 2007).

Table 1: Features of the nine known polyglutamine expansion disorders.

Disease	Gene product	Normal repeat length	Expanded repeat length	Most common areas of degeneration
HD	huntingtin	6-34	36-121	Striatum, cerebral cortex
SBMA	androgen receptor	9-36	38-62	Anterior horn & bulbar neurons, dorsal root ganglion
DRPLA	atrophin	7-34	49-88	Cerebellum, cerebral cortex, basal ganglia, cerebral & brain stem white matter
SCA1	ataxin 1	6-44	39-82	Cerebellar Purkinje cells, brainstem
SCA2	ataxin 2	15-24	32-200	Cerebellar Purkinje cells, brainstem
SCA3	ataxin 3	13-36	61-84	Cerebellar dentate neurons, basal ganglia, brainstem, spinal cord
SCA6	$CACNA1_A$	4-19	10-33	Cerebellar Purkinje cells, brainstem
SCA7	ataxin 7	4-35	37-306	Cerebellar Purkinje cells, brainstem, retina
SCA17	TBP	25-42	47-63	Cerebellar Purkinje cells, brainstem

HD: Huntington's disease; SBMA: spinobulbar muscular atrophy; DRPLA: dentatorubral pallidoluysian atrophy; SCA: spinocerebellar ataxia; TBP: TATA-box binding protein.

Although the causative genes of each of the polyQ expansion disorders are distinct and share no homology outside of the polyQ tract, these diseases share some common features. With the exception of SCA6, the polyQ repeat becomes pathogenic after a threshold of approximately 35 repeats (Table 1; Orr and Zoghbi, 2007). In all of these diseases, a longer polyQ repeat correlates with earlier age of symptom onset and a more severe disease phenotype (Zoghbi and

Orr, 2000). These disorders are inherited in an autosomal dominant fashion (except for SBMA which is X-linked and recessive), suggesting that the polyQ-expanded proteins gain a toxic property or function that mediates neurodegeneration. The causative genes are expressed widely within and outside of the CNS, but specific cell populations are selectively vulnerable to each mutation (Table 1; Orr and Zoghbi, 2007). It is possible that the proteins' normal functions are also disrupted in the context of a polyQ expansion and those cell populations that succumb to the mutation suffer from a combination of loss-of-function and toxic gain-of-function events (Garden and La Spada, 2008). The polyQ-expanded proteins accumulate into proteinaceous aggregates that are most often found in the nucleus, but can also reside in the cytoplasm. These aggregates are observed in many tissues in and outside of the CNS. PolyQ aggregates contain other proteins, including transcription factors and components of the ubiquitin-proteasome system. Aggregates containing polyQ-expanded proteins are a common hallmark of polyQ disease, but their presence is not required for cell death (Garden and La Spada, 2008). Because these commonalities exist amongst the polyQ expansion disorders, it is thought that complete understanding of the pathogenesis of one will provide insight into the others.

SCA7 is caused by an expansion of the CAG trinucleotide tract in the coding region of the ataxin-7 gene (David et al., 1997). Ataxin-7 encodes a protein 892 amino acids in length. The polyQ tract is in the N-terminal region and the protein has one nuclear export signal, three nuclear localization signals, two caspase cleavage sites, and putative sites for post-translational modification via phosphorylation and SUMOylation (Mookerjee et al., 2009). A highly conserved region exists between amino acids 311 and 406 that contains a zinc binding domain (Helmlinger et al., 2004b). Although the normal function of ataxin-7 is largely unknown, studies have shown it is a component of at least two transcriptional regulatory complexes called STAGA

and TFTC (Helmlinger et al., 2004b; McMahon et al., 2005; Palhan et al., 2005; Strom et al., 2005; Helmlinger et al., 2006). Both complexes contain several protein components, including a substituent with histone acetyltransferase (HAT) activity. These complexes regulate gene transcription by preferentially acetylating histone H3, which subsequently promotes access to the associated DNA sequence by transcriptional machinery (Martinez et al., 2001). Several studies *in vivo* and *in vitro* demonstrated mutant ataxin-7 disrupts STAGA and TFTC function, possibly by reducing HAT activity, which leads to the down-regulation of several genes necessary for the function and maintenance of photoreceptors (McMahon et al., 2005; Palhan et al., 2005; Helmlinger et al., 2006; Merienne et al., 2007). The role of ataxin-7 as a subunit of the STAGA and TFTC complexes may explain cone and rod death in the retina, but the normal function of ataxin-7 has yet to be delineated in the cerebellum and brainstem.

Cerebellar Purkinje cells undergo non-cell autonomous degeneration in SCA7

PCs, the most severely affected cell type in SCA7 patients (Zoghbi and Orr, 2000), are also the primary output of the cerebellar cortex (Slemmer et al., 2005). Their cell bodies make up the PC layer, and their extensive dendritic arbors project into the cerebellar molecular layer (Fig. 1). PCs receive two main excitatory, glutamatergic inputs (Slemmer et al., 2005). The first arises from granule cells in the granule cell layer. Granule cells project axons, known as parallel fibers (PFs), which synapse onto PC dendrites in the molecular layer (Fig. 1). The second glutamatergic input originates from the inferior olivary (IO) nucleus. Neurons of the IO project axons known as climbing fibers (CFs; Fig. 1). After development, a single PC is innervated by a CF from one IO neuron. This CF makes approximately 1500 synaptic contacts while as many as

100,000 PFs may innervate a single PC (Slemmer et al., 2005). Bergmann glia (BG) help shape glutamatergic input to PCs (Bellamy, 2006). These non-neuronal cells extend their processes into the molecular layer to ensheath almost all PF-PC and CF-PC synaptic contacts. BG cell bodies reside in the PC layer at a ratio of approximately eight BG per PC. BG highly express the glutamate-aspartate transporter, GLAST, and use this transporter to remove excess glutamate from the synaptic cleft (Rothstein et al., 1994). BG also express a calcium-permeable AMPA receptor (Hollmann et al., 1991; Burnashev et al., 1992). BG with experimentally manipulated AMPA receptors that are impermeable to calcium withdraw their processes from PC synapses, which leads to disrupted glutamatergic signaling and re-innervation by additional CFs (Iino et al., 2001).

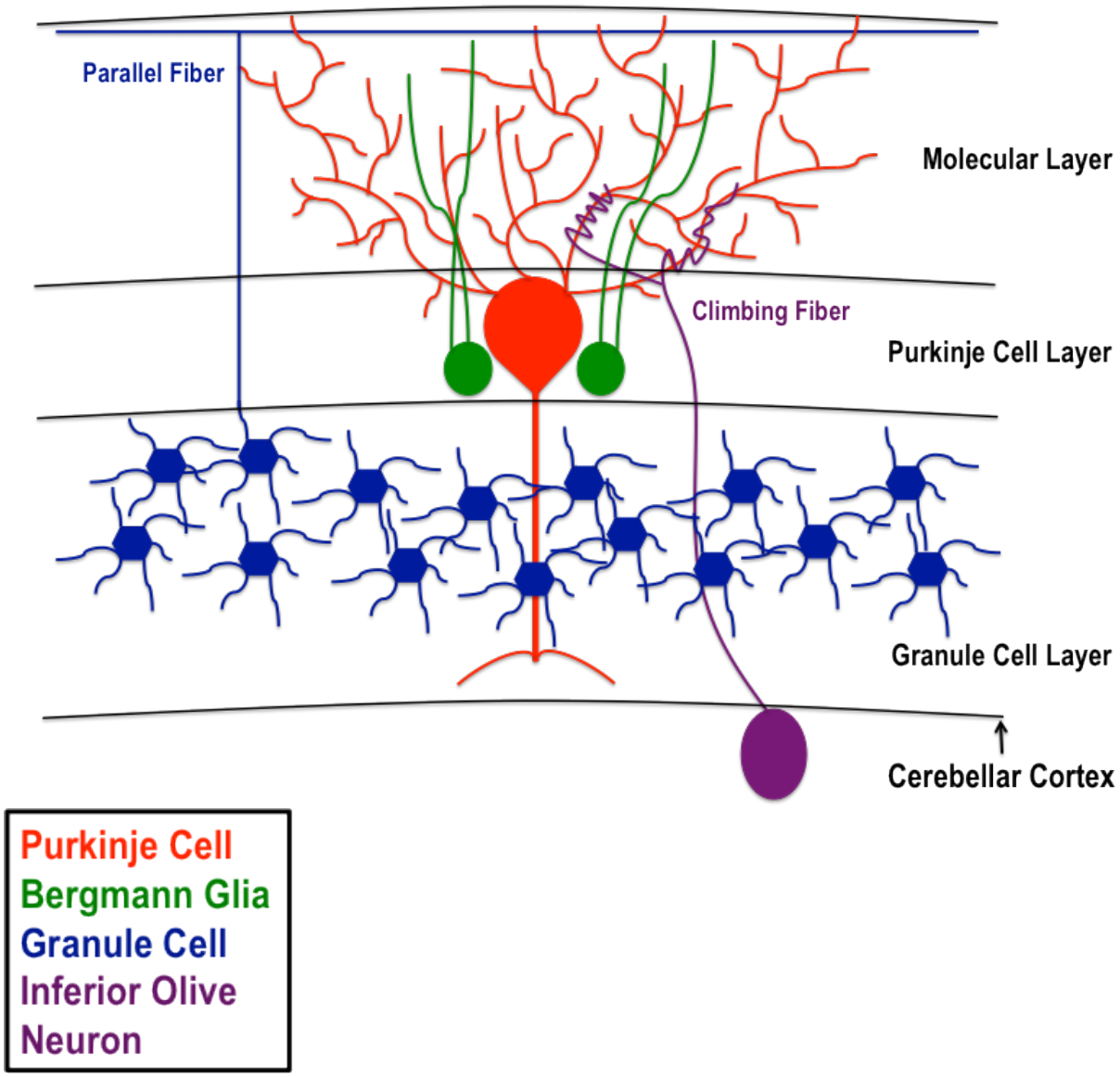

Figure 1: Glutamatergic circuitry of the cerebellar cortex.

Because almost all PCs are lost in SCA7 patients, one of the first SCA7 mouse models was developed by expressing ataxin-7 with 90 CAG repeats (ataxin-7-90Q) solely in PCs using the Purkinje cell protein 2 (Pcp2) promoter (Yvert et al., 2000). This mouse model had a very mild, late-onset ataxic phenotype and only mild changes in the cerebellar cortex at 11-12 months

of age. The same group created another SCA7 mouse model in which ataxin-7-90Q expression was ubiquitously driven under the direction of the platelet derived growth factor beta-chain promoter (Yvert et al., 2001). These mice became visibly ataxic at 5 months of age and their lifespan was reduced to 8-15 months. The La Spada and Garden groups also created a mouse model in which ataxin-7-92Q was expressed throughout brain and body tissues except in PCs (Garden et al., 2002). These mice developed ataxia (at 4-5 months) and succumbed to early mortality (at 8 months). Intriguingly, the cerebellar PCs had shrunken cell bodies and dendritic arbors even though they did not express mutant ataxin-7. Together, these studies demonstrated that PCs expressing polyQ-expanded ataxin-7 alone was not sufficient to cause SCA7 and in fact, PCs could undergo degeneration without expressing the mutant gene. More evidence that PCs undergo non-cell autonomous degeneration came from another La Spada/Garden group mouse model. These mice were engineered to very highly express ataxin-7-92Q specifically in BG (Custer et al., 2006). These mice developed slowly progressive ataxia at 8-12 months of age, and the PCs showed signs of degeneration. BG isolated from these mice had reduced GLAST RNA and protein level expression and a reduction in the ability to take up glutamate through the remaining GLAST protein. Electron microscopic evaluation of the PCs showed a phenotype characteristic of excitotoxic-mediated cell death (a process by which excess glutamatergic signaling leads to deleterious downstream effects, such as elevated intracellular calcium and the activation of proteases and other 'pro-cell death' enzymes; Slemmer et al., 2005). Thus, expression of mutant ataxin-7 solely in BG was sufficient to induce ataxia and PC degeneration, but did not recapitulate a full SCA7 disease phenotype.

What other cell types directly contribute to PC degeneration and atrophy of the cerebellum? When, during the course of SCA7 disease, do these cell types contribute to

neurodegeneration? After symptom onset, is it possible to intervene and delay, stop, or reverse the cellular mechanisms that ultimately lead to cell death? In order to begin to address these questions, we set out to create a novel SCA7 mouse model in which mutant ataxin-7 could be temporally and spatially controlled. Specifically, ataxin-7-92Q could be permanently removed from the genetic material within selected cell populations or globally at pre-designated time points during SCA7 pathogenesis using the Cre-loxP system.

Chapter II

Spinocerebellar ataxia type 7 cerebellar disease requires the coordinated action of mutant ataxin-7 in neurons and glia, and displays non-cell autonomous Bergmann glia degeneration

Summary

Spinocerebellar ataxia type 7 (SCA7) is a dominantly inherited disorder characterized by cerebellum and brainstem neurodegeneration. SCA7 is caused by a CAG/polyglutamine (polyQ) repeat expansion in the ataxin-7 gene. We previously reported that directed expression of polyQ-ataxin-7 in Bergmann glia (BG) in transgenic mice leads to ataxia and non-cell autonomous Purkinje cell (PC) degeneration. To further define the cellular basis of SCA7, we derived a conditional inactivation mouse model by inserting a loxP-flanked ataxin-7 cDNA with 92 repeats into the translational start site of the murine prion protein (PrP) gene in a bacterial artificial chromosome (BAC). The *PrP-floxed-SCA7-92Q BAC* mice developed neurological disease, and exhibited cerebellar degeneration and BG process loss. To inactivate polyQ-ataxin-7 expression in specific cerebellar cell types, we crossed *PrP-floxed-SCA7-92Q BAC* mice with *Gfa2-Cre* transgenic mice (to direct Cre to BG) or *Pcp2-Cre* transgenic mice (which yields Cre in PCs and inferior olive). Excision of ataxin-7 from BG partially rescued the behavioral phenotype, but did not prevent BG process loss or molecular layer thinning, while excision of ataxin-7 from PCs and inferior olive provided significantly greater rescue and prevented both pathological changes, revealing a non-cell autonomous basis for BG pathology. When we prevented expression of mutant ataxin-7 in BG, PCs, and inferior olive by deriving *Gfa2-Cre;Pcp2-Cre;PrP-floxed-SCA7-92Q BAC* triple transgenic mice, we noted a dramatic improvement in SCA7 disease phenotypes.

These findings indicate that SCA7 disease pathogenesis involves a convergence of alterations in a variety of different cell types to fully recapitulate the cerebellar degeneration.

Introduction

Spinocerebellar ataxia type 7 (SCA7) is a progressive, dominantly inherited neurodegenerative disorder characterized by neuron dysfunction, culminating in cell loss in the retina, cerebellum, and brain stem. SCA7 patients consequently exhibit ataxia, motor system abnormalities, blindness, and early mortality. SCA7 is caused by a CAG/polyglutamine (polyQ) repeat expansion in the coding region of the ataxin-7 gene. As in other diseases caused by polyQ repeat expansion, ataxin-7 is ubiquitously expressed. Nonetheless, inheriting polyQ-expanded ataxin-7 yields degeneration in specific neuronal populations that are selectively vulnerable to this mutation (Garden and La Spada, 2008).

A number of mouse models have been generated to investigate SCA7 disease pathogenesis. PolyQ-expanded ataxin-7, expressed in cerebellar Purkinje cells (PCs) using the Pcp2 promoter, produced very mild ataxia with no impact on life span (Yvert et al., 2000). Using the murine prion protein (PrP) transgenic expression system, we expressed polyQ-expanded ataxin-7 throughout the CNS, but not in PCs. The resulting *PrP-SCA7-c92Q* mice developed ataxia and PC degeneration, documenting a role for non-cell autonomous PC degeneration in SCA7 disease pathogenesis (Garden et al., 2002). Transgenic mice that express ataxin-7-92Q protein only in Bergmann glia (BG) in the cerebellum also develop ataxia and PC degeneration, implicating glial dysfunction in polyQ-ataxin-7-mediated PC degeneration (Custer et al., 2006).

While these studies underscored the importance of specific non-neuronal cell types in cerebellar degeneration, PCs are integrated into a complex neural network and receive glutamatergic input from axons projecting from the inferior olive (IO) and cerebellar granule cells. BG remove excess glutamate from PC synapses (Huang and Bordey, 2004), and secrete neurotrophic

factors, which support PCs (Mount et al., 1995). IO neurons produce insulin-like growth factor 1, a neurotrophic factor that promotes PC survival and glutamate-aspartate transporter (GLAST) expression in BG (Nieto-Bona et al., 1993; Gamboa and Ortega, 2002).

To clarify the cellular basis of SCA7, we developed a powerful new mouse model wherein polyQ-ataxin-7 expression could be spatially and temporally regulated. In this model, an ataxin-7-92Q cDNA is flanked by loxP sites at the start site of translation in the murine PrP gene in a bacterial artificial chromosome (BAC). The *PrP-floxed-SCA7-92Q BAC* mice ubiquitously express mutant ataxin-7 protein in all neurons, including PCs, and develop cerebellar ataxia and histopathology. To determine which cell types are required for SCA7 disease pathogenesis, *PrP-floxed-SCA7-92Q BAC* mice were crossed with driver lines expressing Cre-recombinase in BG (*Gfa2-Cre*), or in PCs and IO (*Pcp2-Cre*). *Gfa2-Cre;PrP-floxed-SCA7-92Q BAC* and *Pcp2-Cre;PrP-floxed-SCA7-92Q BAC* bigenic mice each displayed a less severe phenotype than *PrP-floxed-SCA7-92Q BAC* littermates. Excision of ataxin-7-92Q from PCs and IO neurons not only protected against cerebellar atrophy, but also prevented BG pathology. Excision of ataxin-7-92Q from BG, however, did not prevent these pathological features, suggesting that BG pathology is non-cell autonomous in SCA7. When we created triple transgenic (i.e., *Gfa2-Cre; Pcp2-Cre; PrP-floxed-SCA7-92Q BAC*) mice, onset of cerebellar ataxia was delayed up to 20 weeks. These findings indicate that BG, PCs, and IO neurons interact in an intimate and tightly interconnected network, and thus, together contribute to SCA7.

Results

Characterization of the *PrP-floxed-SCA7-92Q BAC* transgenic mouse

To generate a mouse model that can delineate cell type-specific contributions to SCA7 disease pathogenesis, we inserted an ataxin-7 cDNA, carrying 92 CAG repeats and flanked by loxP sites, into a murine prion protein BAC, and placed an EGFP reporter gene downstream of the ataxin-7 cDNA (Fig. 2.1, A). After transgenic microinjection of this BAC construct, we identified founders and established two independent *PrP-floxed-SCA7-92Q BAC* lines. RT-PCR analysis of cerebellar RNA from *PrP-floxed-SCA7-92Q BAC* mice demonstrated that both *PrP-floxed-SCA7-92Q BAC* lines expressed human ataxin-7 (Fig. 2.1, B). Quantitative real-time RT-PCR analysis of ataxin-7 on RNA extracted from cerebellum confirmed that transgene expression was less than endogenous ataxin-7 expression (Fig. 2.1, C). To ensure Cre recombinase-mediated excision of the ataxin-7 cDNA, we crossed *PrP-floxed-SCA7-92Q BAC* mice with *CMV-Cre* transgenic mice. The resulting *CMV-Cre;PrP-floxed-SCA7-92Q BAC* bigenic mice no longer expressed human ataxin-7, confirming successful Cre-mediated gene excision (Fig. 2.1, B). Immunofluorescent labeling of *PrP-floxed-SCA7-92Q BAC* brain sections with an anti-ataxin-7 antibody revealed widespread expression of the mutant protein, as evidenced by aggregate formation in neurons, including granule cell neurons (GCNs) and Purkinje cell neurons (Fig. 2.1, D). *PrP-floxed-SCA7-92Q BAC* mice did not exhibit a significant reduction in calbindin-labeled PC soma (2.6 ± 0.1 PCs per 100 μm; ±SEM) compared with non-transgenic mice (3.0 ± 0.2 PCs per 100 μm; ±SEM) ($p = 0.13$; unpaired two-tailed t-test), similar to previously published mouse models of SCA7 (Garden et al., 2002; Chou et al., 2010).

Motor behavior in *PrP-floxed-SCA7-92Q BAC* mice was assessed using a composite

phenotype scoring system (Guyenet et al., 2010) and by rotarod analysis. Beginning at 20 weeks of age, *PrP-floxed-SCA7-92Q BAC* mice exhibited a more severe behavioral phenotype than non-transgenic mice, based upon composite phenotype score, and this progressively worsened with age (Fig. 2.1, E). *PrP-floxed-SCA7-92Q BAC* mice also performed significantly worse on the accelerating rotarod at 21 weeks of age compared to non-transgenic littermates, and their rotarod performance worsened at 30 weeks of age (Fig. 2.1, F). CMV-Cre-driven excision of the ataxin-7 cDNA prevented these phenotypes in *CMV-Cre;PrP-floxed-SCA7-92Q BAC* bigenic mice, as these bigenic mice performed comparably to non-transgenic mice (Fig. 2.1, E & F). Together, these results indicate that the *PrP-floxed-SCA7-92Q BAC* transgenic mice develop a SCA7 phenotype characterized by progressive ataxia and impaired motor function. Furthermore, the utility of this model for studying cell-type contribution was confirmed by widespread Cre-mediated excision of the mutant ataxin-7 gene.

PolyQ-ataxin-7 expression in Bergmann glia is required for the full SCA7 phenotype

We have previously shown that expression of polyQ-expanded ataxin-7 in BG, driven by a human glial fibrillary acidic protein promoter known as Gfa2 (Besnard et al., 1991), is sufficient to produce SCA7 cerebellar neurodegeneration (Custer et al., 2006). To determine whether mutant ataxin-7 expression in BG is required for the full SCA7 phenotype, we crossed a mouse line expressing Cre recombinase driven by the Gfa2 promoter (Zhuo et al., 2001) with the *PrP-floxed-SCA7-92Q BAC* mice. In *PrP-floxed-SCA7-92Q BAC* mice, EGFP expression is induced upon Cre-mediated excision of the loxP flanked ataxin-7 cDNA, as EGFP is moved adjacent to the murine prion protein promoter. In *Gfa2-Cre;PrP-floxed-SCA7-92Q BAC* mice, EGFP expression is low

and BG cell bodies are very compact, complicating determination of the excision rate in bigenic BG. Thus, to validate this driver line, we crossed *Gfa2-Cre* mice with a robust *Z/EG* reporter line (Novak et al., 2000). Sagittal brain sections from *Gfa2-Cre;Z/EG* mice were immunolabeled for GFP and S100-β, a BG cell body marker. We found that 72% of all S100-β-positive BG were concurrently positive for GFP (Fig. 2.2, A & B), validating the utility of the *Gfa2-Cre* driver line for high-level BG excision.

We assessed the behavioral phenotype of *Gfa2-Cre;PrP-floxed-SCA7-92Q BAC* bigenic mice by again using the composite phenotype score and accelerating rotarod. As expected, *PrP-floxed-SCA7-92Q BAC* mice displayed significantly higher composite phenotype scores, beginning at 20 weeks of age (Fig. 2.2, C). *Gfa2-Cre;PrP-floxed-SCA7-92Q BAC* mice, however, displayed a progressive, but less severe phenotype compared to *PrP-floxed-SCA7-92Q BAC* littermates. On the accelerating rotarod, *PrP-floxed-SCA7-92Q BAC* mice performed poorly at 22 weeks of age and were significantly impaired by 40 weeks of age (Fig. 2.2, D). *Gfa2-Cre;PrP-floxed-SCA7-92Q BAC* mice performed poorly on the accelerating rotarod at 40 weeks as well, but tended to remain on the rotarod longer than their *PrP-floxed-SCA7-92Q BAC* littermates (Fig. 2.2, D). Together, these data suggest that polyQ-expanded ataxin-7 expression in BG contributes to SCA7 pathogenesis and is required to recapitulate the full SCA7 behavioral phenotype.

PolyQ-ataxin-7 expression in inferior olive is required for SCA7 disease phenotype

Restricted expression of polyQ-expanded ataxin-7 in cerebellar PCs in transgenic mice is not sufficient to cause progressive motor impairment (Yvert et al., 2000). Indeed, ataxia and PC degeneration can develop in SCA7 mice in which mutant ataxin-7 is expressed throughout the

brain, but not in PCs (Garden et al., 2002), indicating the importance of non-cell autonomous degeneration in SCA7. To test whether excising mutant ataxin-7 in PCs would significantly alter the disease phenotype, we crossed *PrP-floxed-SCA7-92Q BAC* mice with a Purkinje cell protein 2 (Pcp2)-Cre line, obtained from the Jackson Laboratory (Barski et al., 2000). When we assessed the excision rate in *Pcp2-Cre;PrP-floxed-SCA7-92Q BAC* bigenic mice by immunofluorescent labeling with antibodies to EGFP and calbindin, we noted that 52% of all calbindin-positive PCs were also EGFP positive (Fig. 2.3, A & B). Importantly, in the course of performing this analysis, we documented that expression of Cre in this line is not limited to PCs, but is also present in the inferior olive, the superior olive, and the olfactory bulb (Fig. 2.3, A, and data not shown). These studies thus reconfirmed the integrity of the *PrP-floxed-SCA7-92Q BAC* construct, as singly transgenic *PrP-floxed-SCA7-92Q BAC* cerebellar sections showed no EGFP immunoreactivity, indicating that EGFP expression is only released upon Cre-mediated gene excision (Fig. 2.3, B).

Neurons of the IO degenerate in SCA7 patients (Garden and La Spada, 2008) as well as in SCA7 transgenic mice (Wang et al., 2010). The IO projects climbing fibers (CFs) that form glutamatergic synapses on PC somae and dendrites. The IO also delivers the neurotrophic factor insulin-like growth factor-1 (IGF-1) to PCs (Nieto-Bona et al., 1993). Thus, loss of climbing fiber input to PCs may contribute to non-cell autonomous PC degeneration in SCA7. When we quantified the percentage of calbindin-positive IO neurons that also express GFP to determine excision rate, as was just described for PCs, we found that ataxin-7 cDNA excision had occurred in 58% of IO neurons (Fig. 2.3, A & B). Composite phenotype scoring indicated that *Pcp2-Cre;PrP-floxed-SCA7-92Q BAC* bigenic mice had a significantly milder phenotype than their singly transgenic SCA7 littermates, and, interestingly, neurological impairment in *Pcp2-Cre;PrP-floxed-SCA7-92Q BAC* mice reached a plateau at 30 weeks of age (Fig. 2.3, C). Accelerating rotarod

analysis at 22 weeks of age indicated that *PrP-floxed-SCA7-92Q BAC* mice displayed evidence of motor incoordination at this time, while *Pcp2-Cre;PrP-floxed-SCA7-92Q BAC* bigenic mice performed comparably to non-transgenic and *Pcp2-Cre* controls (Fig. 2.3, D). By 40 weeks of age, the motor performance differences became quite dramatic, as *Pcp2-Cre;PrP-floxed-SCA7-92Q BAC* bigenic mice remained on the rotarod at least four times longer than their *PrP-floxed-SCA7-92Q BAC* littermates. Together, these findings demonstrate that expression of mutant ataxin-7 in IO neurons, and likely also in PCs, is required to recapitulate the full SCA7 phenotype.

PolyQ-ataxin-7 excision in Purkinje cells and inferior olive, but not in Bergmann glia, protects against cerebellar molecular layer degeneration

A prominent feature of SCA7 neurodegeneration in transgenic mice is shortened PC dendritic arbors in the cerebellar molecular layer (Garden et al., 2002; Yoo et al., 2003; Custer et al., 2006; Chou et al., 2010). To investigate whether this loss is mitigated in *Gfa2-Cre;PrP-floxed-SCA7-92Q BAC* or *Pcp2-Cre;PrP-floxed-SCA7-92Q BAC* bigenic mice, we immunostained sagittal cerebellar sections with anti-calbindin antibody. By 40 weeks of age, we noted reduced dendritic calbindin immunoreactivity, abnormal PC morphology, and molecular layer thinning in the cerebellum of *PrP-floxed-SCA7-92Q BAC* mice (Fig. 2.4, A & B). *Gfa2-Cre;PrP-floxed-SCA7-92Q BAC* bigenic mice also exhibited reduced calbindin immunoreactivity and a thinner molecular layer, similar to *PrP-floxed-SCA7-92Q BAC* mice (Fig. 2.4, C); however, *Pcp2-Cre;PrP-floxed-SCA7-92Q BAC* cerebellar sections resembled cerebellar sections from non-transgenic controls (Fig. 2.4, A-D).

To further investigate the effect of conditional ataxin-7 excision from selected cell

populations in the cerebellum, we quantified molecular layer thickness in dorsal cerebellum. When we measured the width of the molecular layer along the outside of each folium from the pial surface to the PC layer boundary at 100 μm intervals (Fig. 2.4, E), we found that molecular layer thickness was significantly reduced from an average of 92.8 μm in non-transgenic controls to 75.5 μm in *PrP-floxed-SCA7-92Q BAC* mice (Fig. 2.4, F). Although *Gfa2-Cre;PrP-floxed-SCA7-92Q BAC* mice had a similarly reduced molecular layer thickness, *Pcp2-Cre;PrP-floxed-SCA7-92Q BAC* bigenic mice exhibited molecular layer thickness values that were comparable to non-transgenic controls and markedly increased versus *PrP-floxed-SCA7-92Q BAC* mice (Fig. 2.4, F). The molecular layer thickness in *Gfa2-Cre* and *Pcp2-Cre* singly transgenic mice did not differ from non-transgenic animals (data not shown). These findings indicate that excision of mutant ataxin-7 from PCs and IO neurons rescues PC neurodegeneration in SCA7 transgenic mice, while excision of mutant ataxin-7 from BG does not prevent such PC pathology.

PolyQ-ataxin-7 excision in Purkinje cells and inferior olive, but not in Bergmann glia, prevents Bergmann glia degeneration

As BG exhibit morphological pathology and dysfunction in SCA7 (Garden et al., 2002; Custer et al., 2006), we examined BG morphology in *PrP-floxed-SCA7-92Q BAC* mice and the two bigenic lines. After staining sagittal cerebellar sections for GFAP to visualize BG processes, we generated 3-D images of dorsal cerebellar folia, deconvolved them, and transformed them into 2-D images by creating brightest-point projections. This analysis revealed that *PrP-floxed-SCA7-92Q BAC* mice have remarkably fewer BG processes in the cerebellar molecular layer (Fig. 2.5, A & B). Although the morphology of BG in *Gfa2-Cre;PrP-floxed-SCA7-92Q BAC* bigenic mice

resembled that of *PrP-floxed-SCA7-92Q BAC* mice, BG in *Pcp2-Cre;PrP-floxed-SCA7-92Q BAC* mice exhibited more prominent processes, indicative of an intermediate pathology between non-transgenic controls and *PrP-floxed-SCA7-92Q BAC* mice (Fig. 2.5, A-D). To quantify BG pathology, we counted the number of GFAP-positive BG processes that crossed a 150 μm line drawn parallel to, and 50 μm from, the pial surface (Fig. 2.5, E). *PrP-floxed-SCA7-92Q BAC* mice harbored significantly fewer BG processes than non-transgenic controls (Fig. 2.5, F). Surprisingly, BG processes were also markedly reduced in *Gfa2-Cre;PrP-floxed-SCA7-92Q BAC* mice, similar to *PrP-floxed-SCA7-92Q BAC* mice. BG process number in *Pcp2-Cre;PrP-floxed-SCA7-92Q BAC* bigenic mice was not significantly different from non-transgenic mice or from *PrP-floxed-SCA7-92Q BAC* mice, indicative of an intermediate phenotype (Fig. 2.5, F). Neither *Gfa2-Cre* nor *Pcp2-Cre* singly transgenic mice differed from non-transgenic controls (data not shown). Hence, excision of mutant ataxin-7 from PCs and IO neurons ameliorated BG histopathology, while elimination of mutant ataxin-7 expression from BG did not improve BG degeneration. This finding represents the first demonstration that BG dysfunction and degeneration in SCA7 is non-cell autonomous.

PolyQ-ataxin-7 excision in Bergmann glia, Purkinje cells, and inferior olive delays SCA7 disease onset

Because excising polyQ-ataxin-7 from BG, or from PCs and IO neurons, partially rescued SCA7 neurodegeneration, we proceeded to test whether eliminating mutant ataxin-7 from all three cell types would further ameliorate SCA7 disease pathogenesis. To do so, we generated triple transgenic mice that carried the *PrP-floxed-SCA7-92Q BAC*, the *Pcp2-Cre* transgene, and the

Gfa2-Cre transgene. Composite phenotype analysis revealed that such triple transgenic mice exhibit very late disease onset, but once manifested, neurological abnormalities are progressive (Fig. 2.6, A). Rotarod analysis, however, indicated that triple transgenic mice retain normal motor coordination function, and perform dramatically better than singly transgenic *PrP-floxed-SCA7-92Q BAC* mice at 40 weeks of age (Fig. 2.6, B).

To quantify the delay in onset, we pooled data from all *PrP-floxed-SCA7-92Q BAC*, non-transgenic, *Gfa2-Cre;PrP-floxed-SCA7-92Q BAC*, *Pcp2-Cre;PrP-floxed-SCA7-92Q BAC*, and triple transgenic mice analyzed during the course of this study. One-way ANOVA testing, followed by a Bonferroni's multiple comparison *post hoc* analysis, was conducted for all composite phenotype data. This analysis showed that *PrP-floxed-SCA7-92Q BAC* mice display neurological abnormalities at 20 weeks of age ($p < 0.001$), establishing the age of onset. Both *Gfa2-Cre;PrP-floxed-SCA7-92Q BAC* and *Pcp2-Cre;PrP-floxed-SCA7-92Q BAC* bigenic mice exhibit significant neurological impairments by 25 weeks of age ($p < 0.01$ and $p < 0.001$, respectively). The triple transgenic mice, however, do not develop statistically significant neurological deficits until 40 weeks of age ($p < 0.01$), a delay of onset of 20 weeks. Thus, SCA7 mice, in which the ataxin-7 transgene is excised from BG, PCs, and IO neurons, exhibit a dramatically improved phenotype, underscoring the combined importance of all these components of the cerebellar circuitry.

To further assess the effect of removing mutant ataxin-7 expression from BG, PCs and IO neurons, we analyzed the histological phenotype of the trigenic animals. Mean cerebellar molecular layer thickness of the triple transgenic mice (100.2 μm) did not significantly differ from that measured in the *Pcp2-Cre;PrP-floxed-SCA7-92Q BAC* bigenic mice (100.0 μm). To address the possibility that mutant ataxin-7-mediated degeneration of cerebellar granule cell neurons could contribute to the SCA7 phenotype, we analyzed the cerebellar granule cell layer in non-transgenic

and *PrP-floxed-SCA7-92Q BAC* mice. No overt morphological changes were noted, and the width of the granule layer was modestly increased in *PrP-floxed-SCA7-92Q BAC* mice compared to non-transgenic controls (data not shown). These results indicate that delay of disease onset until 40 weeks of age in *Gfa2-Cre; Pcp2-Cre; PrP-floxed-SCA7-92Q BAC* transgenic mice is best attributed to incomplete excision of ataxin-7 cDNA from PCs, IO neurons, and BG.

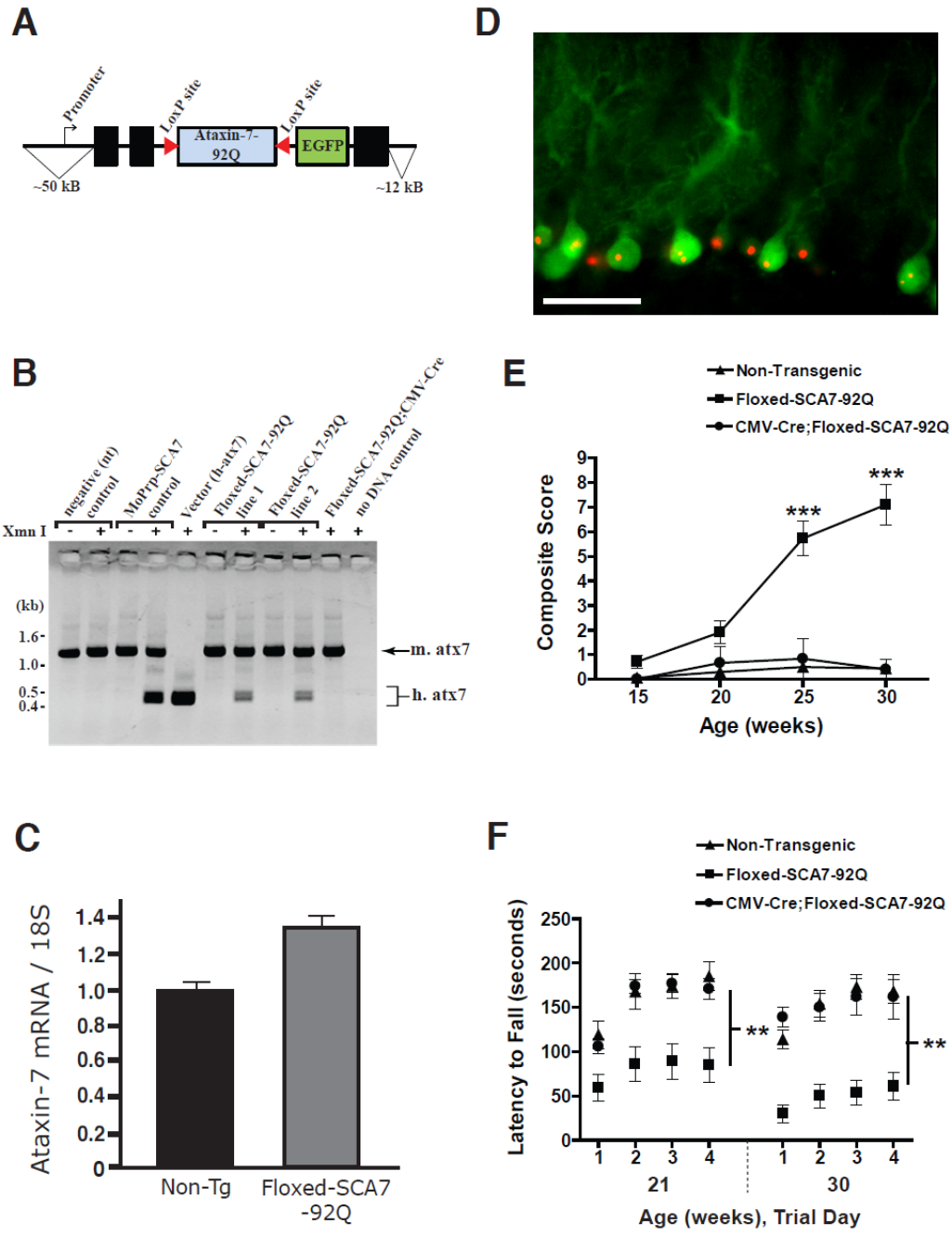

Figure 2.1: *PrP-floxed-SCA7-92Q BAC* mice exhibit Cre-dependent ataxin-7 expression and disease phenotype.

A, Diagram of the PrP-floxed-SCA7-92Q BAC construct, indicating the location of the human ataxin-7 92Q cDNA flanked by loxP sites, a downstream EGFP reporter gene, and the first two exons and last exon from the murine prion protein gene (black boxes; not to scale). **B**, We performed RT-PCR analysis of cerebella with primers that co-amplified murine and human ataxin-7, and then differentiated mouse endogenous ataxin-7 (m. atx7) from human transgenic

ataxin-7 (h. atx7) by XmnI restriction digestion. *PrP-floxed-SCA7-92Q* transgene-positive mice yielded XmnI-cut bands, which were no longer present after crossing with *CMV-Cre* mice that ubiquitously express Cre recombinase. **C**, We performed quantitative RT-PCR analysis of cerebellar RNA with primers that co-amplified murine and human ataxin-7, normalized to mouse 18S RNA levels, for non-transgenic and *PrP-floxed-SCA7-92Q BAC* mice (n = 3/group). We set the total ataxin-7 level to 1 in the non-transgenic control and found that the total ataxin-7 level in the *PrP-floxed-SCA7-92Q BAC* mice is ~ 1.3, indicating that the BAC transgene is expressed at lower than endogenous levels. **D**, Immunofluorescent labeling of ataxin-7 (red) and calbindin (green) in cerebellar sections from 40-week-old *PrP-floxed-SCA7-92Q BAC* mice. Scale bar, 50 μm. **E**, We completed composite phenotype analysis for sets of non-transgenic (n = 14), *PrP-floxed-SCA7-92Q BAC* (n =10), and *CMV-Cre;PrP-floxed-SCA7-92Q BAC* (n = 5) mice. *PrP-floxed-SCA7-92Q BAC* mice develop a significant phenotype, which is eliminated upon Cre-mediated excision (***$p < 0.001$, two-way ANOVA with Bonferroni's *post hoc* test). Error bars indicate SEM. **F**, We measured the mean latency to fall from the accelerating rotarod for sets of non-transgenic (n = 10), *PrP-floxed-SCA7-92Q BAC* (n =10), and *CMV-Cre;PrP-floxed-SCA7-92Q BAC* (n = 5) mice. *PrP-floxed-SCA7-92Q BAC* mice performed significantly worse on the rotarod at 21 and 30 weeks of age compared with non-transgenics, and *CMV-Cre;PrP-floxed-SCA7-92Q BAC* mice performed much better than *PrP-floxed-SCA7-92Q BAC* mice at these time points (**$p < 0.01$, two-way ANOVA with Bonferroni's *post hoc* test). Error bars indicate SEM.

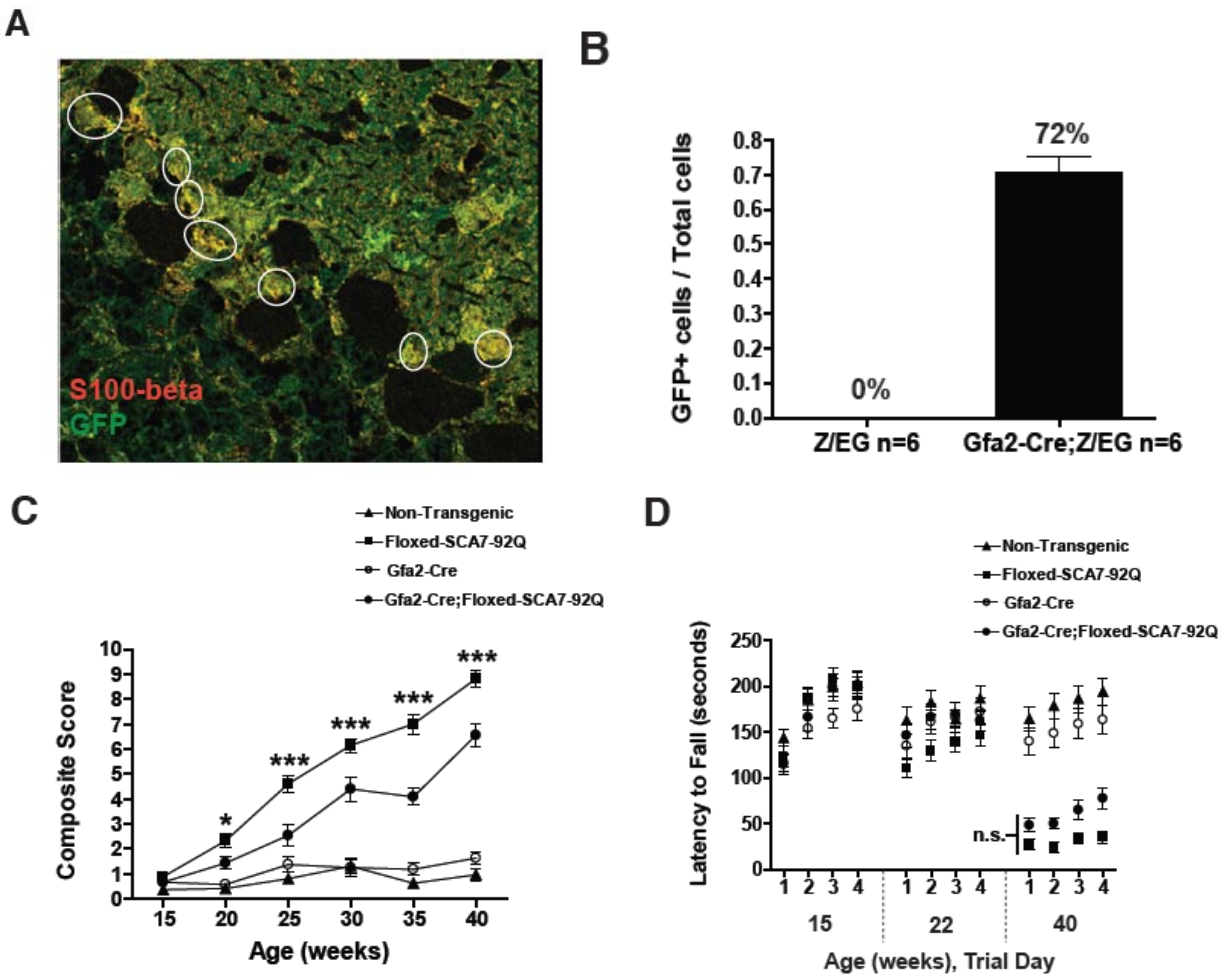

Figure 2.2: Excision of polyQ-ataxin-7 from Bergmann glia partially ameliorates SCA7 neurological phenotypes.

A, Immunofluorescence labeling of EGFP (green) and S100-β (red) in *Gfa2-Cre;Z/EG* cerebellar sections. **B**, Gfa2-Cre expression produced a 72% excision rate in Bergmann glia. **C**, We performed composite phenotype analysis for sets of non-transgenic (n = 16), *PrP-floxed-SCA7-92Q BAC* (n =13), *Gfa2-Cre* (n = 14), and *Gfa2-Cre;PrP-floxed-SCA7-92Q BAC* (n = 11) mice. Excision of polyQ-ataxin-7 from Bergmann glia in *Gfa2-Cre;PrP-floxed-SCA7-92Q BAC* mice yielded a markedly improved composite phenotype compared with *PrP-floxed-SCA7-92Q BAC* mice beginning at 20 weeks of age (*$p < 0.05$, ***$p < 0.001$, two-way ANOVA with Bonferroni's *post hoc* test). Error bars indicate SEM. **D**, When we analyzed these cohorts by accelerating rotarod testing, we found that *PrP-floxed-SCA7-92Q BAC* mice perform significantly worse than non-transgenic and *Gfa2-Cre* mice at 40 weeks of age ($p < 0.001$, two-way ANOVA with Bonferroni's *post hoc* test). *Gfa2-Cre;PrP-floxed-SCA7-92Q BAC* mice exhibited a trend toward improved rotarod performance, but this was not significant. Error bars indicate SEM.

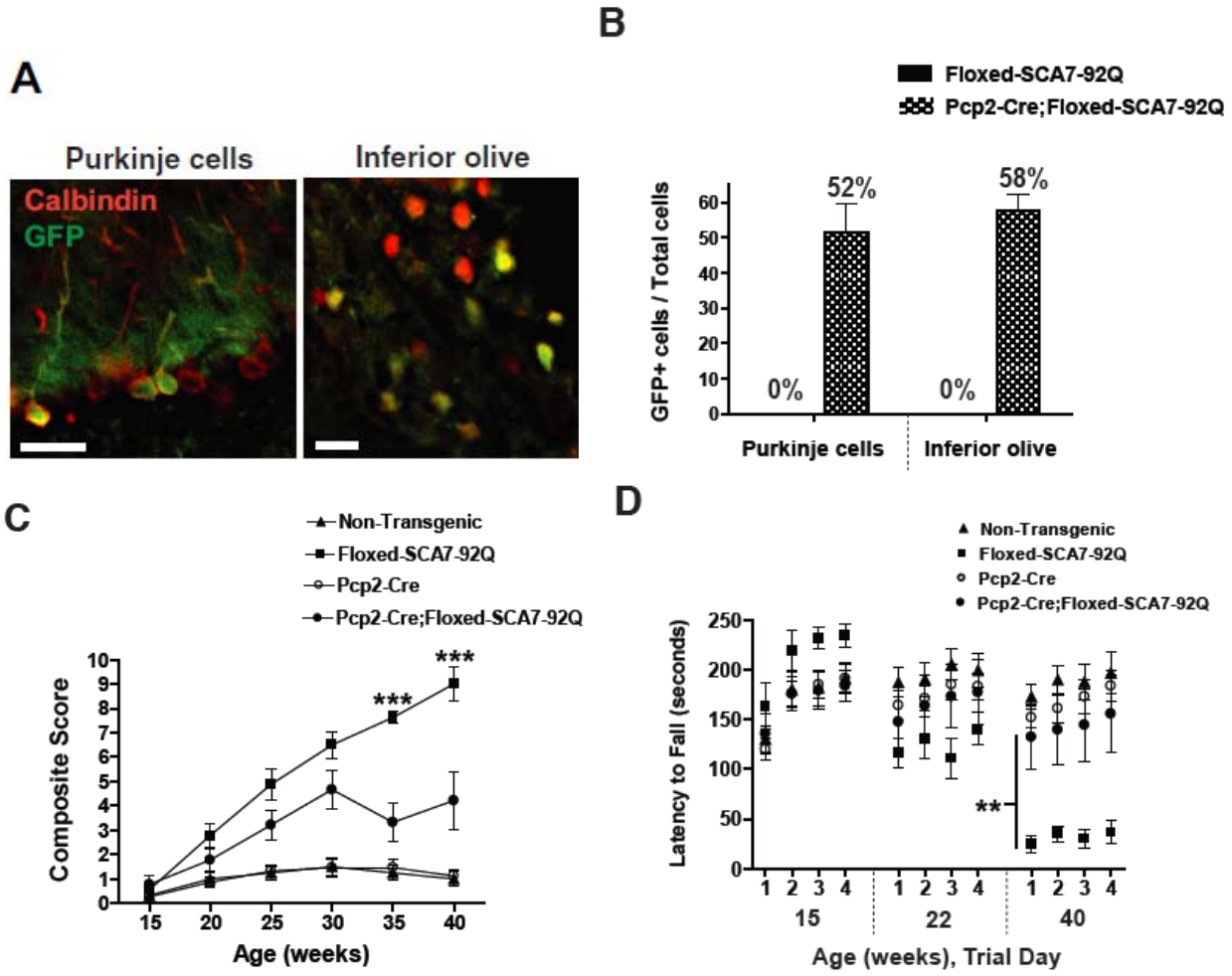

Figure 2.3: Excision of polyQ-ataxin-7 from Purkinje cells and inferior olive partially ameliorates SCA7 neurological phenotypes.

A, Immunofluorescence labeling of EGFP (green) and calbindin (red) in *Pcp2-Cre;PrP-floxed-SCA7-92Q BAC* bigenic cerebellum and brainstem sections. Scale bars, 50 µm. **B**, Pcp2-driven Cre expression yielded a 52% excision rate in Purkinje cells and a 58% excision rate in inferior olive neurons. **C**, Composite phenotyping revealed that *Pcp2-Cre;PrP-floxed-SCA7-92Q BAC* mice (n = 9) are moderately improved compared with *PrP-floxed-SCA7-92Q BAC* mice (n = 8) from 20 to 30 weeks of age, but not compared with non-transgenic (n = 12) or *Pcp2-Cre* (n = 15) controls. Moreover, the neurological phenotype of *Pcp2-Cre;PrP-floxed-SCA7-92Q BAC* mice ceases to progress after 30 weeks of age, and thus becomes dramatically improved compared to their progressing *PrP-floxed-SCA7-92Q BAC* littermates at these time points (***$p < 0.001$, two-way ANOVA with Bonferroni's *post hoc* test). Error bars indicate SEM. **D**, *Pcp2-Cre;PrP-floxed-SCA7-92Q BAC* mice exhibit a trend toward improved rotarod performance at 22 weeks of age. By 40 weeks of age, however, *Pcp2-Cre;PrP-floxed-SCA7-92Q BAC* mice are markedly superior to their *PrP-floxed-SCA7-92Q BAC* littermates, and actually perform comparably to non-transgenic and *Pcp2-Cre* controls on the accelerating rotarod (**$p < 0.01$, two-way ANOVA with Bonferroni's *post hoc* test). Error bars indicate SEM.

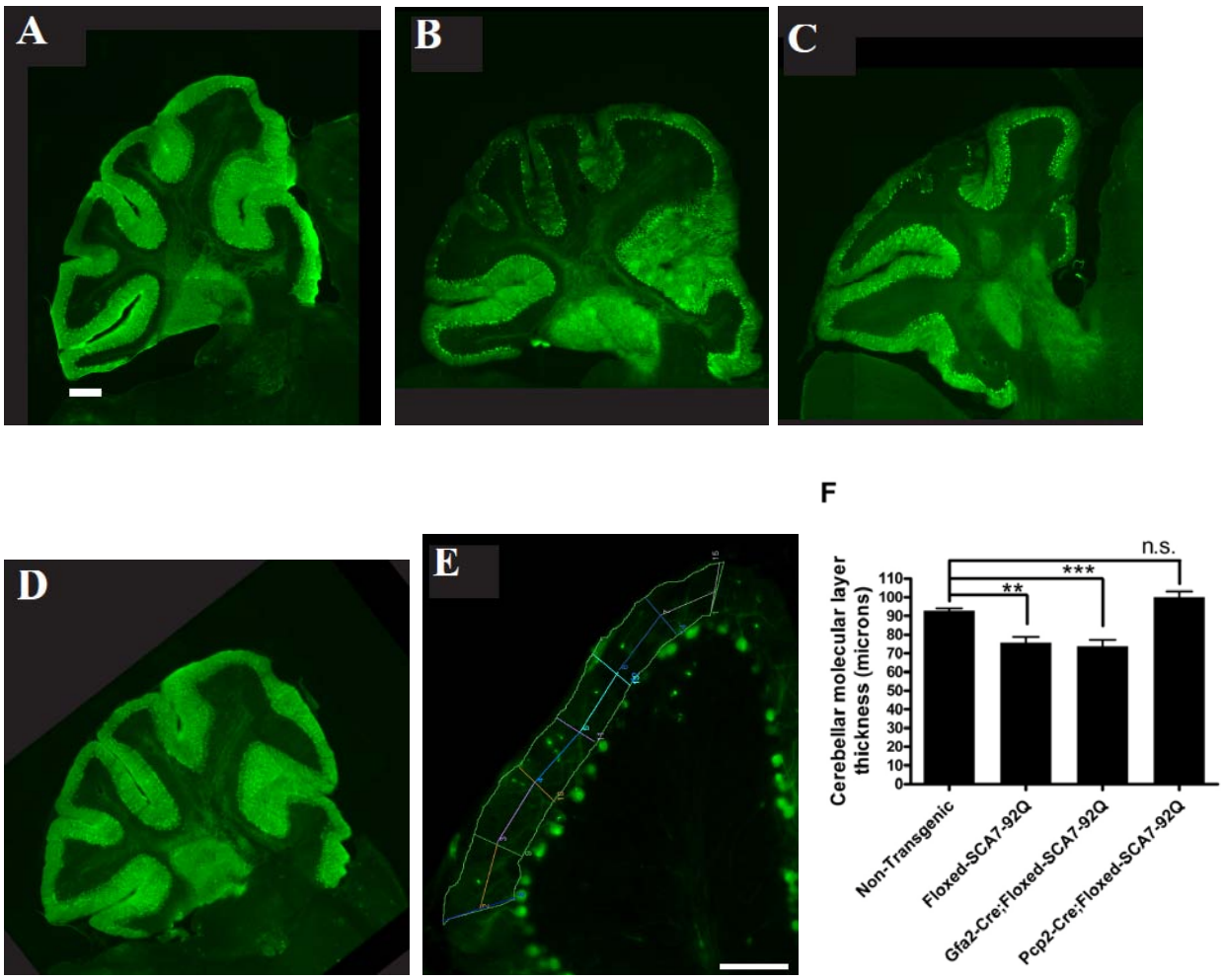

Figure 2.4: Excision of polyQ-ataxin-7 from Purkinje cells and inferior olive prevents cerebellar degeneration in *PrP-floxed-SCA7-92Q BAC* mice.

A-D, Anti-calbindin antibody staining of cerebellar sections. Calbindin immunoreactivity in non-transgenic control cerebellum is intense (**A**), in contrast to the marked loss of calbindin immunoreactivity in the dorsal cerebellar folia of *PrP-floxed-SCA7-92Q BAC* mice (**B**). *Gfa2-Cre;PrP-floxed-SCA7-92Q BAC* mice (**C**) also display reduced calbindin immunoreactivity and molecular layer thinning, but cerebellar sections from *Pcp2-Cre;PrP-floxed-SCA7-92Q BAC* mice (**D**) exhibit intense calbindin staining comparable to non-transgenic controls. **E**, We quantified cerebellar molecular layer thickness by taking measurements at 100 µm intervals (perpendicular lines) along the outer region of three dorsal cerebellar folia per section. **F**, Results of cerebellar molecular layer quantifications (n = 6 - 7/group). *PrP-floxed-SCA7-92Q BAC* and *Gfa2-Cre;PrP-floxed-SCA7-92Q BAC* animals have significantly thinner molecular layers in their dorsal cerebellar folia (**$p < 0.01$, ***$p < 0.001$, one-way ANOVA with Bonferroni's *post hoc* test). Cerebellar molecular layer thickness of *Pcp2-Cre;PrP-floxed-SCA7-92Q BAC* animals, however, was unchanged from non-transgenic controls. Error bars indicate SEM. Scale bars: **A**, 300 µm; **E**, 100 µm.

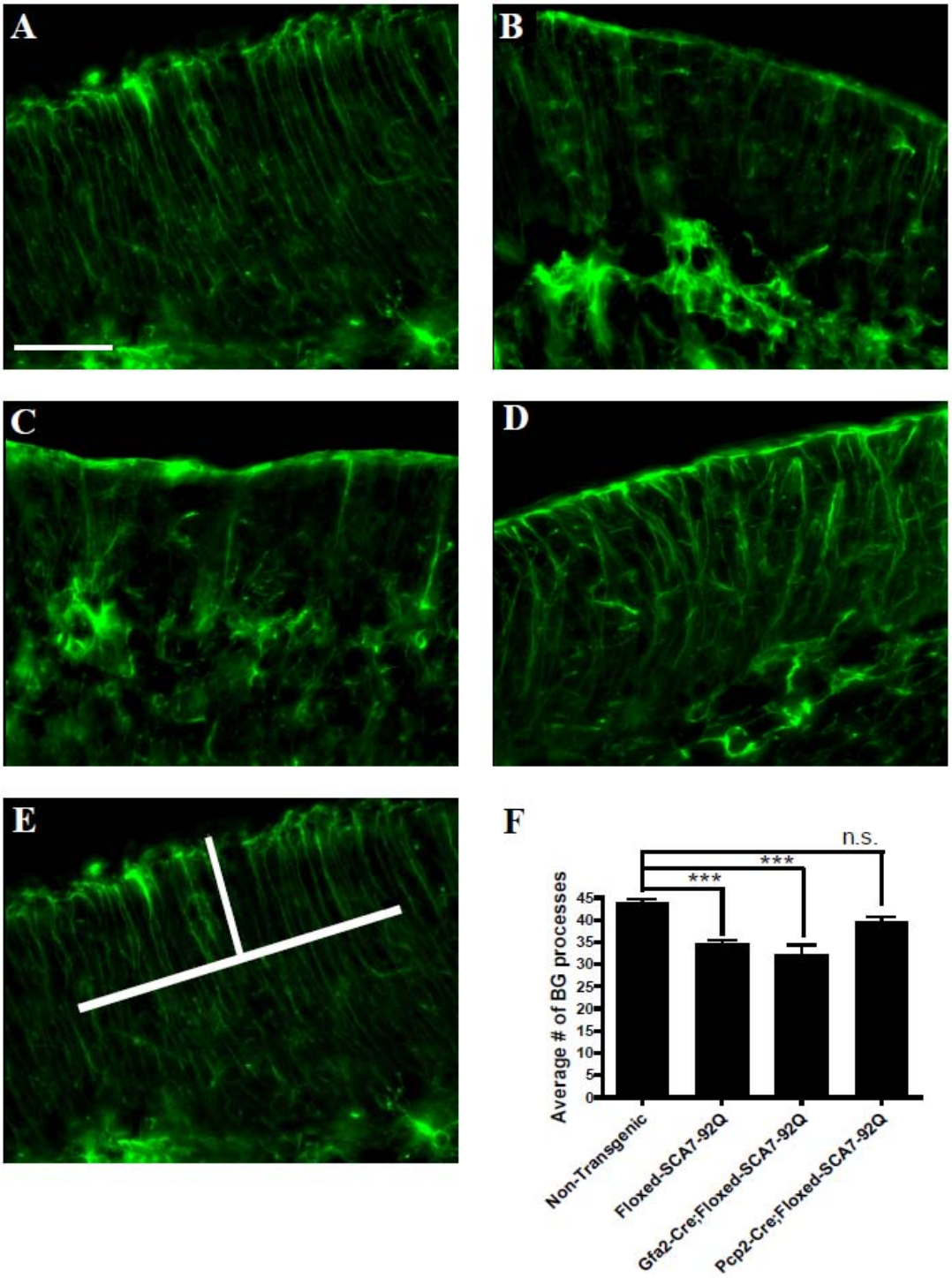

Figure 2.5: Excision of polyQ-ataxin-7 from Purkinje cells and inferior olive, but not Bergmann glia, prevents loss of glial processes.

A-D, Anti-GFAP antibody staining of dorsal cerebellar folia. Comparison of non-transgenic controls (**A**) to *PrP-floxed-SCA7-92Q BAC* mice (**B**) demonstrates an obvious reduction in Bergmann glia processes in the *PrP-floxed-SCA7-92Q BAC* mice. *Gfa2-Cre;PrP-floxed-SCA7-*

92Q BAC cerebellar sections (**C**) resembled *PrP-floxed-SCA7-92Q BAC* sections, while *Pcp2-Cre;PrP-floxed-SCA7-92Q BAC* cerebellar sections (**D**) appeared comparable to non-transgenic controls. Scale bar, 30 μm. **E**, We quantified Bergmann glia processes by counting the number of GFAP-positive processes that cross a 150 μm line drawn parallel to, and approximately 50 μm from, the pial surface (white lines). **F**, Results of quantifications of Bergmann glia processes (n = 6/group). *PrP-floxed-SCA7-92Q BAC* and *Gfa2-Cre;PrP-floxed-SCA7-92Q BAC* animals have significantly fewer Bergmann glia processes compared with non-transgenic mice (***$p < 0.001$, one-way ANOVA with Bonferroni's *post hoc* test). However, the number of Bergmann glia processes in *Pcp2-Cre;PrP-floxed-SCA7-92Q BAC* mice is intermediate between non-transgenic controls and *PrP-floxed-SCA7-92Q BAC* mice. Error bars indicate SEM.

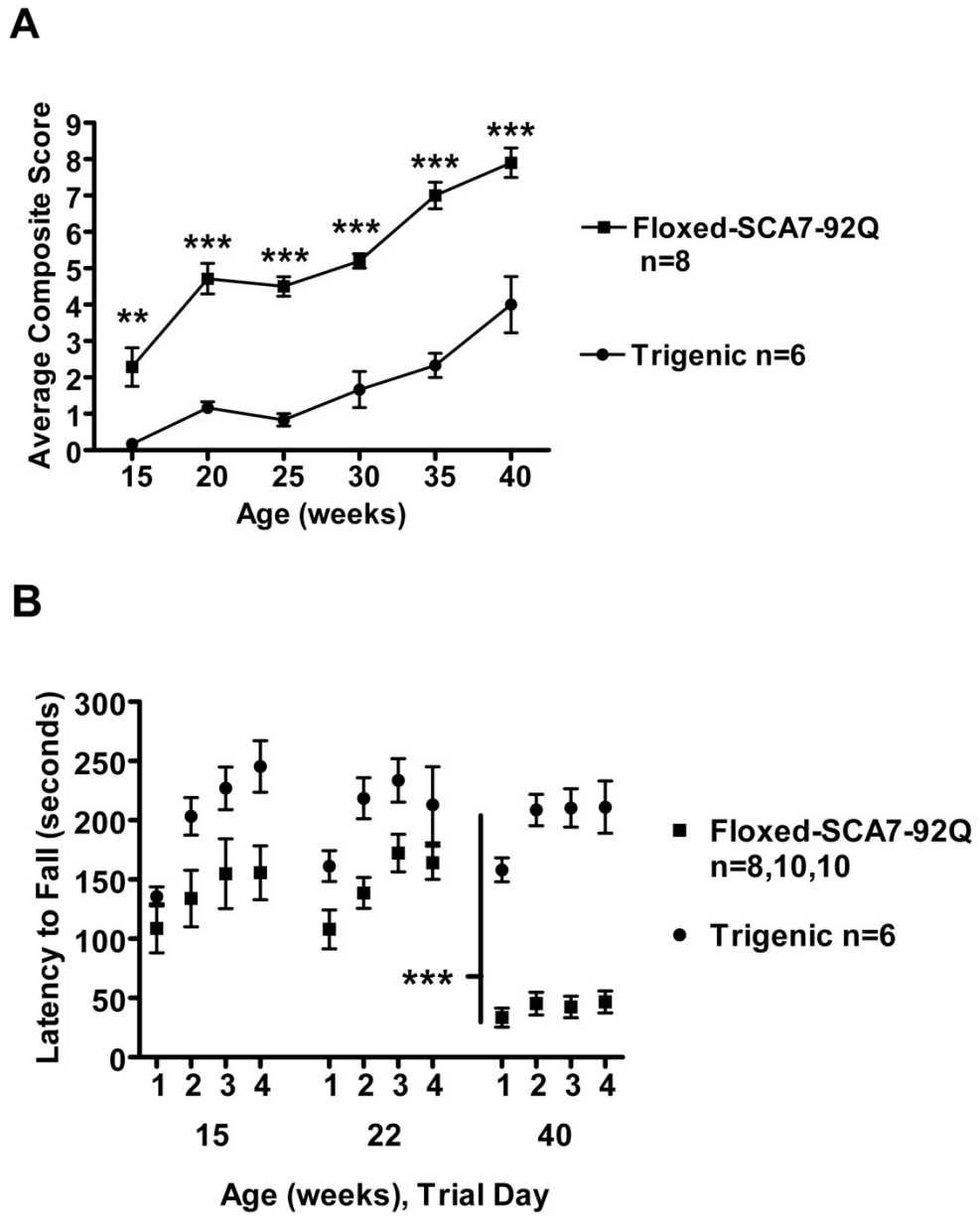

Figure 2.6: Excision of polyQ-ataxin-7 from Bergmann glia, Purkinje cells, and inferior olive greatly retards neurological disease onset in *PrP-floxed-SCA7-92Q BAC* mice.

A, Composite phenotype scoring of *Gfa2-Cre;Pcp2-Cre;PrP-floxed-SCA7-92Q BAC* (trigenic) mice reveals markedly delayed onset of a progressive behavioral phenotype and superior performance scores compared with *PrP-floxed-SCA7-92Q BAC* mice at all time points tested (**$p < 0.01$, ***$p < 0.001$, two-way ANOVA with Bonferroni's *post hoc* test). Error bars indicate SEM. **B**, Trigenic mice consistently performed better on the accelerating rotarod than *PrP-floxed-SCA7-92Q BAC* mice at all time points, and rotarod performance was dramatically superior at 40 weeks of age (***$p < 0.001$, two-way ANOVA with Bonferroni's *post hoc* test). Error bars indicate SEM.

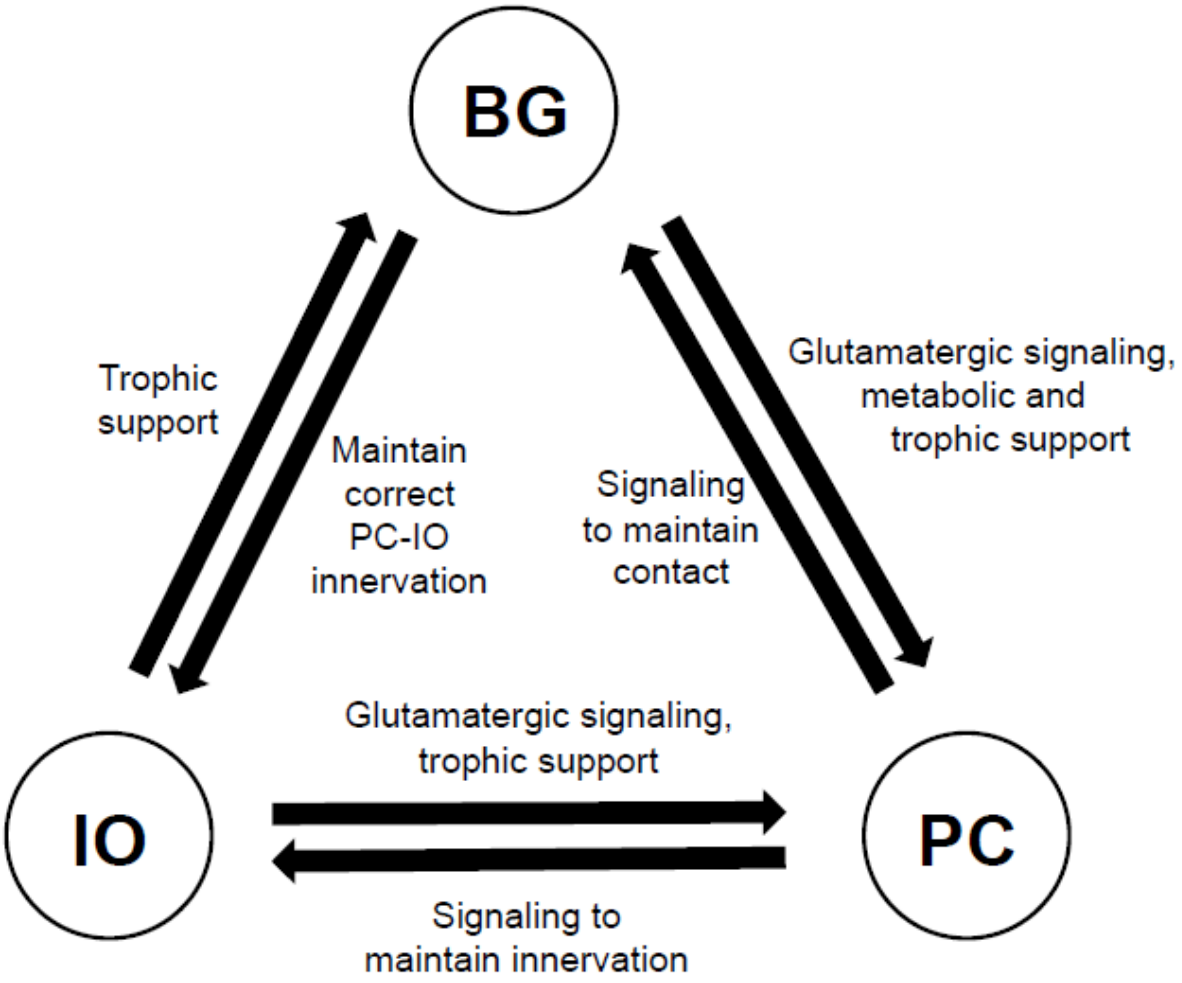

Figure 2.7: Interdependent connections between Bergmann glia (BG), Purkinje cells (PC), and inferior olive (IO) account for the multi-cell type origin of SCA7 neurodegeneration.

BG, PCs, and IO neurons each engage in bilateral interactions to yield an interdependent neural-glial network in which the function and survival of all cell types are assured together. During SCA7 disease pathogenesis, dysfunction of one cell type will inevitably impact the other connected cell types due to loss of trophic support and/or release of excitotoxic or inflammatory mediators. Altered function in one cell type thus culminates in all cell types failing to maintain appropriate signaling or other key functions, thereby exacerbating damage in the initial cell type while propagating abnormalities in the other connected cell types.

Discussion

In this study, we report a new SCA7 mouse model in which ataxin-7 gene expression can be controlled by Cre recombinase. In this model, a murine PrP BAC containing > 50 kb of DNA 5' to the PrP translational start site produced widespread expression of ataxin-7-92Q, including in PC neurons. In a prior study, a smaller PrP promoter fragment lacking key regulatory elements to drive broad expression of ataxin-7-92Q was used, but expression in PCs was not observed (Garden et al., 2002). *PrP-floxed-SCA7-92Q BAC* mice developed progressive ataxia and cerebellar degeneration typical of other SCA7 models (Garden et al., 2002; Yoo et al., 2003; Custer et al., 2006; Wang et al., 2010). When *PrP-floxed-SCA7-92Q BAC* mice were crossed with mice with ubiquitous Cre expression, mutant ataxin-7 was no longer produced and no behavioral phenotype developed, validating the loxP sites. Excision of ataxin-7-92Q from BG in the cerebella of *Gfa2-Cre;PrP-floxed-SCA7-92Q BAC* bigenic mice significantly ameliorated neurological abnormalities measured by composite phenotype scoring (Guyenet et al., 2010), but did not prevent cerebellar molecular layer thinning or BG process loss. Excision of ataxin-7-92Q from PCs and IO neurons improved motor behavior and protected against cerebellar molecular layer thinning and BG process loss. These findings indicate that expression of mutant ataxin-7 in BG is not required for glial degeneration. However, expression of mutant ataxin-7 in PCs and IO neurons contributes to BG pathology. Thus, SCA7 exhibits non-cell autonomous BG degeneration, revealing for the first time that neuronal health directly impacts BG in SCA7.

Studies over the last decade support the realization that the cellular basis of neurodegenerative disorders is not simply cell autonomous. An important example comes from a series of studies on familial amyotrophic lateral sclerosis (ALS) due to dominant, gain-of-

function mutations in superoxide dismutase 1 (SOD1). This form of ALS has been extensively studied since its genetic basis was defined in 1993 (Rosen et al., 1993). Transgenic expression of disease-causing SOD1 mutations in mice recapitulated key features of human ALS motor neuron degeneration (Gurney et al., 1994). These early mouse models utilized the native SOD1 promoter, resulting in ubiquitous expression of the mutant SOD1 protein. When transgenic strategies relying upon neuron-restricted expression of mutant SOD1 failed to produce significant motor neuron disease in mice (Pramatarova et al., 2001; Lino et al., 2002), many groups theorized that motor neuron degeneration might be non-cell autonomous in this form of ALS. Production of chimeric mice containing different mixtures of normal and mutant-expressing SOD1 cells allowed investigators to definitively show that motor neuron expression of mutant SOD1 is not sufficient for disease (Clement et al., 2003). Instead, non-neuronal cells must express mutant SOD1 for neighboring motor neurons to degenerate. Current models of ALS postulate that a variety of different molecular pathologies contribute to the motor neuron degeneration by eliciting damage within different cell types, and that death of the motor neuron does not occur in isolation from its connected glial, vascular, and immune system partners (Ilieva et al., 2009).

In SCA7, it is also clear that neurodegeneration is not simply cell autonomous. Our study examined the roles of BG, PCs, and IO neurons, and found that all of these cell types contribute to SCA7 PC degeneration. We previously reported that expression of mutant ataxin-7 in BG in *Gfa2-SCA7-92Q* transgenic mice is sufficient to cause PC degeneration (Custer et al., 2006). In the current study, removal of ataxin-7-92Q in PCs and IO neurons prevented PC degeneration (as measured by cerebellar molecular layer thinning), despite continued expression of mutant ataxin-7 protein in BG. One likely explanation for the difference between these two studies is that *PrP-*

floxed-SCA7-92Q BAC mice express mutant ataxin-7 at levels less than that of the endogenous gene, while expression in *Gfa2-SCA7-92Q* transgenic mice exceeded endogenous levels. Furthermore, isolated expression of mutant ataxin-7 in BG resulted in late-onset ataxia and PC degeneration in the *Gfa2-SCA7-92Q* model. When mutant ataxin-7 is expressed ubiquitously at low levels, reduction of mutant ataxin-7 expression in PCs and IO neurons is more beneficial than excision of mutant ataxin-7 in BG. Thus, expression of mutant ataxin-7 in IO neurons, in combination with expression in PCs, produces greater cerebellar toxicity than mutant ataxin-7 expression in BG. Nonetheless, our current findings continue to support an important role for BG in SCA7 pathogenesis. Excision of the disease gene from BG alone does ameliorate the disease phenotype, and excision of mutant ataxin-7 from BG in combination with PCs and IO neurons yields a synergistic effect on the delay of symptom onset.

An important and unexpected observation in this study is that a well established *Pcp2-Cre* transgenic driver line (Barski et al., 2000) expresses Cre recombinase in both PCs and IO neurons. This permitted us to evaluate the contribution of IO neurons and PCs to cerebellar degeneration in SCA7, but prevented us from delineating the individual role of each cell type in SCA7 pathogenesis. Previous studies in transgenic mice have shown that polyQ-ataxin-7 expression restricted to PCs produces a very mild, late-onset phenotype (Yvert et al., 2000). However, expression in other cerebellar cell types, but not in PCs, yields more severe SCA7 disease (Garden et al., 2002; Custer et al., 2006). Together, these studies in conjunction with data presented here, suggest that IO neuron dysfunction is a major contributor to SCA7 disease pathogenesis. A principal role for IO neurodegeneration in SCA7 is suggested not only by our findings, but also by work done independently on a different SCA7 transgenic mouse model (Wang et al., 2010).

How might IO neuron dysfunction result in cerebellar degeneration in SCA7? One function of IO neurons is to deliver IGF-1, an important survival factor for PCs, to the cerebellar molecular layer (Nieto-Bona et al., 1993). Exogenous IGF-1 ameliorates PC degeneration (Tolbert and Clark, 2003; Carrascosa et al., 2004) and promotes glial glutamate transporter gene expression in BG (Gamboa and Ortega, 2002). Impaired GLAST transcription has been documented in SCA7 transgenic mice (Custer et al., 2006), thus loss of IGF-1 delivery from IO neuron CFs may contribute to reduced GLAST gene expression in SCA7. Loss of CFs may also explain the observation that the GluRδ2 AMPA receptor subunit is upregulated in cerebellar lysates from ataxin-7-52Q transgenic mice (Chou et al., 2010). GluRδ2 is found exclusively at PC-parallel fiber (PC-PF) synapses (Kurihara et al., 1997). Deletion of GluRδ2 in mice causes reduced PC-PF synapses and abnormal extra PC-CF synapses (Kashiwabuchi et al., 1995). It is possible that loss of CF input due to cell autonomous degeneration of IO neurons leads to increased PC-PF synapses and thus increased GluRδ2 expression (Chou et al., 2010). Another explanation might involve transcriptional dysregulation resulting in increased GluRδ2 expression, increased PC-PF synapses, and subsequent reduction of PC-CF synapses, contributing to degeneration of IO neurons. BG are a component of both the PC-PF and PC-CF tripartite synapse; thus, disruption of inputs to PCs may in turn cause BG dysfunction and/or degeneration. Because mutant ataxin-7 disrupts normal gene transcription (McMahon et al., 2005; Palhan et al., 2005; Helmlinger et al., 2006), it is also possible that the molecular pathways involved in maintaining appropriate connections between PCs, IO neurons, and BG are altered by transcriptional dysregulation in a cell type-specific fashion. It will be critical to identify the cellular processes that mutant ataxin-7 disturbs within each cell type and how these abnormalities lead to disruptions in the PC-IO neuron-BG network (Fig. 2.7).

Triple transgenic mice harboring the *PrP-floxed-SCA7-92Q BAC*, *Gfa2-Cre*, and *Pcp2-Cre* transgenes exhibited a dramatic rescue from neurological disease and PC degeneration. Remarkably, removing mutant ataxin-7 from these cell populations delayed disease onset by 20 weeks (i.e., twofold). Although disease pathology in the triple transgenic mice could stem from expression of mutant ataxin-7 in cerebellar GCNs, we carefully evaluated GCN morphology, but did not observe any GCN abnormalities, suggesting instead that incomplete excision of mutant ataxin-7 expression from PCs, IO neurons, and BG likely accounts for the ultimate development of a disease phenotype in these mice. Our results demonstrate that PCs, IO neurons, and BG are all involved in SCA7 disease pathogenesis (Fig. 2.7). PolyQ-ataxin-7 consequently leads to dysfunction in each of these different cell types, preventing them from performing key functions or maintaining healthy connections with their interdependent neighbors. Cerebellar neurodegeneration in SCA7 may thus be viewed as a coincident set of pathological alterations that occur within a highly interconnected network composed of neurons and glia. Our findings underscore the complexity of SCA7 disease pathogenesis and suggest that reversing toxicity in a single cell type is unlikely to reverse the course of disease. However, these findings suggest that effective gene-silencing strategies delivered to any involved cell type should yield significant benefit to afflicted patients.

Materials and Methods

Generation of *PrP-floxed-SCA7-92Q BAC* mice

We obtained a 90 kb fragment containing the murine PrP in a BAC vector backbone (RPCI mouse BAC library 24; clone ID RP24-92I12). The murine PrP BAC targeting vector was constructed in five steps, as follows: (1) 5' and 3' targeting arms were inserted by PCR onto the ends of a minimal 1.8 kb, chloramphenicol-resistant vector; (2) an ampicillin resistance cassette was cloned into the MluI, XmaI sites of the targeting vector; (3) a 234 bp fragment encoding the last 50 amino acids of ataxin-7, followed by a loxP site, was inserted into the XhoI, HpaI restriction sites of the targeting vector; (4) an 824 bp fragment encoding a 3X FLAG tag fused to EGFP was cloned into the NheI, PacI restriction sites of the targeting vector; and (5) a 2.8 kb fragment containing a loxP site, followed by the remaining ataxin-7-92Q sequence, was cloned into the MluI, XhoI restriction sites to complete the targeting vector. The targeting vector was recombined into the BAC vector backbone and replaced all coding information for the murine PrP gene. The final PrP-floxed-SCA7-92Q BAC vector was microinjected into C57BL/6J:C3H/HeJ F1 hybrid oocytes. Of four founders identified, two gave rise to *PrP-floxed-SCA7-92Q BAC* lines with comparable phenotypes. Of these lines, we chose to focus our studies principally on line "258".

PCR genotyping

Mice tissue (~2-4 mm^2) was placed in a 1.5 mL Microfuge tube containing 175 µL of 0.1 M NaOH and 175 µL of mineral oil. Tubes were briefly centrifuged and then heated in an Oster

Food Steamer (Target) for 45 min. The tubes were removed from the steamer, inverted several times, and then centrifuged at 13,000 X g in a benchtop centrifuge for 3 min. Eighty microliters of base solution was carefully taken from the middle of the aqueous phase. This material was transferred to a new 0.65 mL Microfuge tube containing 80 µL of 1M Tris-HCl. This neutralized tissue extract was stored at 4°C prior to PCR analysis. PCR conditions included 60ºC annealing temperature, 38 cycles, and 1 min extension period. Primer sequences are shown in Table 2.

Table 2: Primer sequences for PCR genotyping.

Transgene		**Primer Sequence**	**Product (bp)**
PrP-floxed-SCA7-92Q BAC	Forward	CATTTTAGGCCCCACGTATCAC	587
	Reverse	GGCCCGCTCCGACAT	
CMV-Cre	Forward	CAAAATTTGCCTGCATTACCG	553
	Reverse	CATTCTCCCACCGTCAGTACG	
Z/EG	Forward	GACGACGGCAACTACAAGACC	561
	Reverse	GCCAGAAGTCAGATGCTCAAG	
Gfa2-Cre	Forward	GTGCTGGGATTACAAGCATGA	400
	Reverse	CAGGCAAATTTTGGTGTACGG	
Pcp2-Cre	Forward	GATGGATTTCCGTCTCTGGTG	428
	Reverse	CATTATAAGCTGCAATAAACAAGTTCTGC	

RT-PCR analysis

Mouse brains were homogenized in Trizol (Life Technologies), and total RNA was extracted according to the manufacturer's instructions. Total RNA was reverse transcribed in independent duplicate reactions using random hexamers and SuperScript II reverse transcriptase (Life Technologies), and quantification of mouse and human ataxin-7 RNA expression by co-amplification and subsequent restriction digestion was performed as previously described (La

Spada et al., 2001). Total RNA was isolated from the cerebellum of 6 week-old mice using an RNeasy isolation kit (Qiagen). Total RNA was reverse transcribed using SuperScriptII Reverse Transcriptase according to manufacturer's instructions (Invitrogen). The cDNA's were subjected to real-time PCR using custom ataxin-7 primers and probe selected with Primer Express v3.0 software (Applied Biosystems), as follows: forward primer, TTTGGGAGCCGGCAGAT; reverse primer, GCTGTGCATTCAGATGCTTCTC; probe, TGTTTGACTCCAGGTGGA. Samples were analyzed on a StepOnePlus Real-Time PCR system using a 64ºC annealing temperature and normalized to mouse 18S RNA using Applied Biosystems assay Hs99999901_s1. Average ataxin-7 RNA level for non-transgenic (n=3) and *PrP-floxed-SCA7-92Q BAC* (n=3) mice was calculated using Microsoft Excel. Ataxin-7 levels in non-transgenic animals were normalized to 1.0 and data were plotted and statistically analyzed in Graphpad Prism 4.0.

Behavioral Phenotyping

All studies and procedures were approved by the University of Washington and University of California, San Diego, Institutional Animal Care and Use Committees (IACUC). Females and males were used in all studies, and experiments were performed by a blinded examiner.

Composite Phenotype Score

The composite phenotype score was performed as previously described (Guyenet et al., 2010). An average composite phenotype score for each genotype was calculated and plotted using Microsoft Excel. Statistical analyses were conducted in Graphpad Prism 4.0.

Accelerating Rotarod

Mice were placed on the rotarod (Economex, Columbia Instruments) and trained on day 0 by running freely up to 5 min. On days 1-4, mice were placed on the rotarod and underwent the following regimen: at time 0, the rotarod was started with 4 rotations per min, and an acceleration of 0.1 rotations per sec. The time each mouse dismounted was recorded (in seconds), and mice had at least 5 min of rest between trials. Trials were repeated 5 times daily for a maximum of 300 sec per trial. The best four times per day were recorded and averaged for each mouse. Average latency to fall for each trial day was calculated for each genotype and plotted using Microsoft Excel. Statistical analyses were conducted in Graphpad Prism 4.0.

Immunohistochemistry

Deeply anesthetized mice were transcardially perfused with phosphate buffered saline (PBS) followed by 4.0% paraformaldehyde (PFA) in 0.1M phosphate buffer (PB), pH 7.4. Brains were removed and post-fixed in 4.0% PFA in 0.1M PB overnight, then moved into 0.4% PFA in 0.1M PB for storage at 4ºC. Free-floating 40 μm sagittal brain sections were cut on the Leica Vibratome 1000S and stored in 0.03% PFA in PBS. Free-floating sections were incubated with 5% normal goat serum (NGS), 0.2% bovine serum albumin (BSA), and 1.0% Triton X-100 for 1 hr at room temperature. Sections were then incubated overnight at 4ºC with anti-calbindin antibody (#300, Swant) at 1:1,000 dilution; anti-GFP antibody (ab6556, Abcam) at 1:1,000 dilution; anti-GFAP antibody (Z0334, DAKO) at 1:1,000 dilution; anti-S100β antibody (ab11178, Abcam) at 1:1,000 dilution; or anti-ataxin-7 antibody (PA1-749, Affinity Bioreagents) at 1:500 dilution in PBS with 5% NGS and 0.1% Triton X-100. After 3 washes in 1X PBS,

AlexaFluor 488 anti-rabbit or anti-mouse IgG (Invitrogen) at 1:500 dilution, and/or AlexaFluor 594 anti-rabbit or anti-mouse IgG (Invitrogen) at 1:500 dilution were applied to sections and incubated at room temperature for 2-3 hr. After 3 washes in 1X PBS, sections were mounted on glass slides and coverslipped in Fluoro-Gel with Tris Buffer (Electron Microscopy Sciences). Sections were viewed and 2-D or 3-D z-stack digital images were created using a Zeiss Axiovert 200M inverted microscope and Slidebook 5.0 software (Intelligent Imaging Innovations).

To quantify *PrP-floxed-SCA7-92Q BAC* gene excision, 2-D images were collected from three areas per section, one section per animal, for *Gfa2-Cre;Z/EG* and *Z/EG* animals (n = 6/group). 2-D images were collected of four areas per section, one section per animal, for *Pcp2-Cre;PrP-floxed-SCA7-92Q BAC* (n = 7) and *PrP-floxed-SCA7-92Q BAC* (n = 4) mice. Two independent observers counted the number of either calbindin-positive Purkinje cells or S-100β-positive Bergmann glia, then counted the number of those that were GFP positive. Results were reported as a ratio of GFP and marker double-positive cells to total marker-positive cells. Average ratios for each genotype were calculated, plotted, and analyzed statistically in Graphpad Prism 4.0.

To quantify cerebellar molecular layer thickness, 2-D images of calbindin-immunostained cerebellar sections were collected. The three most dorsal cerebellar folia per section, using three sections per individual (n = 6/group), were imaged. In each image, a boundary line around the molecular layer from, but excluding, the Purkinje cell bodies to the pial surface was drawn by hand using Slidebook 5.0. In the center of the molecular layer, 100 µm-long lines were drawn. Every 100 µm, a measurement was taken from the pial surface to the Purkinje cell layer. Molecular layer measurements were averaged for each genotype, plotted, and analyzed statistically in Graphpad Prism 4.0.

To quantify the number of Bergmann glia processes, brightest-point projection images were created using Slidebook 5.0. 3-D image z-stacks were collected for two areas per section, three sections per individual (n = 6/group). 3-D images were deconvolved using the Nearest Neighbors algorithm of Slidebook 5.0. The brightest-point projection images were created through the z-axis to produce 2-D images. In each 2-D image, a 150 μm line was drawn using Slidebook 5.0 (Intelligent Imaging Innovations) approximately 50 μm from the pial surface of the cerebellar molecular layer. Three independent observers drew this line and then counted the number of GFAP-positive processes that crossed the line. The average number of processes for each genotype was calculated, plotted, and analyzed statistically in Graphpad Prism 4.0.

Chapter III:

Cre recombinase-mediated removal of polyglutamine-expanded ataxin-7 after symptom onset arrests disease progression in a mouse model of spinocerebellar ataxia type 7

Summary

Neurodegenerative disorders caused by polyglutamine (polyQ) expansions typically manifest in mid-life and symptoms worsen slowly. During the progressive stage, it is unknown whether neurological dysfunction is reversible. Conditional mouse models of Huntington's disease and spinocerebellar ataxia (SCA) type 1 recover motor function after expression of the disease genes is stopped. To address whether the same phenomenon occurs in SCA type 7 (SCA7), we crossed the *PrP-floxed-SCA7-92Q BAC* mouse line to a transgenic mouse line ubiquitously expressing a tamoxifen-inducible Cre recombinase. Bigenic mice were orally administered tamoxifen citrate four weeks after the onset of behavioral abnormalities and showed improved motor function compared to bigenic mice treated with vehicle. Symptom progression was arrested as measured with a composite phenotype scoring system. Poor performance on the accelerating rotatod reverted to wildtype performance. Tamoxifen treatment did not significantly alter two hallmarks of cerebellar pathology in this SCA7 model, molecular layer thinning and Bergmann glia process loss. In fact, Bergmann glia pathology continued to progress after disease gene excision. However, tamoxifen treatment after symptom onset did prevent changes in the distribution of climbing fiber terminals and reduced the number of Purkinje cell nuclei containing ataxin-7 aggregates. Our results demonstrate that suppression of polyQ-expanded ataxin-7 gene expression prevents further symptom progression, even when initiated after symptom onset and at a time when some histopathological changes cannot be

reversed. These findings support the hypothesis that some features of SCA7 are irreversible and suggest that symptom progression may be linked with degeneration of inferior olive input to cerebellar Purkinje neurons.

Introduction

Spinocerebellar ataxia type 7 (SCA7) is a dominantly inherited progressive neurodegenerative disease caused by a polyglutamine (polyQ) expansion in the ataxin-7 gene. PolyQ-expanded ataxin-7 leads to cell loss in the retina, brainstem, and cerebellum resulting in blindness and progressive loss of motor control (Garden and La Spada, 2008). Other known disorders caused by a CAG trinucleotide repeat expansion encoding an elongated polyQ tract in their causative proteins are Huntington's disease (HD), spinobulbar muscular atrophy (SBMA), dentatorubral pallidoluysian atrophy (DRPLA), and spinocerebellar ataxia (SCA) types 1, 2, 3, 6, 7, and 17. A common feature of polyQ expansion disease is mid-life onset with slowly progressive neurological abnormalities that worsen over years or decades before early mortality (Orr and Zoghbi, 2007).

Previous studies suggest that the negative impact of the polyQ-expanded gene on neuronal function may be reversible, and the affected cells possess the capacity to recover if mutant gene expression is stopped prior to cell death (Yamamoto et al., 2000; Zu et al., 2004). In a conditional model of HD utilizing the tetracycline-responsive transgene system, cessation of mutant huntingtin expression after the onset of detectable abnormalities of motor behavior resulted in a near complete reversal of motor symptoms and clearance of mutant huntingtin aggregates from the striatum. The progression of striatal volume loss, reactive astrocytosis, and loss of dopamine-1 receptors was also prevented (Yamamoto et al., 2000). In a conditional model of SCA1 using the same tetracycline-responsive system, turning off expression of the mutant transgene at early, middle, or late stage disease was assessed. Motor function and Purkinje cell (PC) histopathology were improved, even at late disease stages, suggesting that

SCA1 pathology may be reversible throughout disease progression. The earlier the intervention, the more closely conditional SCA1 mice resembled control mice (Zu et al., 2004). At all stages of SCA1 disease, polyQ-ataxin-1 aggregates were cleared from PCs. Taken together, these two studies suggest that polyQ expansion disorders require continued expression of the causative gene in order to maintain disease progression and neuronal dysfunction may not be completely irreversible.

In this study, we characterized the timeline of some features of disease pathogenesis and discovered not all features were reversible in a mouse model of SCA7. Recently we reported the novel mouse model *PrP-floxed-SCA7-92Q BAC*, which expresses a human polyQ-expanded ataxin-7 cDNA that can be controlled spatially and temporally by use of the Cre-loxP system. *PrP-floxed-SCA7-92Q BAC* mice first show significant motor impairment at 20 weeks of age as assessed by a composite phenotype scoring system (Guyenet et al., 2010). This neurological pathology continues to worsen with age until end stage at 40-50 weeks (Furrer et al., 2011). At end stage, the cerebellar molecular layer is significantly thinned and Bergmann glia radial processes are fewer (Furrer et al., 2011). Here we show molecular layer thinning occurs at the onset of behavioral abnormalities, but well before Bergmann glia (BG) processes are lost. The inferior olive (IO) projects climbing fibers (CFs) into the molecular layer that synapse onto PCs. Similar to findings reported in SCA1 mice (Duvick et al., 2010; Barnes et al., 2011), we document CF pathology in end stage *PrP-floxed-SCA7-92Q BAC* mice.

In order to stop polyQ-ataxin-7 expression after behavioral symptom onset, we crossed a mouse line ubiquitously expressing tamoxifen-inducible Cre recombinase onto the *PrP-floxed-SCA7-92Q BAC* line. Bigenic mice administered tamoxifen citrate four weeks after symptom onset demonstrated prevention of neurological symptom progression. However, histopathology

of PCs and BG in tamoxifen-treated bigenic mice resembled *PrP-floxed-SCA7-92Q BAC* singly transgenic mice. Tamoxifen treatment of bigenic mice did reduce the number of ataxin-7 aggregates found within PC nuclei and prevented the development of an abnormal pattern of CF synapses, suggesting that IO input may have an important role in the progression of motor dysfunction in SCA7. Removing the polyQ-expanded ataxin-7 gene after symptom onset did not reverse PC pathology or prevent BG pathology, but it prevented dislocation of CF terminals and reduced ataxin-7 aggregate formation. This study supports the hypothesis that reduction of polyQ-ataxin-7 expression prevents neurological symptom progression, even after the onset of behavioral dysfunction and PC degeneration. Future treatments developed to reduce or halt mutant ataxin-7 gene expression will likely benefit patients, even if administered after symptom onset.

Results

Purkinje cell degeneration is first detected concurrently with the onset of motor dysfunction in *PrP-floxed-SCA7-92Q BAC* mice

Several studies have suggested that certain mouse models for polyQ diseases have detectable pathological abnormalities prior to behavioral symptom onset (Gatchel et al., 2008; Chou et al., 2010; Vig et al., 2011; Xiang et al., 2011). Such very early pathology may be reversible if transgene expression is inactivated during early life (Barnes et al., 2011). To determine if *PrP-floxed-SCA7-92Q BAC* mice develop presymptomatic PC pathology, sagittal brain sections from 10 week-old *PrP-floxed-SCA7-92Q BAC* and non-transgenic mice were labeled with antibodies against calbindin. The number of PCs and their dendritic arborization in the cerebellar molecular layer appeared similar between the two groups (Fig. 3.1, A & B). Quantification of cerebellar molecular layer thickness using a previously reported approach (Furrer et al., 2011) demonstrated no difference between *PrP-floxed-SCA7-92Q BAC* and non-transgenic mice (Fig. 3.1, C). Thus, *PrP-floxed-SCA7-92Q BAC* mice have no histological abnormalities of PCs at 10 weeks of age, confirming normal development of PC dendritic arbors and suggesting that PC pathology may correlate with the onset of behavioral deficits.

We recently reported that *PrP-floxed-SCA7-92Q BAC* mice have detectable motor deficits at 20 weeks of age (Furrer et al., 2011). To determine whether PC pathology coincides with the onset of the neurological phenotype, we examined sagittal cerebellar sections labeled for calbindin in early symptomatic animals. We observed that 20 week-old *PrP-floxed-SCA7-92Q BAC* mice have visible degeneration of PC dendrites compared to non-transgenic mice (Fig. 3.2, A & B). Molecular layer thickness measurements revealed that *PrP-floxed-SCA7-92Q BAC*

mice display significantly thinner cerebellar molecular layers than non-transgenic animals (Fig. 3.2, C). The degree of molecular layer thinning in 25 week-old animals is similar to 20 week-old animals (data not shown). These observations indicate that behavioral symptom onset in *PrP-floxed-SCA7-92Q BAC* mice coincides with reduced cerebellar molecular layer thickness and PC pathology.

Previously we observed that dysfunctional or degenerating PCs can cause BG pathology, including loss of BG processes in the cerebellar molecular layer (Furrer et al., 2011). To determine if BG pathology develops coincident with PC pathology in early symptomatic *PrP-floxed-SCA7-92Q BAC* mice, we immunostained sagittal cerebellar sections for glial fibrillary acidic protein (GFAP) and quantified the number of BG processes using previously reported methods (Furrer et al., 2011). BG in *PrP-floxed-SCA7-92Q BAC* mice at 20 and 25 weeks of age were not significantly affected compared to non-transgenic mice. We observed some features previously reported in mice expressing polyQ-expanded ataxin-7 exclusively in BG (Custer et al., 2006), including excessive branching and fewer BG processes reaching the pial surface (Fig. 3.2, D & E; data not shown). However, quantification of the number of BG processes in the cerebellar molecular layer showed *PrP-floxed-SCA7-92Q BAC* mice did not exhibit significant BG process loss in comparison to non-transgenic mice at either time point (Fig. 3.2, F & G). These findings suggest that BG degeneration occurs after PC pathology is present, further supporting the hypothesis that damaged PCs cause injury to BG in a non-cell autonomous manner.

Tamoxifen-inducible Cre recombinase permits temporal inactivation of polyQ-ataxin-7 in the *PrP-floxed-SCA7-92Q BAC* mice

To determine if PC pathology and neurological symptoms are reversible in our *PrP-floxed-SCA7-92Q BAC* mice, we crossed a tamoxifen-inducible Cre recombinase transgenic line (Hayashi and McMahon, 2002) to the *PrP-floxed-SCA7-92Q BAC* model. Bigenic mice (*PrP-floxed-SCA7-92Q BAC;CAGG-Cre-ER^{TM}*) express Cre recombinase ubiquitously, though Cre is sequestered into the cytoplasm due to fusion with a mutant form of the estrogen receptor (ER) ligand-binding domain. Once tamoxifen binds, the Cre-ER^{TM} fusion protein translocates to the nucleus where Cre recombinase can excise the loxP-flanked polyQ-expanded ataxin-7 cDNA (Fig. 3.3, A). Because symptom onset in *PrP-floxed-SCA7-92Q BAC* mice is 20 weeks (Furrer et al., 2011), we orally administered a single 20 mg dose of tamoxifen citrate dissolved in corn oil, or corn oil alone, to bigenic (*PrP-floxed-SCA7-92Q BAC;CAGG-Cre-ER^{TM}*), singly transgenic (*CAGG-Cre-ER^{TM}* or *PrP-floxed-SCA7-92Q BAC*), and non-transgenic littermate controls at 24 weeks of age (Fig. 3.3, A). *CAGG-Cre-ER^{TM}* and non-transgenic animals were pooled together in one group designated "SCA7-negative".

To determine the efficiency of polyQ-ataxin-7 gene excision after orally administered tamoxifen, cerebella were collected from *PrP-floxed-SCA7-92Q BAC;CAGG-Cre-ER^{TM}* bigenic mice dosed with tamoxifen or oil and from *PrP-floxed-SCA7-92Q BAC* mice dosed with tamoxifen. Real-time RT-PCR analysis was then conducted to determine the relative abundance of transgene mRNA upon Cre-mediated excision of the ataxin-7-92Q sequence. Oil-treated bigenic mice exhibited a small number of Cre-mediated excision events, as shown previously in the *CAGG-Cre-ER^{TM}* line (Hayashi and McMahon, 2002). Importantly, bigenic mice displayed

a nine-fold increase in ataxin-7 transgene excision after a single dose of tamoxifen in comparison to oil-treated bigenic mice (Fig. 3.3, B).

Cessation of polyQ-ataxin-7 expression after symptom onset prevents SCA7 symptom progression

SCA7-negative (*CAGG-Cre-ER^{TM}* or non-transgenic), SCA7-positive (*PrP-floxed-SCA7-92Q BAC*), and bigenic (*PrP-floxed-SCA7-92Q BAC;CAGG-Cre-ER^{TM}*) mice were administered either tamoxifen or vehicle four weeks after symptom onset, at 24 weeks of age. At 23 weeks (pre-treatment), bigenic mice exhibited significant abnormalities in composite phenotype score, similar to SCA7-positive mice. All bigenic and SCA7-positive mice were significantly impaired compared with SCA7-negative mice (Fig. 3.4, A). Singly transgenic SCA7 mice treated with tamoxifen or oil progressively worsened in accordance with a previous report (Furrer et al., 2011). Bigenic mice administered oil at 24 weeks also exhibited a progressive neurological phenotype. Bigenic mice treated with a single dose of tamoxifen worsened slightly at 25 weeks, but their composite phenotype score reached a plateau and remained consistent throughout the remainder of the study period (Fig. 3.4, A). Although the bigenic tamoxifen-treated mice exhibited neurological abnormalities, they no longer had progressive symptoms nor were their symptoms as severe as those exhibited by SCA7-positive mice or bigenic oil-treated mice. Hence, Cre-mediated excision of the ataxin-7 transgene four weeks after symptom onset arrested SCA7 disease progression. This finding was corroborated by assessment of performance on an accelerating rotarod. At 23 weeks of age (pre-treatment) and prior to transgene excision, SCA7-positive and bigenic mice dismounted the accelerating rotarod sooner than SCA7-negative mice,

suggesting a trend toward deficiencies in motor coordination (Fig. 3.4, B). Bigenic mice were significantly impaired on trial days 3 and 4 (two-way ANOVA with Bonferroni's *post hoc* test; data not shown). At 42 weeks of age (19 weeks post-treatment and at end stage for this SCA7 mouse model), SCA7-positive mice administered tamoxifen or oil performed significantly worse on the rotarod compared with SCA7-negative mice. Bigenic mice administered oil also performed poorly. Bigenic tamoxifen-treated mice, however, performed similarly to the SCA7-negative mice (Fig. 3.4, B), suggesting that termination of polyQ-ataxin-7 expression can reverse some neurological abnormalities in SCA7 transgenic mice.

Cessation of polyQ-ataxin-7 expression after symptom onset does not arrest neuronal or glial pathology in SCA7 mice

We next tested whether excision of the polyQ-ataxin-7 transgene prevented the onset or progression of cerebellar histopathology in *PrP-floxed-SCA7-92Q BAC* transgenic mice. We collected sagittal cerebellar sections from 43 week-old SCA7-negative mice, SCA7-positive mice, and bigenic mice and immunolabeled with anti-calbindin antibodies to evaluate PC histopathology (Fig. 3.5, A-D). Cerebella from tamoxifen-treated SCA7-positive and oil-treated bigenic mice had PCs with shrunken somae and reduced dendritic arborization, while tamoxifen-treated bigenic mice exhibited PCs appearing healthier. However, quantification of cerebellar molecular layer thickness revealed that while tamoxifen-treated SCA7-positive mice had a thinner molecular layer than control mice given tamoxifen (Fig. 3.5, E), the molecular layer thickness of tamoxifen-treated bigenic mice did not significantly differ from oil-treated bigenics or tamoxifen-treated SCA7-positive mice (Fig. 3.5, E). Because molecular layer thinning is

present in 20 week-old *PrP-floxed-SCA7-92Q BAC* mice (Fig. 3.2, A-C), these findings suggest that cessation of polyQ-ataxin-7 expression after this thinning has occurred cannot reverse the pathology. Nonetheless, as the appearance of PC pathology was reduced in tamoxifen-treated bigenics, PC degenerative changes distinct from molecular layer thickness may be slowed or prevented when polyQ-ataxin-7 expression is ceased.

Although ataxin-7-92Q transgene excision after symptom onset did not reverse thinning of the molecular layer, we tested if SCA7 disease gene excision would prevent the progressive loss of BG processes, which was only detectable at a later timepoint. Cerebellar sections from SCA7-negative, SCA7-positive, and bigenic mice were immunostained with antibodies against GFAP to visualize BG. Tamoxifen-treated SCA7-positive mice displayed cerebella with disorganized and stunted BG processes compared with tamoxifen-treated SCA7-negative mice (Fig. 3.6, A & B). BG from tamoxifen-treated bigenic mice appeared slightly healthier than tamoxifen-treated SCA7-positive BG, while oil-treated bigenic mice harbored BG more similar in appearance to SCA7-positive tamoxifen-treated BG (Fig. 3.6, A-D). Quantification of BG process numbers revealed significant reductions in tamoxifen-treated SCA7-positive mice. Both tamoxifen-treated and oil-treated bigenic mice exhibited BG pathology similar to tamoxifen-treated SCA7-positive mice (Fig. 3.6, E). Thus excision of the ataxin-7 transgene at 24 weeks does not prevent BG process loss, even though BG degeneration occurs after gene excision in *PrP-floxed-SCA7-92Q BAC* mice (Fig. 3.2, D-G). These findings suggest that once PC pathology occurs, removal of the causative gene cannot prevent BG damage, further supporting the hypothesis that BG dysfunction in SCA7 develops in response to non-cell autonomous factors.

Cessation of polyQ-ataxin-7 expression after symptom onset ameliorates the redistribution of climbing fiber-Purkinje cell synapses in SCA7 mice

Our recently published findings demonstrated that PCs, BG, and neurons of the inferior olivary (IO) nucleus are important contributors to SCA7 disease onset and pathogenesis (Furrer et al., 2011). CFs originating from IO neurons synapse onto PC dendrites. Antibodies against vesicular glutamate transporter 2 (VGLUT2) specifically label CF terminals in the cerebellar molecular layer (Fremeau et al., 2001). In a mouse model of SCA1, CF synapses labeled with antibodies to VGLUT2 are decreased near the pial surface in the cerebellar molecular layer of symptomatic mice (Duvick et al., 2010). Because the IO degenerates in SCA7 patients and is likely involved in disease pathogenesis in both SCA7 and SCA1 (Duvick et al., 2010; Wang et al., 2010; Barnes et al., 2011; Furrer et al., 2011; Ingram et al., 2011), we investigated whether loss of CF-PC synapses also occurs in our mouse model of SCA7. Sagittal cerebellar sections from non-transgenic and *PrP-floxed-SCA7-92Q BAC* mice were collected and immunostained for VGLUT2. VGLUT2 immunolabeled CF terminals were evenly distributed throughout the molecular layer along PC dendrites in 20 week-old non-transgenic and *PrP-floxed-SCA7-92Q BAC* mice and 40 week-old non-transgenic mice (Fig. 3.7, A-C). In 40 week-old *PrP-floxed-SCA7-92Q BAC* mice, however, the CF-PC synapses were aberrantly distributed and more CF terminals were located nearer the PC bodies than in non-transgenic controls (Fig. 3.7, A-D). Oil-treated bigenic mice appeared to have VGLUT2 CF terminals arranged in a pattern more similar to 40 week-old *PrP-floxed-SCA7-92Q BAC* mice than to non-transgenic controls (Fig. 3.7, C-E). CF terminal distribution in tamoxifen-treated bigenic mice appeared more similar to 40 week-old non-transgenic mice than to *PrP-floxed-SCA7-92Q BAC* mice (Fig. 3.7, C-F).

In order to quantify the distribution of CF terminals labeled with VGLUT2 immunostaining, 3-D images of sagittal cerebellar sections from each experimental group were collected. Then, a line was drawn to separate the distal and proximal halves of the cerebellar molecular layer relative to the PCs. A 3-D box was next created in each of the two regions of the molecular layer (distal to PCs and proximal to PCs), and the volume within the box with intense VGLUT2 immunolabeling of CF terminals was measured. The total volume of VGLUT2 immunolabeling in the distal and in the proximal regions of the molecular layer was calculated using Slidebook 5.0 (Fig. 3.7, G). The results from this quantification are presented as a ratio of the volume of VGLUT2 immunofluorescence in the distal molecular layer to the volume in the proximal molecular layer (Fig. 3.7, H-J). At 20 weeks of age, the ratio of distal to proximal VGLUT2 volume was similar between non-transgenic and *PrP-floxed-SCA7-92Q BAC* mice and indicated more CF terminal volume was located in the region proximal to the PC somae (ratio < 1; Fig. 3.7, H). At 40 weeks of age, this ratio is significantly decreased in *PrP-floxed-SCA7-92Q BAC* mice compared to non-transgenic controls (Fig. 3.7, I), indicating a redistribution of CF terminals in symptomatic SCA7 mice. At 43 weeks of age, tamoxifen-treated bigenic mice have a significantly increased ratio of distal to proximal VGLUT2 volume compared to oil-treated bigenic mice (Fig. 3.7, J). Thus, cessation of polyQ-ataxin-7 gene expression at 24 weeks prevents SCA7-induced redistribution of CF-PC synapses in the cerebellar molecular layer.

PolyQ-ataxin-7 accumulates in PC nuclei over time except after polyQ-ataxin-7 gene excision

Previous studies of HD and SCA1 transgenic mice documented rapid clearance of intranuclear inclusions containing the aggregated form of the mutant protein upon cessation of mutant gene expression (Yamamoto et al., 2000; Zu et al., 2004). We monitored the progressive accumulation of polyQ-ataxin-7 aggregates in PCs in cerebella collected from *PrP-floxed-SCA7-92Q BAC* mice at 10, 20, and 25 weeks of age (Fig. 3.8, A & B). Using an anti-ataxin-7 antibody, we quantified the number of aggregates in PC nuclei as a function of total number of PCs. *PrP-floxed-SCA7-92Q BAC* mice have no appreciable loss of PCs (Furrer et al., 2011). Fewer than 10% of PCs have an intranuclear ataxin-7-positive inclusion at 10 weeks of age, but almost 30% of PCs display aggregates by 25 weeks of age (Fig. 3.8, B). Next we examined the number of polyQ-ataxin-7 aggregates in tamoxifen-treated SCA7-positive and bigenic mice. Approximately 50% of PCs in 43 week-old tamoxifen-treated SCA7-positive mice and oil-treated bigenic mice had inclusions, while only 23% of PCs in tamoxifen-treated bigenic mice did, similar to 25 week-old *PrP-floxed-SCA7-92Q BAC* mice (Fig. 3.8, B). These findings demonstrate that cessation of poly-Q-ataxin-7 gene expression can reduce the number of ataxin-7 aggregates in PC nuclei. However, polyQ-ataxin-7 aggregates may be more resistant to degradation and/or clearance than those that develop in mice expressing mutant huntingtin or polyQ-ataxin-1.

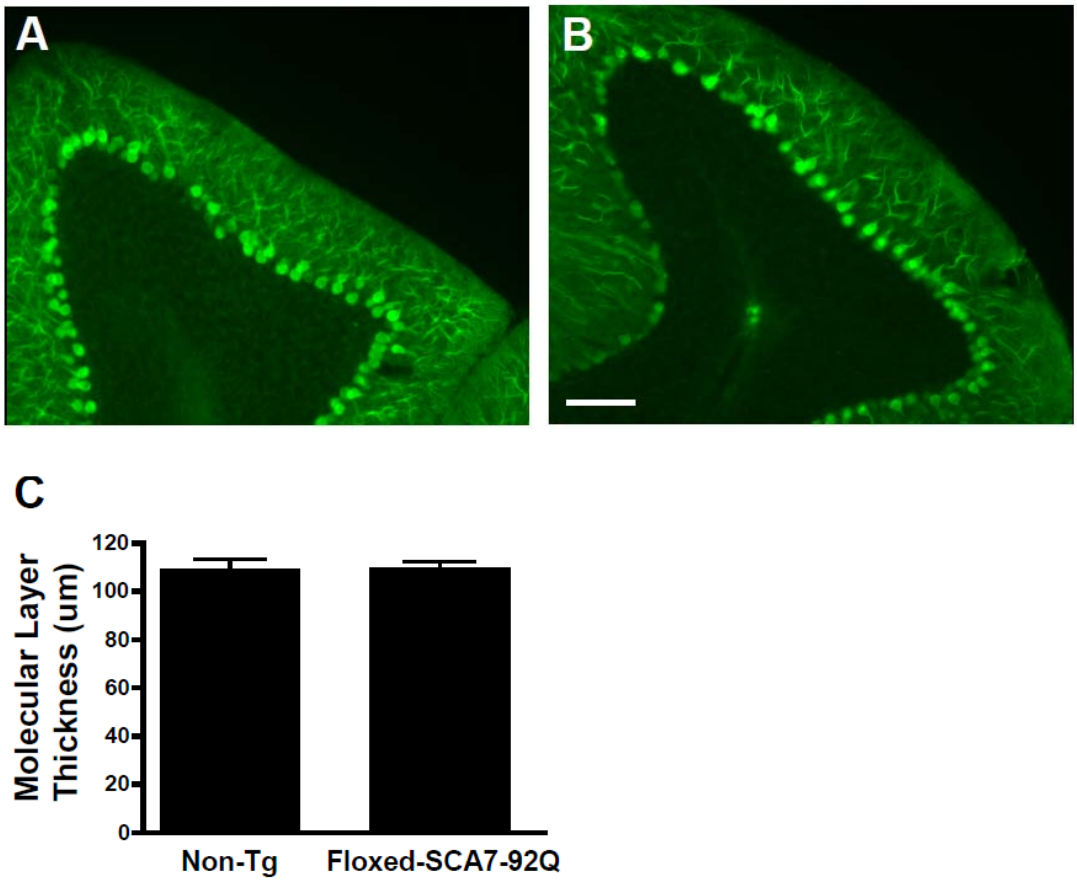

Figure 3.1: *PrP-floxed-SCA7-92Q BAC* mice develop normal cerebellar structure.

A-B, Sagittal cerebellar sections immunostained for anti-calbindin from 10 week-old mice. Non-transgenic (**A**) and *PrP-floxed-SCA7-92Q BAC* (**B**) mice both have strong calbindin immunolabeling of PC bodies and extensive dendritic arbors. Scale bar, 100 µm. **C**, Quantification of cerebellar molecular layer thickness. Cerebellar molecular layer thickness is similar between non-transgenic (Non-Tg; n = 4) and *PrP-floxed-SCA7-92Q BAC* (Floxed-SCA7-92Q; n = 6) mice (unpaired, two-tailed t-test). Error bars indicate SEM.

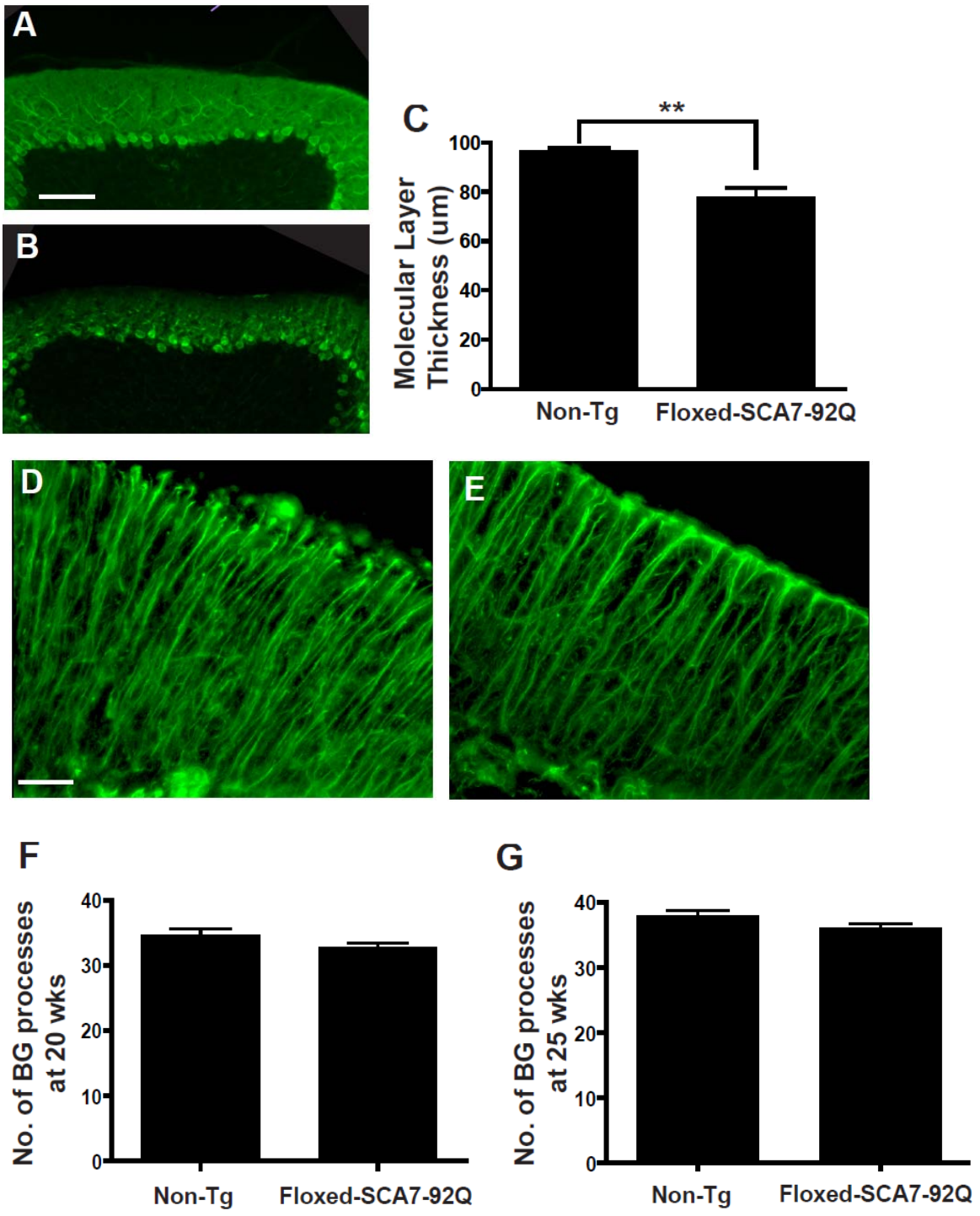

Figure 3.2: *PrP-floxed-SCA7-92Q BAC* mice develop significant Purkinje cell, but not Bergmann glia, pathology by 20 weeks of age.

A-B, Calbindin immunolabeled sagittal cerebellar sections. Non-transgenic mice (**A**) have more extensive PC dendritic branching and a thicker molecular layer than *PrP-floxed-SCA7-92Q BAC*

mice (**B**) at 20 weeks of age. Scale bar, 100 μm. **C**, Quantification of cerebellar molecular layer thickness. Significant thinning of the molecular layer has occurred in *PrP-floxed-SCA7-92Q BAC* mice (Floxed-SCA7-92Q; n = 6) compared to non-transgenic mice (Non-Tg; n = 4) by 20 weeks of age (unpaired, two-tailed t-test; $^{**}p < 0.01$). **D-E**, Sagittal cerebellar sections stained for anti-GFAP. Non-transgenic mice (**D**) and *PrP-floxed-SCA7-92Q BAC* mice (**E**) appear similar. Scale bar, 25 μm. **F-G**, Quantification of BG process number at 20 (**F**) and 25 (**G**) weeks of age. The number of GFAP-positive BG processes is not different between *PrP-floxed-SCA7-92Q* mice (n = 6) and non-transgenic mice (n = 4-5) at 20 or 25 weeks of age (unpaired, two-tailed t-tests). Error bars indicate SEM.

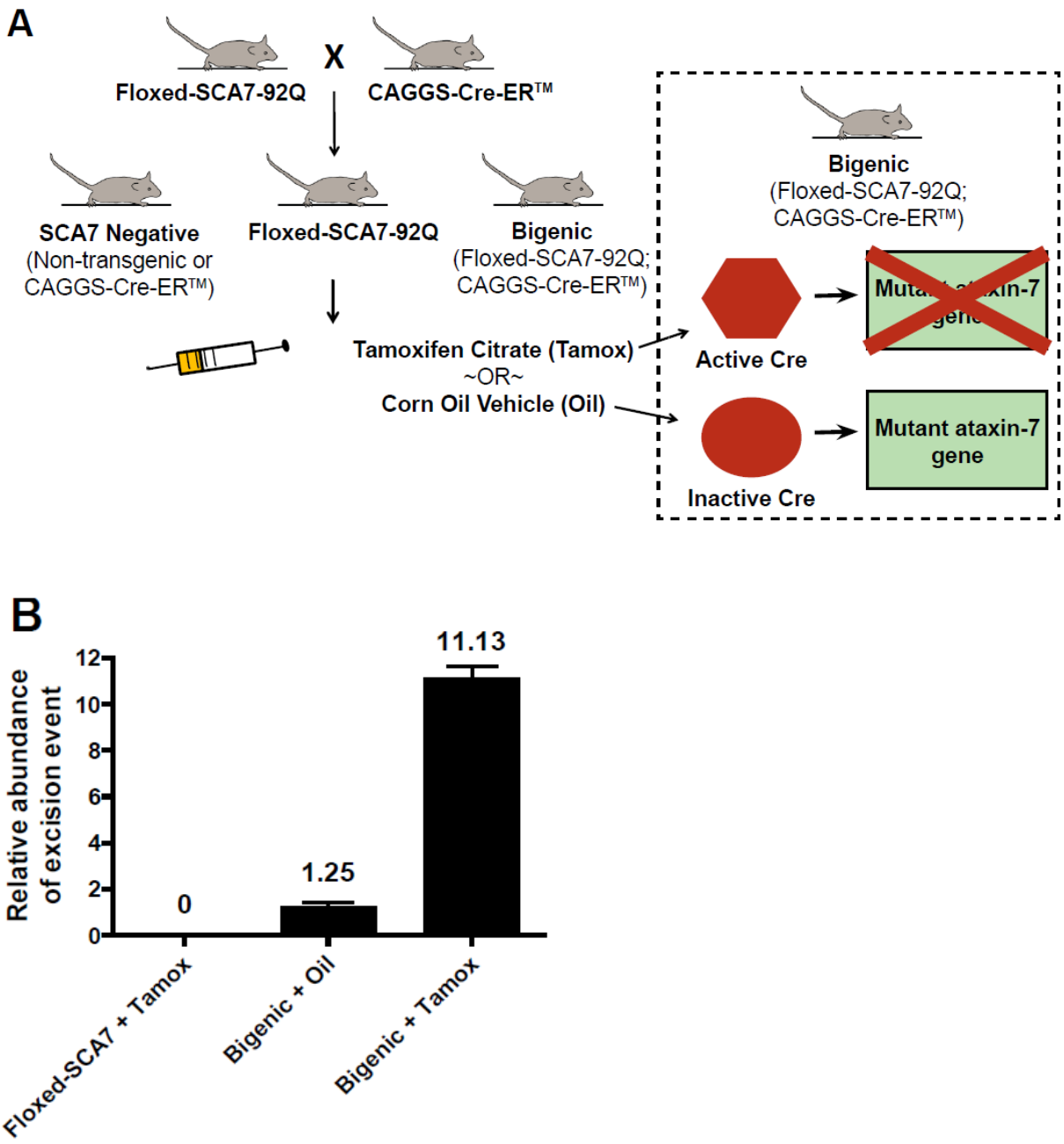

Figure 3.3: Inducible Cre-mediated excision of polyQ-ataxin-7 in *PrP-floxed-SCA7-92Q BAC* mice.

A, Schematic illustrating the breeding and treatment paradigm employed to compare time dependent disease gene suppression in an SCA7 mouse model. **B**, Quantitative real-time RT-PCR of relative mRNA levels of the SCA7 transgene that no longer harbors the ataxin-7-92Q cDNA sequence in cerebella (n = 3/group). Error bars indicate SEM.

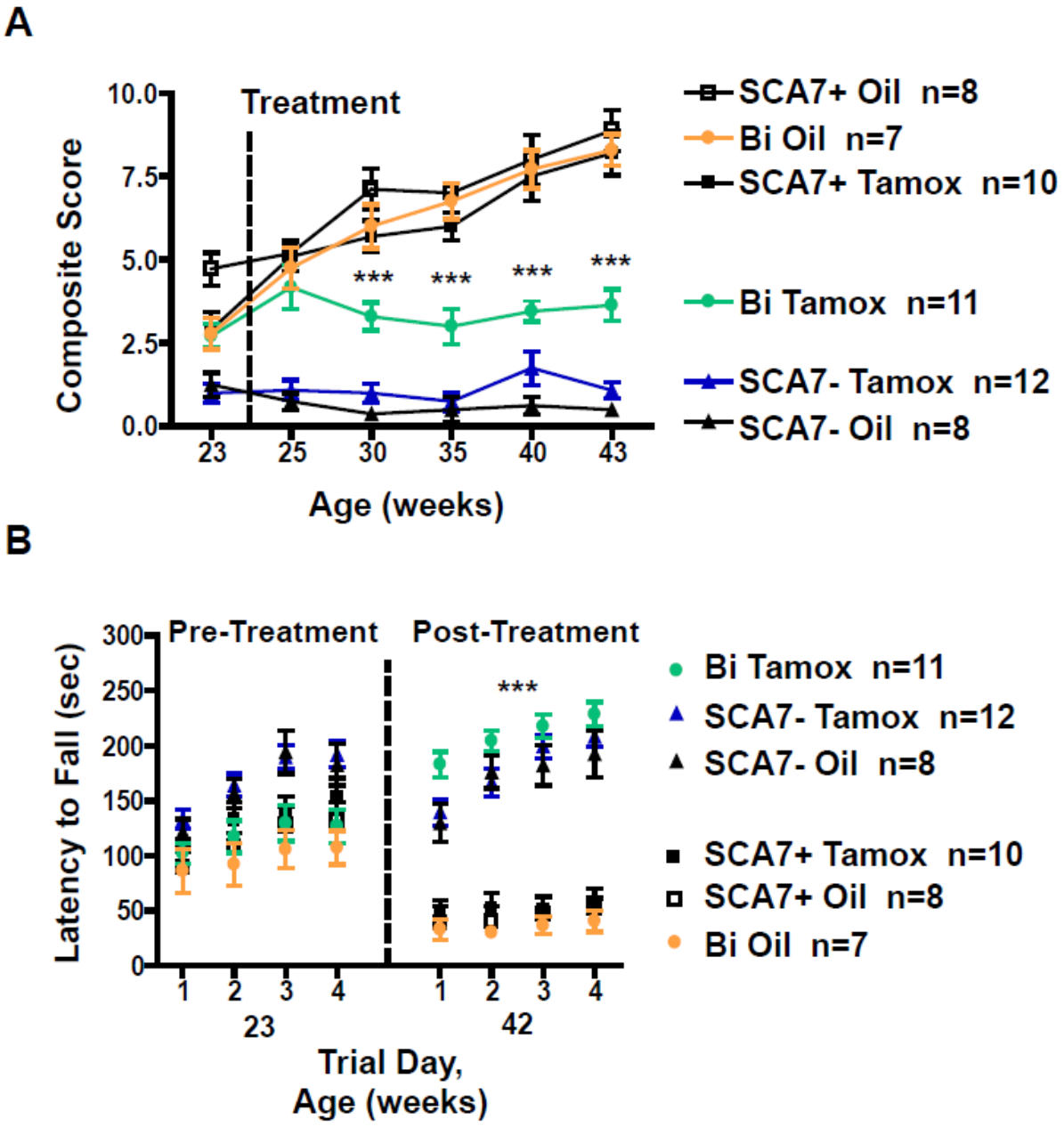

Figure 3.4: Cre-mediated excision of polyQ-ataxin-7 after symptom onset prevents further progression of behavioral symptoms.

A, Composite phenotype score. After tamoxifen (Tamox) treatment at 24 weeks, bigenic (Bi) mice perform significantly better than oil-treated bigenic mice from 30-43 weeks of age (***$p <$ 0.001, two-way ANOVA with Bonferonni's *post hoc* test). **B**, Accelerating rotarod assessment. After treatment with tamoxifen at 24 weeks, bigenic mice perform as well as SCA7-negative mice and significantly better than oil-treated bigenic mice at 42 weeks (***$p < 0.001$, two-way ANOVA with Bonferonni's *post hoc* test). Bars represent SEM.

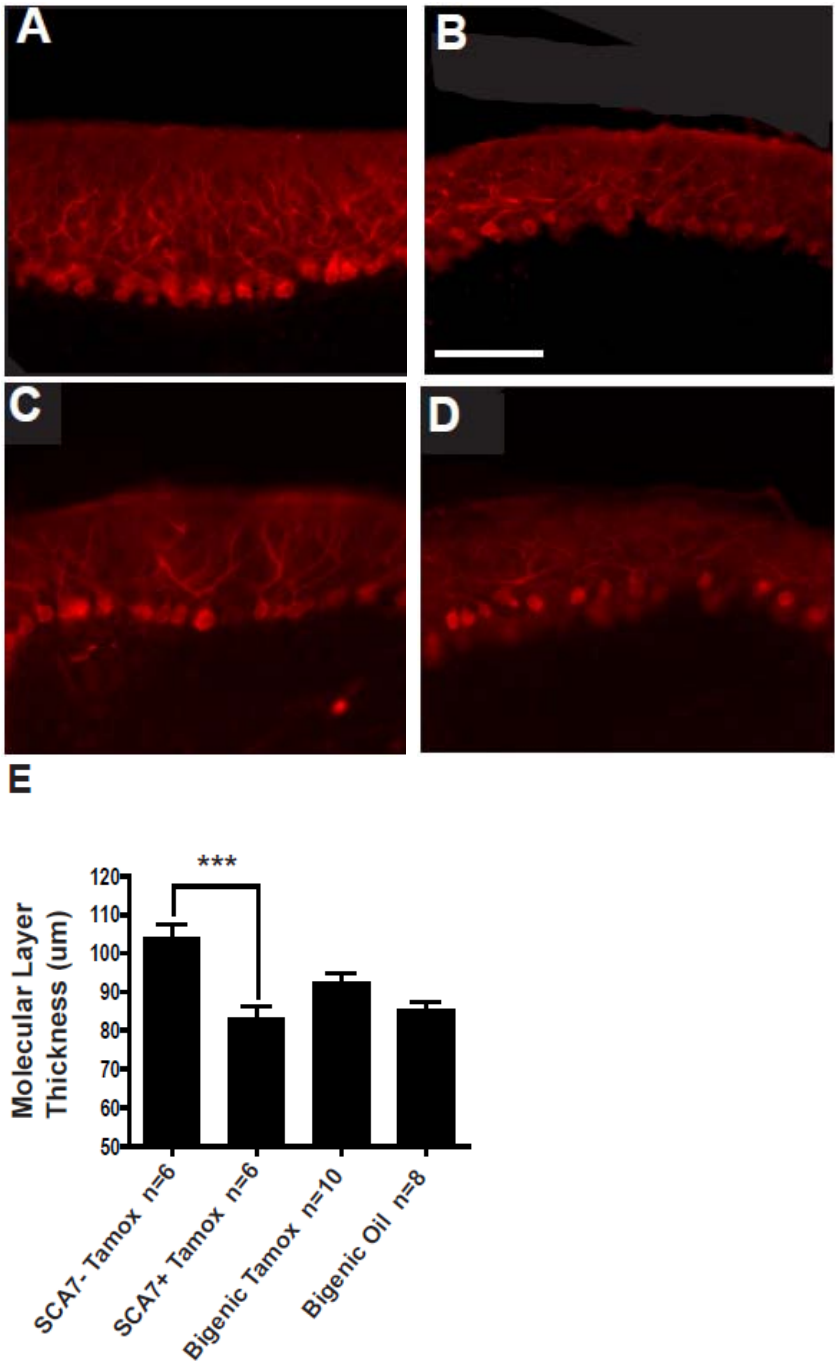

Figure 3.5: Cre-mediated excision of polyQ-ataxin-7 after symptom onset does not reverse cerebellar molecular layer thinning or PC pathology.

A-D, Calbindin immunolabeled sagittal cerebellar sections from 43 week-old animals. SCA7-negative mice treated with tamoxifen at 24 weeks (**A**) have extensive PC dendrite branching while age-matched tamoxifen-treated SCA7-positive mice (**B**) have reduced calbindin

immunoreactivity and a shrunken molecular layer. Tamoxifen-treated (**C**) and oil-treated (**D**) bigenic mice appear to have intermediate morphology. Scale bar, 100 μm. **E**, Quantification of cerebellar molecular layer thickness. Although tamoxifen-treated bigenic mice have a thicker cerebellar molecular layer compared to tamoxifen-treated SCA7-positive mice, this difference is not statistically significant (***$p < 0.001$, one-way ANOVA with Bonferonni's *post hoc* test). Error bars indicate SEM.

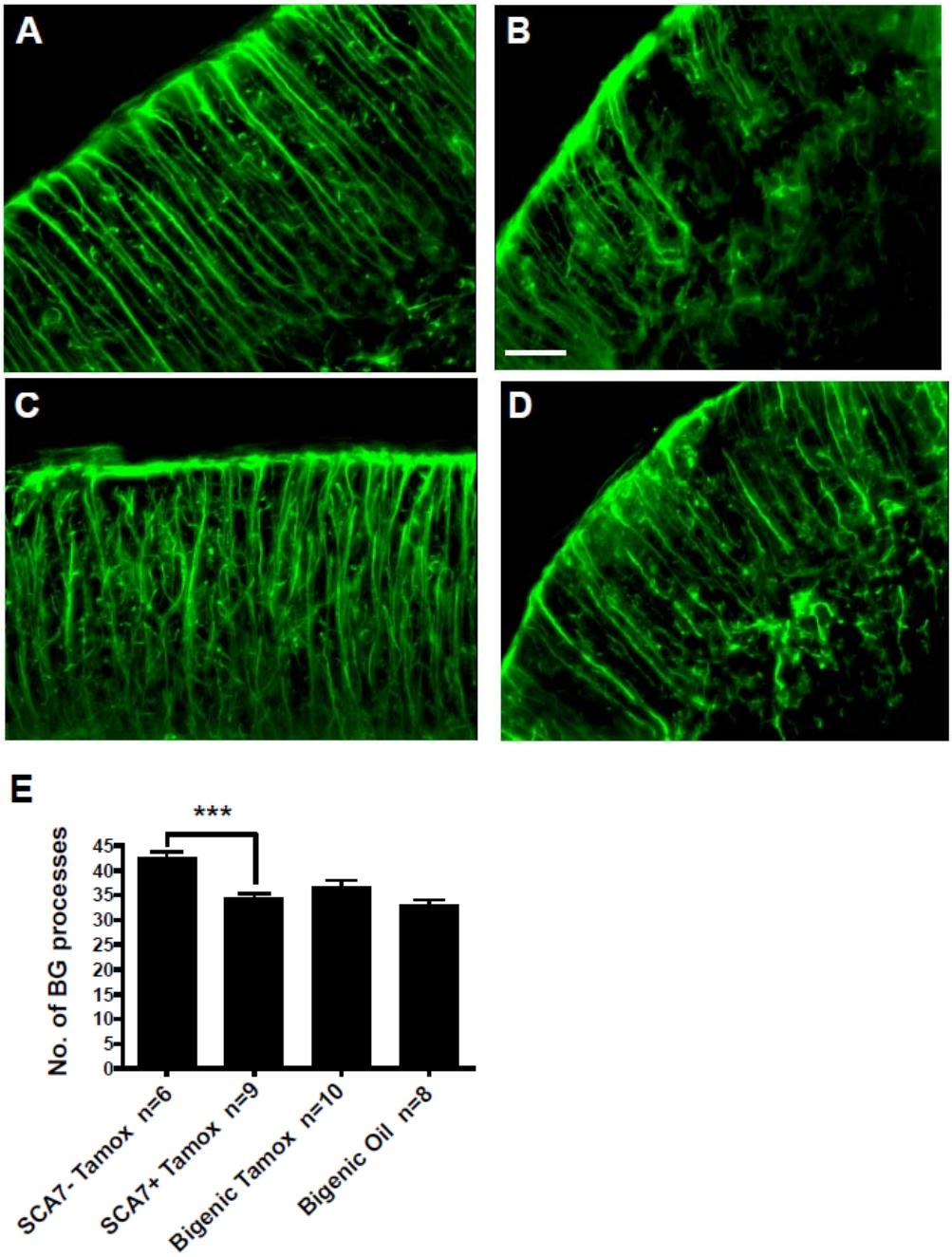

Figure 3.6: Cre-mediated excision of polyQ-ataxin-7 after symptom onset does not prevent loss of BG processes in the cerebellar molecular layer.

A-D, Sagittal cerebellar sections from 43 week-old animals stained for anti-GFAP. Compared to tamoxifen-treated SCA7-negative mice (**A**), tamoxifen-treated SCA7-positive mice (**B**) have fewer, less organized, and more stunted BG processes. BG are pathologic in both tamoxifen-treated (**C**) and oil-treated (**D**) bigenic mice. Scale bar, 25 μm. **E**, Quantification of BG process number. Tamoxifen-treated bigenic mice are not significantly different from tamoxifen-treated SCA7-positive mice or oil-treated bigenic mice (***$p < 0.001$, one-way ANOVA with Bonferonni's *post hoc* test). Error bars indicate SEM.

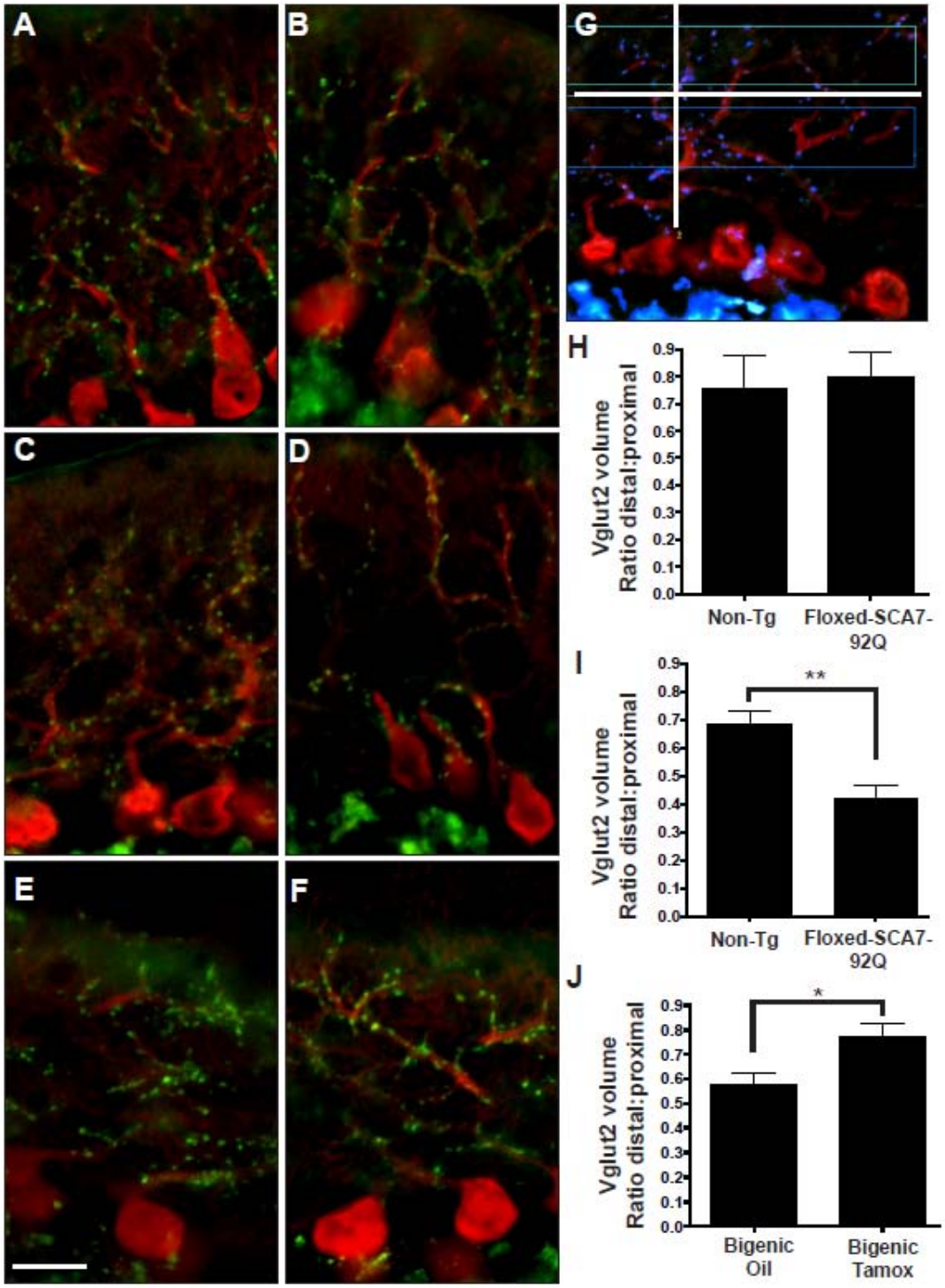

Figure 3.7: Redistribution of climbing fiber-Purkinje cell synapses in *PrP-floxed-SCA7-92Q BAC* mice is ameliorated after Cre-mediated polyQ-ataxin-7 gene excision.

A-F, Sagittal cerebellar sections stained for anti-calbindin (red) and anti-vesicular glutamate transporter 2 (VGLUT2; green), a marker of CF-PC synapses. VGLUT2-positive puncta are evenly distributed throughout the cerebellar molecular layer in non-transgenic (**A**) and *PrP-*

floxed-SCA7-92Q BAC (**B**) mice at 20 weeks of age and in 40 week-old non-transgenic mice (**C**). In 40 week-old *PrP-floxed-SCA7-92Q BAC* mice (**D**), the VGLUT2 immunolabeled CF-PC synapses appear to aggregate in the molecular layer proximal to the PC bodies and are no longer evenly distributed. 43 week-old oil-treated bigenic mice (**E**) and tamoxifen-treated bigenic mice (**F**) appear to have an intermediate phenotype. Scale bar, 20 μm. **G**, Quantification of the volume of VGLUT2 immunolabeling in the cerebellar molecular layer. For each 3-D image, a line was drawn from the PC layer to the pial surface (white line). A second line (white line) was drawn perpendicular to the first line at the midpoint of the molecular layer in order to assign one area proximal to, and one area distal to, the PC layer. A mask was generated (blue) and the volume of total VGLUT2 immunolabeled synapses was calculated using Slidebook 5.0 for the distal and proximal regions (colored boxes). **H-J**, Results of the quantification reported as the ratio of VGLUT2 immunolabeled volume in the region distal to the PC layer to the region proximal to the PC layer. **H**, At 20 weeks of age, the distribution of VGLUT2-positive CF-PC synapses in the molecular layer is even and similar in non-transgenic (Non-Tg) and *PrP-floxed-SCA7-92Q* (Floxed-SCA7-92Q) mice (n = 6-7/group). **I**, At 40 weeks, the distribution of CF-PC synapses has been significantly altered such that more are found proximal to the PCs than distal in *PrP-floxed-SCA7-92Q BAC* mice compared with non-transgenic mice (n = 6/group; $^{**}p < 0.01$, unpaired, two-tailed t-test). **J**, Tamoxifen-treated bigenic mice, however, have a significantly improved distribution of VGLUT2 immunolabeled CF-PC synapses compared to oil-treated bigenic mice (n = 6/group; $^{*}p < 0.05$, unpaired, two-tailed t-test). Error bars indicate SEM.

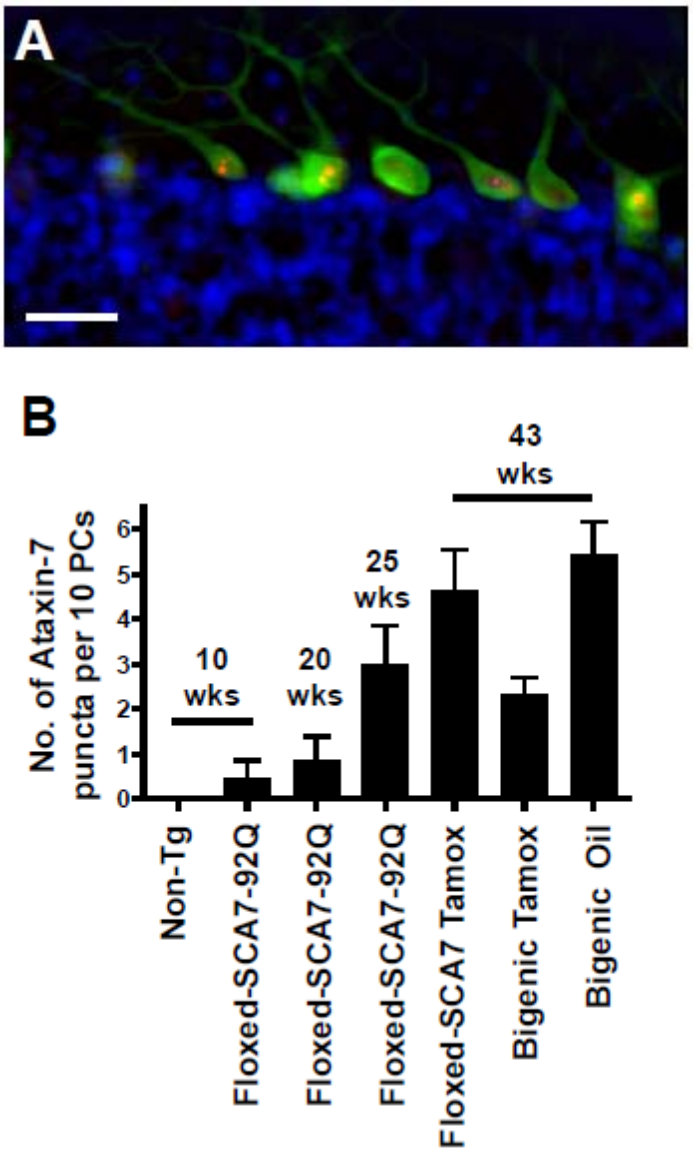

Figure 3.8: Accumulation of ataxin-7-positive puncta in PC nuclei is progressive except after Cre-mediated polyQ-ataxin-7 gene excision.

A, Sagittal cerebellar section from a 43 week-old mouse immunolabeled for anti-ataxin-7 (red), anti-calbindin (green), and DAPI (blue). Scale bar, 25 μm. **B**, Quantification of the number of ataxin-7-positive nuclear inclusions in PCs divided by the total number of PCs observed. *PrP-floxed-SCA7-92Q BAC* mice accumulate ataxin-7 aggregates from 10 weeks until 43 weeks, when approximately 50% of PCs have aggregates. Only about 25% of PCs in 43 week-old tamoxifen-treated bigenic animals, however, have ataxin-7 nuclear aggregates (n = 3/group at 10, 20, and 25 weeks; n = 5 *PrP-Floxed-SCA7-92Q BAC* animals and n = 8 tamoxifen- or oil-treated bigenic animals at 43 weeks). Error bars indicate SEM.

Discussion

An important question in therapy development for neurodegenerative disease is the optimal stage at which a therapeutic intervention should be offered. For rare diseases such as SCA7, determining the extent of reversibility for neurological phenotypes and neuronal dysfunction is especially crucial, as opportunities for performing clinical trials will be limited by the small size of affected patient populations. With these issues in mind, we developed an inducible mouse model for SCA7, based upon our *PrP-floxed-SCA7-92Q BAC* transgenic model that features a floxed human ataxin-7 cDNA carrying 92 CAG repeats, inserted at the first coding exon of the PrP gene contained within a BAC (Furrer et al., 2011). Unlike earlier polyQ disease inducible/conditional models (Yamamoto et al., 2000; Zu et al., 2004), these SCA7 transgenic mice express mutant ataxin-7 protein in neurons, glia, and other cell types in the CNS, thereby allowing for an evaluation of the effect of expression termination upon a network of interconnected neurons and glia. Using this model, we have previously shown that excising polyQ-ataxin-7 from PCs, BG, and IO neurons delays neurological disease onset by 20 weeks, extending the age of onset by a factor of two (Furrer et al., 2011). In the present study, we crossed the *PrP-floxed-SCA7-92Q BAC* transgenic mice with a *CAGG-Cre-ER^{TM}* line (Hayashi and McMahon, 2002), and then achieved effective termination of polyQ-ataxin-7 expression in bigenic mice by oral administration of tamoxifen at 24 weeks of age, which is roughly a month after the onset of visible neurological abnormalities and detectable motor incoordination. By comparing *PrP-floxed-SCA7-92Q BAC;CAGG-Cre-ER^{TM}* bigenic mice treated with tamoxifen versus vehicle, and including singly transgenic *PrP-floxed-SCA7-92Q BAC* mice as well as non-SCA7 control mice, we were able to assess the effect of excising the polyQ-ataxin-7 transgene on a range of neurological, histological, and neurodegenerative phenotypes. Our findings

indicate that disease gene excision improves motor incoordination and PC morphology, maintains normal CF-PC synapses, and restores PC proteostasis, but that other aspects of SCA7 neuropathology do not respond to cessation of mutant ataxin-7 protein expression.

Motor incoordination is a hallmark feature of SCA7 and related cerebellar degenerations, and stems from dysfunction of neuronal pathways involving cerebellar granule cells, PCs, and brainstem neurons in the IO. This circuitry has been extensively studied, and lesions of PCs are sufficient to produce profound ataxia in mouse models (Chakrabarti et al., 2010), confirming the importance of PC afferent and efferent pathways in coordinated movement. In this study, we waited until SCA7 mice exhibited significant impairment in motor coordination before oral administration of tamoxifen to terminate polyQ-ataxin-7 expression. We found that bigenic mice receiving tamoxifen performed comparably to non-SCA7 controls on the accelerating rotarod. This recovery of motor function occurred despite an apparent persistence of neuropathological findings typically considered to be indicative of cerebellar dysfunction, including thinning of the cerebellar molecular layer and BG process loss. Although molecular thickness and BG process number in bigenic mice undergoing polyQ-ataxin-7 expression termination were comparable to vehicle-treated bigenic mice and to singly transgenic SCA7 mice, careful examination of these measurements does reveal a trend toward improvement, though this trend did not achieve statistical significance (Fig. 3.5 and 3.6). Nonetheless, the extent of cerebellar histopathology in bigenic mice subjected to tamoxifen-mediated termination of expression was significant. These findings underscore that pathology does not always equate with disease, and that additional measures of neural function are required to fully evaluate the status of the cerebellar network.

Several mouse models of SCA7 manifest symptoms and histopathological findings at different time points during pathogenesis. Ataxin-7-90Q expressed only in PCs leads to a

rotarod deficiency at 11 months of age but no overt ataxic phenotype up to one year (Yvert et al., 2000). In this model, PCs have a shrunken dendritic arbor and one large NI in almost all PCs at 16 months. Ubiquitous expression of ataxin-7-128Q under the direction of the platelet derived growth factor beta chain (PDGF-β) promoter causes visible motor abnormalities at 5 months of age while nuclear ataxin-7 staining is clearly observed by 3 months (Yvert et al., 2001). Another group expressed ataxin-7-52Q using the same promoter and observed a rotarod deficiency by 9 months of age and gross motor abnormalities at 10-11 months. Neurological symptom onset was concurrent with the onset of PC dendrite degeneration, formation of nuclear inclusions in PCs, and detection of a decreased number of neurons in the IO (Chou et al., 2010; Wang et al., 2010). When ataxin-7 with 266 CAG repeats was knocked into the murine *SCA7* locus (Yoo et al., 2003) mice developed ataxia, weight loss, muscle wasting and severe motor dysfunction by 5 weeks of age but NIs did not form until 10-12 weeks of age. Our group previously generated an SCA7 mouse model by expressing ataxin-7-92Q under the direction of a fragment of the murine prion protein promoter (Garden et al., 2002). This mouse developed detectable motor dysfunction by rotarod by 8 weeks of age and exhibited visible ataxia by 13 weeks, even though the mutant protein was not expressed in PCs. Neuronal NIs in the cerebellar granular and molecular layers were first apparent at 8 weeks, coincident with rotarod deficits. Our group also used the human glial fibrillary acidic protein promoter to drive expression of ataxin-7-92Q solely in BG in the cerebellum (Custer et al., 2006). Rotarod deficiencies at 12 months were followed by abnormal gait at 16 months. Before rotarod performance was significantly impacted, PC dendrites were reduced and BG had swollen, disoriented, and stunted radial fibers by 9 months. BG also expressed significantly less GLAST RNA and protein, leading to aberrant glutamatergic signaling. In the most recent mouse model generated by our group, polyQ-ataxin-7 is expressed

ubiquitously, including in PCs. The mice develop an ataxic phenotype by 20 weeks of age, coincident with significant thinning of the cerebellar molecular layer and degeneration of PC dendrites (Furrer et al., 2011; Fig. 3.2), but significant BG process loss and aberrant redistribution of CF terminals labeled with VGLUT2 occur later than this time point (Fig. 3.2 & 3.7). Ataxin-7 NIs begin to form as early as 10 weeks of age and accumulate over time (Fig. 3.8). In the future, changes in cerebellar circuitry and function will be a more informative readout of cellular changes that correlate with, or directly cause, motor incoordination.

In the current study, we demonstrate that end stage *PrP-floxed-SCA7-92Q BAC* mice have an abnormal distribution of CF-PC synapses. The distribution of CF-PC synapses is normal in SCA7 mice at 20 weeks of age, and inducible Cre recombinase-mediated excision of the ataxin-7-92Q cDNA at 24 weeks of age prevented the development of aberrant CF-PC synapse distribution in 43 week-old SCA7 mice (Fig. 3.7). CF-PC synapse dislocation occurs after molecular layer thinning and onset of behavioral symptoms, yet the preservation of the CF-PC circuitry in SCA7 animals with polyQ-ataxin-7 expression eliminated after symptom onset correlates with improved motor behavior (Fig. 3.4 and 3.7). This suggests that PC function is maintained despite the presence of significant PC and BG pathology. SCA1 is a related neurodegenerative disorder characterized by PC and IO degeneration (Ingram et al., 2011). In a transgenic SCA1 mouse model, PCs displayed a reduced responsiveness to excitatory stimulation from CFs at 6 weeks of age, the age at which rotarod deficits are first detectable (Clark et al., 1997). Additionally, when disease gene expression was initiated after cerebellar development was complete (5 weeks), CF-PC synaptic inputs were preserved (Barnes et al., 2011). These findings suggest that very early changes in CF-PC synaptic function can contribute to motor deficits. The CF-PC synapse findings in this SCA1 model raise two interesting issues. First, it is

possible that functional abnormalities in CF-PC synapses in SCA7 may develop prior to anatomic abnormalities, but that anatomic methods of detection are not sufficiently sensitive to identify the reversible component of this finding. Second, in SCA1 mice, changes in CF-PC synapses are secondary to changes in PCs because this model specifically expresses the disease gene only in PCs (Barnes et al., 2011). It is possible that preservation of the CF-PC synapse distribution in the cerebellar molecular layer upon termination of mutant gene expression in our SCA7 mouse model likely indicates a preservation of normal CF-PC synaptic connectivity and function.

In addition to improved motor function and maintenance of CF – PC synapses, termination of polyQ-ataxin-7 protein expression also prevented further formation of polyQ-containing nuclear aggregates in PCs. Indeed, tamoxifen-treated bigenic mice, sacrificed at 43 weeks, exhibited roughly the same percentage of PCs with ataxin-7 aggregates as 25 week-old *PrP-floxed-SCA7-92Q BAC* mice. Because the bigenic mice received tamoxifen at 24 weeks of age, this indicates that termination of polyQ-ataxin-7 expression prevented further ataxin-7 nuclear aggregate formation. The impact of disease gene excision on aggregate formation mirrors the effect of disease gene expression termination on motor behavior in this cohort of mice. Perhaps PCs spared from forming nuclear aggregates are more capable of effectively maintaining physiological function despite minor retraction of their dendritic arbors. As proteotoxic stress imposes a heavy burden on energy utilization (Tsunemi et al., 2012), termination of expression of misfolded polyQ-expanded ataxin-7 likely permits PCs to achieve a more favorable bioenergetics profile, consistent with their ability to better support synaptic activity and behavioral function. Therefore, nuclear aggregates may serve as a surrogate marker for cellular stress, and likely correlate with high levels of toxic oligomers and protofibrils that are

present in the cell (Poirier et al., 2002; Wacker et al., 2004). Hence, their continued presence in PCs would be expected to prevent proper neural function. Persistence of protein aggregates in a fraction of PCs in bigenic mice subjected to polyQ-ataxin-7 expression termination may account for the observed lack of complete reversal of molecular layer thickness defects and non-cell autonomous BG degeneration. Failure to eliminate ataxin-7 protein aggregates in this study also differs from prior investigations of polyQ disease reversibility in HD and SCA1, where termination of disease gene expression allowed for the eventual removal of polyQ-containing protein aggregates in these models (Yamamoto et al., 2000; Zu et al., 2004). One prior study of mice expressing ataxin-7-90Q under rhodopsin promoter control revealed that the proportion of rods in the retina with ataxin-7-positive nuclear aggregates declined from >95% at 26 weeks to ~50% by one year of age. However, the rods never completely cleared the nuclear aggregates even at 2 years of age, despite the fact that polyQ-ataxin-7 expression became negligible at 9 weeks of age in this model (Helmlinger et al., 2004a). These findings suggest that aggregates containing mutant ataxin-7, unlike polyQ-expanded huntingtin and ataxin-1, are not easily cleared from cells, even when expression of the mutant gene is inactivated. As the aggregate itself is no longer believed to be the toxic species, further studies geared towards detection of polyQ-ataxin-7 oligomers and other toxic conformers will be required to assess the true extent of proteotoxic stress in such situations.

Interestingly, significant BG process loss was not detectable in *PrP-floxed-SCA7-92Q BAC* mice until after 25 weeks of age, but polyQ-ataxin-7 gene excision at 24 weeks of age did not protect against BG degeneration (Fig. 3.2, D-G & 3.6). In contrast, cerebellar molecular layer thickness appeared improved in tamoxifen-treated bigenic mice at end stage although the molecular layer is significantly thinned four weeks prior to tamoxifen treatment (Fig. 3.2, C &

3.5). One possible explanation for this finding is that BG are more sensitive than PCs to the cumulative effects of polyQ-ataxin-7 expression during their first 24 weeks. After ataxin-7-92Q is excised, PCs may be able to recover some function while BG cannot and instead continue to degenerate. A second possible explanation is that PC pathology at 20 weeks may negatively impact BG in an irreversible manner. We have previously shown that BG undergo non-cell autonomous degeneration in *PrP-floxed-SCA7-92Q BAC* mice as cell type-specific removal of polyQ-ataxin-7 from PCs and neurons of the IO protected mutant protein-expressing BG from degeneration (Furrer et al., 2011). In the current study, we show that BG process loss is detectable well after PCs begin to degenerate. Additionally, BG degeneration is not prevented when the polyQ-ataxin-7 gene is removed before signs of morphological alteration become apparent. It is possible that early PC damage promotes active BG degeneration that cannot be reversed by cessation of mutant ataxin-7 gene expression.

In this study we demonstrate that suppressing polyQ-ataxin-7 gene expression even after the onset of cerebellar degeneration arrests progressive loss of motor function. Patients with neurodegenerative diseases are often diagnosed after symptoms begin. The prospect of preventing the worsening of symptoms after diagnosis would be of immeasurable benefit to patients and their caregivers. Gene silencing strategies are actively being pursued in the polyQ disease field (Scholefield and Wood, 2010). Current research is directed towards developing sequence-specific nucleic acid based technologies such as RNA interference in order to knock down polyQ-expanded gene expression. Understanding how disease protein termination therapies impact disease progression in model systems may yield a more representative picture of expected outcomes in human patients, who, for a growing subset of neurodegenerative disorders, are currently being recruited to receive experimental RNA interference or antisense

oligonucleotide gene knock-down therapies. Our results confirm that development of these therapeutic approaches for SCA7 patients may prevent progressive loss of motor function and improve quality of life.

Materials and Methods

Animals

Mice were bred and housed in the Department of Comparative Medicine facilities at the University of Washington Seattle. Up to five mice were housed per cage with food and water available *ad libitum*. Mice were maintained in a temperature- and humidity-controlled environment on a 12 hr light/dark cycle with light onset at 6:00 AM. All studies and procedures were approved by an Institutional Animal Care and Use Committee at the University of Washington or the University of California, San Diego.

Bigenic mice (*PrP-floxed-SCA7-92Q BAC;CAGG-Cre-ER^{TM}*) were generated by breeding either a single *PrP-floxed-SCA7-92Q BAC* or *CAGG-Cre-ER^{TM}* male with two *PrP-floxed-SCA7-92Q BAC* or *CAGG-Cre-ER^{TM}* females in a single cage. Non-transgenic, *PrP-floxed-SCA7-92Q BAC*, *CAGG-Cre-ER^{TM}*, and bigenic littermates were orally administered either a single 20 mg dose (80 mg/mL in 0.25 mL) of tamoxifen citrate dissolved in corn oil or corn oil alone at 24 weeks of age. Mice dosed with tamoxifen were housed separately from those dosed with corn oil.

Behavioral Phenotyping

Females and males were used in all studies. The composite phenotype score and accelerating rotarod assessments were performed exactly as previously described (Furrer et al., 2011). An examiner blinded to genotype performed all behavioral measurements.

PCR genotyping

Mice tissue was harvested and processed as previously described (Furrer et al., 2011). PCR conditions included 60ºC annealing temperature, 38 cycles, and 1 min extension period. Primer sequences are listed in Table 3.

Table 3: Primer sequences for PCR genotyping.

Transgene		Primer Sequence	Product (bp)
PrP-floxed-SCA7-92Q BAC	Forward	CATTTTAGGCCCCACGTATCAC	587
	Reverse	GGCCCGCTCCGACAT	
CAGG-Cre-ER^{TM}	Forward	CAAAATTTGCCTGCATTACCG	553
	Reverse	CATTCTCCCACCGTCAGTACG	

Quantitative RT-PCR analysis

Total RNA was isolated from the cerebellum of mice using an RNeasy isolation kit (Qiagen). Total RNA was reverse transcribed using SuperScriptII Reverse Transcriptase according to manufacturer's instructions (Invitrogen). The cDNA's were subjected to real-time PCR using custom ataxin-7 primers and probe selected with the Primer3 (version 4.0) primer design program (Rosen and Skaletsky, 1998), as follows: forward primer, GATCAGCAGACCGATTCTGG; reverse primer, TAATCGCCGTCATGGTCTTT; probe, AGCATTCTGCCTTCCTAGTGG. Samples were analyzed on a StepOnePlus Real-Time PCR system and normalized to mouse 18S RNA using Applied Biosystems assay Hs99999901_s1. Primers were designed such that amplification of the sequence could only take place when the human ataxin-7 cDNA was successfully excised. Average 'excision product' mRNA level in cerebella from tamoxifen-treated *PrP-floxed-SCA7-92Q BAC*, tamoxifen-treated bigenic, and oil-

treated bigenic mice (n = 3/group) was calculated using Microsoft Excel.

Immunohistochemistry

Deeply anesthetized mice were transcardially perfused with phosphate buffered saline (PBS) followed by 4.0% paraformaldehyde (PFA) in 0.1M phosphate buffer (PB), pH 7.4. Brains were removed and post-fixed in 4.0% PFA in 0.1M PB overnight, then moved into 0.4% PFA in 0.1M PB for storage at 4ºC. Free-floating 40 µm sagittal brain sections were cut on the Leica Vibratome 1000S and stored in 0.03% PFA in PBS. Free-floating sections were immunostained as previously described (Furrer et al., 2011), except for VGLUT2 immunostaining. Primary antibodies used were anti-calbindin antibody (#300, Swant) at 1:1,000 dilution; anti-GFAP antibody (Z0334, DAKO) at 1:1,000 dilution; or anti-ataxin-7 antibody (PA1-749, Affinity Bioreagents) at 1:500 dilution. For VGLUT2 immunostaining, floating sections were incubated in 0.1M urea at 85ºC for 30 mins, followed by cooling to room temperature for 30 mins. After a 5 min incubation with 1X PBS, sections were blocked overnight in 5% normal goat serum (NGS), 1.0% Triton X-100, and 0.2% bovine serum albumin (BSA) at 4ºC with shaking. Sections were then incubated with anti-VGLUT2 primary antibody (MAB5504, Millipore) at 1:500 dilution in antibody buffer (5% NGS, 0.3% Triton X-100, and 0.2% BSA) at 4ºC with shaking overnight. After sections were washed in 1X PBS for 10 mins 3 times, they were incubated with secondary antibody in antibody buffer without BSA at 4ºC with shaking overnight. After 3 x 10-min washes in 1X PBS, the sections were blocked overnight a second time before adding a second primary antibody (anti-calbindin, Swant) in antibody buffer and incubating overnight at 4ºC with shaking. After 3 x 10-min 1X PBS washes, sections were incubated with a second secondary antibody in antibody buffer without BSA overnight at 4ºC

with shaking. Finally, sections were briefly washed in 1X PBS and mounted on glass slides and allowed to dry. Fluro-Gel with Tris Buffer mounting media (Electron Microscopy Sciences) was added to the sections before coverslips were applied. For all immunostaining, the secondary antibodies used were AlexaFluor 488 anti-rabbit or anti-mouse IgG (Molecular Probes, Invitrogen) at 1:500 dilution, and/or AlexaFluor 594 anti-rabbit or anti-mouse IgG (Molecular Probes, Invitrogen) at 1:500 dilution. DAPI was used at a final concentration of 1:10,000. A Zeiss Axiovert 200M inverted microscope and Slidebook 5.0 software (Intelligent Imaging Innovations) was used to capture, process, and analyze images of stained sections.

Cerebellar molecular layer thickness was quantified as previously described (Furrer et al., 2011). Briefly, 2-D images of calbindin immunostained sections were collected. The three most dorsal cerebellar folia per section, and three sections per individual (n = 6/group) were imaged. Every 100 μm, a measurement was taken from the pial surface to the Purkinje cell layer along a folium by a blinded observer. Molecular layer measurements were averaged for each genotype, plotted, and analyzed statistically in Graphpad Prism 4.0.

Bergmann glia process number was quantified as described previously (Furrer et al., 2011). Briefly, 2-D brightest-point projection images were created from 3-D image z-stacks using Slidebook 5.0. Two areas per section, three sections per individual (n = 6/group) were imaged. The number of Bergmann glia processes crossing a 150 μm line drawn approximately 50 μm from the pial surface was counted by three independent observers. Average number of processes for each genotype was calculated, plotted, and analyzed statistically in Graphpad Prism 4.0.

To quantify the volume of VGLUT2 immunofluorescence, 3-D image z-stacks were

collected from the three most dorsal folia in each section, three sections per animal (n = 6/group). A blinded observer deconvolved the images using the Nearest Neighbors algorithm of Slidebook 5.0 and then rotated the images using bicubic interpolation to position the PC layer parallel to the horizontal axis. A line was drawn from the PC layer to the pial surface. A second line was drawn perpendicular to, and at the midpoint of, the first line to separate the molecular layer into two halves; one 'distal' to the PC layer and one 'proximal' to the PC layer. A segment mask was then generated to encompass VGLUT2 immunofluorescence. A rectangular box measuring 450 by 60 pixels extending through the z-stack was drawn in the distal region, and a second box was drawn in the proximal region. The total volume of VGLUT2 immunofluorescence was calculated within each distal and proximal box and the data was plotted, graphed, and analyzed statistically in Graphpad Prism 4.0.

Ataxin-7 positive nuclear inclusions were quantified using calbindin, ataxin-7, and DAPI triple-labeled cerebellar sections. 2-D images were created of the three most dorsal folia per section, three sections per individual except those collected at 43 weeks (2 dorsal folia/section and 1 section/individual). n = 3 animals/group at 10, 20, and 25 weeks. n = 5 *PrP-Floxed-SCA7-92Q BAC* animals at 43 weeks. n = 8 tamoxifen- or oil-treated bigenic animals at 43 weeks. The number of ataxin-7-positive nuclear inclusions and total number of PC somae was quantified in each image. Average number of ataxin-7 nuclear inclusions/10 PCs was plotted in Graphpad Prism 4.0.

Chapter IV
Discussion & Conclusions

Systems analysis of PCs, IO neurons, and BG

This work has highlighted the importance of PCs, IO neurons, and BG to SCA7 pathogenesis. The next logical step is to fully characterize the interactions between these cell types and how they are specifically altered by mutant ataxin-7 expression. Previous studies have shown that polyQ-expanded ataxin-7 can disrupt transcriptional regulation, leading to aberrant expression of many of genes (Palhan et al., 2005; Helmlinger et al., 2006; Gatchel et al., 2008; Chou et al., 2010). Microarray analysis of whole cerebellum provides a useful start to identifying the molecular mechanisms disrupted in SCA7, but pinpointing the genes that are dysregulated in a specific population of cells would provide more complete understanding of how the system is changing and which specific cell types and processes should be targeted for therapeutic development. Recent developments in systems biology and informatics make it possible to characterize global changes in epigenetic modifications (Guo et al., 2011; Kramer et al., 2011; Agrawal-Singh et al., 2012), expression of coding and non-coding RNAs (Cahoy et al., 2008; Chou et al., 2010; Kang et al., 2011; Sun et al., 2012), and relative concentrations of proteins, modified proteins and metabolites (Hanrieder et al., 2011; Liu et al., 2011; Reitman et al., 2011; Yata et al., 2011; Ipser et al., 2012; James et al., 2012). The ability to specifically profile the transcriptome, proteome, metabolome and epigenetic changes in PCs, IO neurons, and BG will help elucidate patterns of intra- and inter-cellular change associated with SCA7 disease. To accomplish this, each cell type must be successfully isolated from the cerebellum.

PCs have been isolated from mouse cerebellum using fluorescence-activated cell sorting (FACS). Green fluorescent protein (GFP) was highly expressed in PCs using the Pcp2/L7 promoter (Tomomura et al., 2001). Enzymatically dissociated cerebellar tissue from the L7-GFP mice subjected to a cell sorting machine allows the recovery of highly fluorescent PCs. PCs have been isolated and collected using FACS from mice expressing the L7-GFP transgene at ages 6-13 days (Tomomura et al., 2001), 4 weeks (Donald et al., 2008), and 9 months (Chung et al., 2011). Crossing the *PrP-floxed-SCA7-92Q BAC* mice into the L7-GFP transgenic mouse line would allow for the isolation of PCs from SCA7 mice at different ages. Molecular profiles of PCs at pre-, early-, and late-symptomatic time points will shed light into which inter- and intra-cellular pathways in PCs are disrupted during SCA7 pathogenesis. However, limitations of FACS include causing damage to PCs that may activate signaling cascades that would confound profiling data, and the potential for contamination by other cells and debris. Additionally, these experiments rely on the expression of GFP faithfully in every PC and at a level that is distinguishable from background fluorescence. Recently, laser capture microdissection (LCM) has been used to isolate PCs for further analysis (Chen et al., 2010; Euler et al., 2012). Preparation of cerebellar tissue for LCM includes generating and staining cerebellar slices such that PCs can be easily identified. During LCM, each PC body is identified and cut out of the cerebellar slice with a laser. The individual PC samples are then collected for further analysis. LCM can be more time intensive and potentially more expensive than FACS. However, more PCs can be collected with less contamination as the cell bodies are hand-picked from each slice, as opposed to a FACS machine relying on the transgenic expression of a fluorescent marker. LCM could be a better approach to profiling PCs in *PrP-floxed-SCA7-92Q BAC* mice as one

group has already set a precedent for gene expression profiling of singly captured PCs in a mouse model of Huntington's disease (Euler et al., 2012).

Neurons of the IO are, at present, difficult to isolate as they make up a small population within the mouse brainstem and are difficult to distinguish from surrounding tissue without the use of chemical markers. However, the Allen Brain Institute in Seattle, WA, is currently developing several lines of transgenic mice that highly express Cre recombinase in the IO. A93-Cre, Crh-Cre, and Gpr26-Cre are all candidate mouse lines (Travis Baughan, personal communication). Once validated and fully characterized, these promoters can be linked to a fluorescent marker protein, such as GFP, and GFP-expressing transgenic mice can be generated. In the future, perhaps neurons of the IO can be isolated from dissociated brainstem tissue using FACS. In the meantime, it may be more feasible and/or informative to collect mRNA samples from the terminals of the CFs in the cerebellar molecular layer, rather than from the cell bodies in the IO. mRNA translation and protein synthesis are not restricted to the cell body of neurons, but instead can take place in dendrites (Sutton and Schuman, 2006) and in axons (Jung and Holt, 2010). Perhaps gene expression changes at the CF-PC synapse more directly influence the changing dynamics of CF-PC interactions in SCA7 mice than gene expression changes within the cell bodies found in the IO. Possible methods of isolating mRNA at the CF terminal include culturing IO cells or microdissecting regions of the molecular layer from cerebellar slices. It is possible to separate the neurites from cell bodies in culture and collect mRNA solely from isolated neurites for profiling analysis (Miyashiro et al., 1994; Moccia et al., 2003). However, a protocol for culturing IO neurons has not been previously published. Typically, neuronal cell cultures are derived from young animals still undergoing development. If a protocol for IO neuron culture were to be developed, it will be optimal to culture from more mature animals, if

possible, to reduce confounding effects of developmental processes on the mRNA expression profile. Alternatively, brain slices can be generated from animals at any age. LCM (described briefly above) could be used to collect areas of CF-PC synapses in the cerebellar molecular layer. These samples would be processed for mRNA isolation and evaluation with either cDNA microarrays or PCR-based strategies. LCM of cerebellar molecular layer may also include PF-PC synapses, so samples enriched for PF-PC synapses should be collected as a control. mRNA hits identified in PF-PC enriched samples would be excluded in the analysis of CF-PC synapse mRNA expression. Once mRNA expression profiles are obtained from either IO neuron cell bodies or CF terminals from *PrP-floxed-SCA7-92Q BAC* mice at different disease stages, identification of candidate intra- and inter-cellular pathways affected in SCA7 will guide hypothesis-driven experimentation.

Currently there exists no published method to isolate and purify glia from adult rodents more than 10 weeks old, making a systems biology approach to investigate the disease-relevant molecular changes in adult BG in SCA7 impossible. Therefore, we have recently proposed to develop novel protocols for the isolation of adult BG from mouse brain. Recently, Jungblut et al. (2012) generated a novel monoclonal antibody against GLAST that recognizes an extracellular epitope and does not interfere with transporter function or astrocyte viability in culture. This GLAST antibody was conjugated to biotin and used in a multi-step magnetic separation protocol to isolate and purify astrocytes. However, astrocytes in animals older than 10 days were not successfully separated (Jungblut et al., 2012). Past studies have utilized FACS methods to isolate glia from transgenic animals expressing fluorescent markers under the direction of glia-specific promoters in animals younger than 30 days (Malatesta et al., 2000; Belachew et al., 2002; Cahoy et al., 2008; Pinto et al., 2008; Lichter-Konecki et al., 2008). While only animals of

younger ages were employed in these studies, other cell types have been successfully isolated from adult CNS tissue (Frank et al., 2006; Marko et al., 2011), suggesting that with refinement the age limits of earlier studies may be surmountable. Adult tissues are more difficult to employ using the approach in Jungblut et al. (2012) because of increased myelin and more extensive glial processes and intercellular connections. These factors make adult CNS tissue more difficult to dissociate. The resulting cell suspension also has more debris, increasing both specific and non-specific anti-GLAST antibody binding, thus diminishing the efficacy of anti-GLAST separation. We have proposed to optimize the methods in Jungblut et al. (2012) to isolate BG from adult mouse brain as outlined in Figure 4, and as follows:

Step 1: Optimize the enzymatic and mechanical elements of dissociation.

Step 2: Optimize incubation times.

Step 3: Optimize the purification of BG.

Step 1: Optimize the enzymatic and mechanical elements of dissociation.

First, determine the optimum protease(s) and concentration(s) for enzymatic dissociation. Trypsin is a widely used enzyme for the generation of single cell suspensions but causes a large amount of debris to form in tissue collected from older animals. Papain is gentler, causing less debris formation but can disrupt a later separation step using anti-GLAST (ACSA-1) antibodies (Jungblut et al., 2012). However, increased debris in the cell suspension also increases non-specific antibody binding and decreases the efficacy of glial enrichment. Therefore, test optimized concentrations of papain and trypsin both independently and in combination.

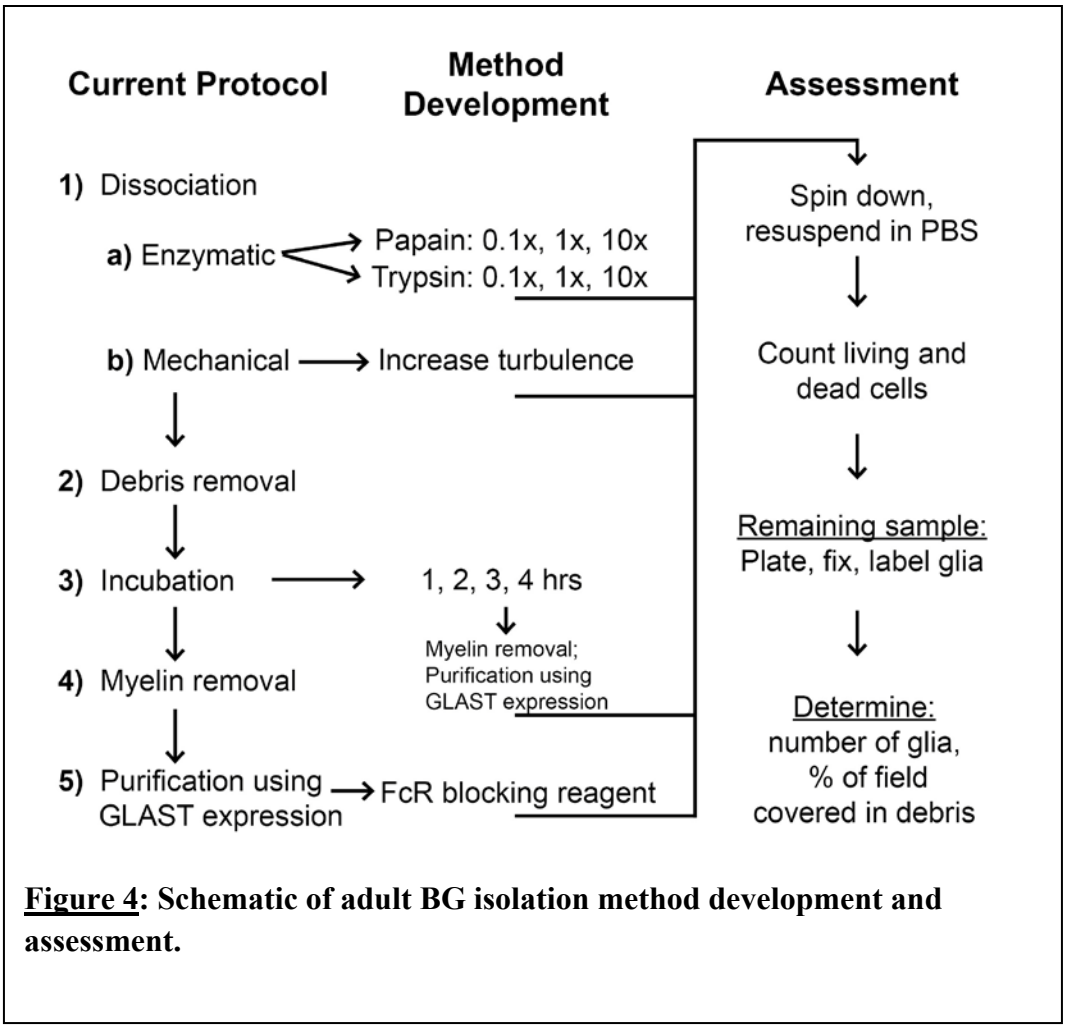

Figure 4: Schematic of adult BG isolation method development and assessment.

The goals of this step are to: 1) increase the number of GLAST-positive BG with intact plasma membrane and 2) reduce cellular debris. To accomplish these goals, use one C57BL/6J (B6) mouse cerebellum per treatment of 0.1x, 1x, and 10x papain or trypsin. Dissociate tissue using MACS® neural tissue dissociation kits and the gentleMACS™ dissociator (Miltenyi Biotech). After dissociation, filter the cell suspensions through a 100 μm nylon filter, resuspend in PBS, and assess for membrane integrity using vital dyes. Plate the samples and use gentle centrifugation to encourage cells and debris to settle at the bottom, fix and label with

fluorescently tagged ACSA-1 antibody and/or additional glial specific marker proteins (e.g., GFAP or glutamate transporter 1 (GLT-1)). Use a fluorescent microscope to determine the number of GLAST-positive BG with membrane integrity intact and the percentage of total space taken up by cellular debris. In the next phase of protocol development, use the concentrations of papain and/or trypsin that produce the greatest number of viable BG and the least amount of debris to optimize the mechanical phase of dissociation using the Miltenyi gentleMACS™ dissociator (Miltenyi Biotech). Place one adult B6 cerebellum into each tube with buffer containing optimum papain or trypsin concentration. Insert the tubes into the dissociator, which can perform physical dissociation of varying intensity. We have successfully isolated and collected cerebellar BG but with low yield (approximately 65,000 BG out of a theoretical 6 million, or ~1%). One possible explanation for the low yield is that older animals have well-established synaptic contacts and complex intercellular connections; thus, dissociator programs developed for neonatal neural tissue do not adequately separate these cells. Because a debris removal step based on size exclusion follows dissociation, large clumps of cells and/or cells with long processes may be excluded from isolation. Therefore, assess dissociator programs with increasing force using pre-programmed protocols (Miltenyi Biotech). Analyze the cell suspensions as described above and quantify the number of dead and membrane-intact BG and the percentage of debris. Use the mechanical dissociation steps that yield the most BG and the least debris next in step 2.

Step 2: Optimize incubation times.

Papain can degrade the GLAST epitope, making use of anti-GLAST (ACSA-1) antibodies less effective during the separation step (Jungblut et al., 2012). However, it is possible to reconstitute surface GLAST expression by incubating the cell suspension at 37ºC

after the dissociation step (M. Jungblut, personal communication). To test this, use the optimized concentration of papain and/or trypsin and their respective most effective gentleMACS™ dissociator program to generate single cell suspensions from adult B6 cerebellum. Following debris removal with a 100 μm filter, incubate the cell suspensions at 37ºC with rotation in serum-free media with L-glutamine and heparin-binding epidermal growth factor (Foo et al., 2011) at 1, 2, 3, or 4 hours. Because this incubation step is expected to improve the ability of anti-GLAST (ACSA-1) antibodies to recognize the epitope and successfully separate BG from other cell types, follow the remainder of the protocol before analyzing each sample for number of BG and amount of debris (Fig. 4). Use the optimized incubation time when carrying out step 3.

Step 3: Optimize the purification of BG.

The goal of this step is to maximize binding of biotinylated-anti-GLAST (ACSA-1) antibodies (Jungblut et al., 2012). One possibility limiting the yield of GLAST-based glial enrichment is that cellular debris non-specifically binds ACSA-1 and will decrease the availability for specific binding to BG. We hypothesize that Fc receptor (FcR) block will decrease non-specific binding and therefore increase the number of adult glia selected using this method. Dissociate adult B6 cerebellum tissue using the protocol as optimized above and incubate the resulting cell suspension either with or without FcR blocking reagent (Miltenyi Biotech). If FcR blocking reagent increases yield of isolated BG, then this step will become integrated into the protocol.

In the event that two different protocols consistently yield similar positive results (e.g., 0.1x papain and 1x papain), both should be taken forward until one becomes less effective and

then discarded. If optimization of this protocol does not result in greater yield of BG, then different components of dissociation buffers and incubation media that may increase viability of adult glia during the procedure shall be tested. In addition, it is possible that alternate glial specific epitopes may be preferable to the one recognized by ACSA-1 antibody. If the efforts described above improve viability, but do not improve yield, we can work with our collaborators at Miltenyi Biotech to develop alternate biotin conjugated antibodies that can be employed for magnetic separation of BG.

Once BG can be successfully isolated from adult mouse brain, systems analysis can be utilized to characterize molecular changes in BG over the course of disease in *PrP-floxed-SCA7-92Q BAC* mice. Recall in this mouse model of SCA7 that BG do not significantly retract their processes until after 25 weeks of age (Chapter III, Fig. 3.2). However, global excision of the mutant ataxin-7 transgene at 24 weeks does not prevent loss of BG processes at end stage (Chapter III, Fig. 3.6). We hypothesize that irreversible damage occurs prior to 24 weeks of age, and analyzing molecular profiles of BG isolated from cerebella of 15, 20, 25, and 30 week-old *PrP-floxed-SCA7-92Q BAC* and non-transgenic mice will shed light into which cellular events lead to this damage. Additionally, these profiling data will add to our understanding of how BG are contributing to the neuron-glia network of the cerebellar molecular layer in health and in a disease state.

Interactions amongst PCs, IO neurons, and BG

PCs, CFs from the IO, and BG make up a tripartite synapse and each cell type influences the others' function and survival in several ways. Some of these interactions, first discussed in Chapter II (Fig. 2.7), are reviewed here.

Mice harboring mutations that lead to PC loss can cause neurons of the IO to degenerate secondarily, but only during a critical period. For example, *lurcher* and *nervous* mice display PC degeneration at post-natal day 8 (P8) and 22 (P22), respectively (Zanjani et al., 2004). Approximately 75% of IO neurons in *lurcher* and 30% in *nervous* are lost as a result. In *leaner* mice, PCs are not lost until after ~ P30 and no IO neurons degenerate (Zanjani et al., 2004). Thus, there is a critical period during which IO neurons must establish contact with their post-synaptic targets, the PCs. After this critical period, it appears that loss of PCs does not cause degeneration of the IO (Zanjani et al., 2004). In SCA7, it is more likely that neurons of the IO undergo cell autonomous degeneration. One group demonstrated that ataxin-7-52Q expression leads to an increase in active (phosphorylated) p53, which increases the transcription of the pro-apoptotic genes Bax and Puma and leads to cell loss within the IO (Wang et al., 2010). Quantifying the number of calbindin labeled IO neurons in *PrP-floxed-SCA7-92Q BAC* mice at various stages of SCA7 disease would help delineate whether IO neuron loss occurs before, during, or after symptom onset and thinning of the cerebellar molecular layer. The CF terminals at CF-PC synapses appear to be normally distributed throughout the molecular layer at 20 weeks, the age of symptom onset (Chapter III, Fig. 3.7), but IO loss may still occur before this time as there is evidence that surviving CFs may re-innervate PCs after IO lesion (Fernandez et al., 1999).

The mechanism by which PC degeneration influences BG morphology remains unexplained. One possible mediator of this process is the Delta/Notch-like EGF-related receptor (DNER). During cerebellar development, PC dendrites express DNER, which is a ligand for the Notch receptor found on BG (Eiraku et al., 2005). DNER acts to signal the differentiation of BG via a noncanonical Deltex-dependent Notch signaling pathway. This signaling cascade may still be active in the adult cerebellum to maintain the juxtaposition of BG processes to PC synapses. A second potential mechanism of signaling involved in PC-BG neuron-glia interaction is mediated by glutamate transport and signaling. Excitatory amino acid transporter 4 (EAAT4) is expressed solely by PCs in the cerebellum (Slemmer et al., 2005). The expression levels of EAAT4 alter the glutamate concentration profile within the synapse to regulate the degree to which BG are activated via AMPA receptors (Tsai et al., 2012). Additionally, glutamate receptor signaling in BG plays a role in regulating protein synthesis at the elongation phase (Barrera et al., 2010). Further investigation is required to characterize other methods by which BG and PCs maintain contact.

Chemical ablation of the IO in *shaker* mice accelerates the loss of PCs in this mouse model of PC neurodegeneration, suggesting CFs provide trophic support to PCs that becomes lost (Tolbert and Clark, 2000). In fact, the IO has been shown to deliver IGF-1 to the molecular layer of the cerebellum (Nieto-Bona et al., 1993). PCs express IGF-1 receptor (Garcia-Segura et al., 1997) and respond to IGF-1 (Nieto-Bona et al., 1995). Exogenous IGF-1 promotes PC survival, recovery of motor behavior, and re-innervation of surviving CFs onto PCs after IO ablation (Fernandez et al., 1999). We hypothesize that IO degeneration in SCA7 leads to a decrease in IGF-1 signal, exacerbating the non-cell autonomous and cell autonomous damage wrought on PCs (Chapter II, Discussion). It is possible exogenous delivery of IGF-1 to the

cerebellum of *PrP-floxed-SCA7-92Q BAC* mice may prove an efficacious treatment. As discussed above (Chapter II, Discussion), the IGF-1 in the cerebellar molecular layer also influences BG. Specifically, IGF-1 increases the activity and upregulates the surface expression of GLAST (Gamboa and Ortega, 2002). Additional mechanisms by which the IO supports the health and function of PCs and BG have yet to be elucidated.

BG carry out a wide array of functions within the cerebellar molecular layer. They provide structural support (Cui et al., 2001), are indispensible for the maintenance, function, and plasticity of synapses (Muller and Kettenmann, 1995; Bellamy, 2006; Lopez-Bayghen et al., 2007), and buffer ions and supply neurons with glutamine (Ottersen et al., 1992; Muller and Kettenmann, 1995). BG express GLAST which takes up a large majority of the extracellular glutamate at PF-PC and CF-PC synapses (Bellamy, 2006). This shapes glutamate synaptic transmission by modulating post-synaptic receptor activation (Takahashi et al., 1996; Otis et al., 1996) and limiting the escape of glutamate to extrasynaptic receptors and adjacent synapses (Brasnjo and Otis, 2001; Barbour, 2001; Reichelt and Knopfel, 2002). Glutamate uptake via GLAST also protects PCs against prolonged glutamate exposure that can lead to excitotoxic cell death (Slemmer et al., 2005; Custer et al., 2006). Two previous SCA7 mouse models demonstrated mutant ataxin-7 expressing BG have reduced RNA and protein levels of GLAST and the remaining GLAST protein does not take up glutamate as efficiently (Custer et al., 2006). Both cell autonomous (mutant ataxin-7 mediated transcriptional dysregulation) and non-cell autonomous (loss of IGF-1 from the IO) mechanisms are likely to contribute to decreased GLAST expression and activity in SCA7.

Ongoing intercellular communication between PCs and BG prevents axonal outgrowth and synaptogenesis in adult cerebellum (Bellamy, 2006). Retraction of BG processes from PC

synapses allows multiple CFs to innervate a single PC in contradiction to the one-to-one CF-PC ratio (Iino et al., 2001). In addition to helping maintain structure and function at synapses, BG are a source of neurotrophic factors. BG synthesize glial-derived neurotrophic factor (GDNF, Springer et al., 1994) and brain-derived neurotrophic factor (BDNF, Poblete-Naredo et al., 2011). GDNF promotes the survival and differentiation of PCs (Mount et al., 1995) and can ameliorate PC degeneration (Tolbert et al., 2001; Tolbert and Clark, 2003). Similarly, BDNF is required for cerebellar development (Schwartz et al., 1998), and it induces CF re-innervation onto PCs (Sherrard and Bower, 2001; Dixon and Sherrard, 2006; Willson et al., 2008). Further study is needed to determine which BG-mediated processes are disrupted in SCA7 and how mutant ataxin-7 expression causes their disruption.

It is clear from our work that PCs, IO neurons, and BG are all pivotal players in SCA7 onset and progression. Once characterization of their network interactions is complete, progress can be made to understand which molecular mechanisms are disrupted in SCA7 and which are good targets for therapeutic intervention.

Functional analysis of the PC-IO-BG circuit

Given that morphological abnormalities do not always directly correlate with behavioral outcome in models of neurodegenerative disease (Chapter III), the characterization of functional circuits that do correlate with behavior is needed. In a mouse model of SCA1, PCs are less responsive to CF stimulation as measured with flavoprotein autofluorescence optical imaging and extracellular field potential recordings (Barnes et al., 2011). VGLUT2 labeled CF terminals were not present near the pial surface of the cerebellar molecular layer, distal to the PC layer.

We have shown CF terminals are redistributed nearer to PC bodies in end stage *PrP-floxed-SCA7-92Q BAC* mice (Chapter III, Fig. 3.7). It is likely this SCA7 mouse model has disrupted CF-PC synaptic transmission as in the SCA1 mouse model, and further experimentation is warranted.

There are a number of methods already established which can be used to investigate changes in cerebellar molecular layer circuitry in SCA7 mice. Whole cell patch clamp recordings of PCs can be made in organotypic cultures of cerebellar slices (Hirai et al., 2005; Zanjani et al., 2009). Whole cell and other intracellular recordings and calcium imaging of IO neurons can be performed in organotypic cultures of brainstem slices (Li et al., 2012; Rekling et al., 2012). To investigate an intact olivocerebellar system, one group developed a method to isolate the brain stem-cerebellum of guinea pigs (Llinas and Muhlethaler, 1988). They were able to collect data from cerebellar and inferior olive extracellular field potentials, extracellular recordings of single PCs, intrasomatic and intradendritic PC recordings, extra- and intra-cellular IO neuron recordings, and intracellular recordings from pontine nuclei neurons (a major source of mossy fiber input to the cerebellar granule cells). More recently, another group developed a preparation of arterially perfused hindbrain and upper body from rat (Cerminara et al., 2010). This preparation preserves connections of the hindbrain with the upper spinal cord and the peripheral nervous system of the head and forelimbs. Extracellular field potentials of mossy fibers, CFs, and PFs; electromyography (EMG) activity in forelimb muscles; and single unit activity of PCs, molecular layer interneurons, and neurons in the deep cerebellar nuclei can all be observed using this preparation (Cerminara et al., 2010).

To investigate BG signaling and its role in shaping synaptic transmission, one group used cerebellar slice preparations from transgenic mice in which increased intracellular calcium in BG

can be induced with bath application of a peptide ligand (Wang et al., 2012). Combined whole cell recordings of PCs and two-photon calcium imaging confirmed increased calcium in BG leads to an increase of PC spiking activity. Agonist induced calcium concentration increases in BG also cause a decrease in extracellular potassium concentration as measured by simultaneous calcium imaging, whole cell recording of BG, and ion-sensitive microelectrodes. Dual whole cell recordings of neighboring PCs and BG are also possible (Wang et al., 2012).

Perhaps the most exciting is the potential to record from the intact cerebellum of alert or anesthetized animals. Local field potentials and single- and multiple-unit extracellular recordings from PCs have been accomplished in awake, alert mice (Marquez-Ruiz and Cheron, 2012). In another study, calcium imaging was combined with recordings of cerebellar electrocortical activity (ECoG) in intact cerebellum in anesthetized mice (Wang et al., 2012). Acute cranial windows were placed over the vermis of the cerebellum and the cerebellar cortex was loaded with calcium indicator dye. Time-lapse imaging of the live intact cerebellum allowed the researchers to determine calcium transients in BG regulate PC firing activity *in vivo*.

Future studies utilizing the techniques discussed above to describe brain stem and cerebellar circuit function in pre-, early-, and late-symptomatic *PrP-floxed-SCA7-92Q BAC* mice will provide a direct link between motor abnormalities and neural network function. This will enhance our understanding of what causes motor abnormalities directly and help hone our search for potential therapeutic targets.

Conclusions

This work has described several important characteristics of SCA7 pathogenesis. Like PCs, BG undergo non-cell autonomous degeneration. BG, PCs, and the IO are the major players in SCA7 symptom onset, severity, and progression. Symptom progression can be arrested after symptom onset. Behavioral measures of dysfunction do not uniformly correlate with observed histopathological change, either in timing of onset or the ability to arrest disease progression. Thus, functional markers, as opposed to morphological markers, of cerebellar circuit dysfunction must be described in order to define the molecular mechanisms that correlate directly with motor behavior abnormalities.

Bibliography

1. Agrawal-Singh S, Isken F, Agelopoulos K, Klein HU, Thoennissen NH, Koehler G, Hascher A, Baumer N, Berdel WE, Thiede C, et al. (2012) Genome-wide analysis of histone H3 acetylation patterns in AML identifies PRDX2 as an epigenetically silenced tumor suppressor gene. Blood 119:2346-2357.

2. Bang OY, Huh K, Lee PH, Kim HJ. (2003) Clinical and neuroradiological features of patients with spinocerebellar ataxias from Korean kindreds. Arch Neurol 60:1566-1574.

3. Barbour B. (2001) An evaluation of synapse independence. J Neurosci 21:7969-7984.

4. Barnes JA, Ebner BA, Duvick LA, Gao W, Chen G, Orr HT, Ebner TJ. (2011) Abnormalities in the climbing fiber-Purkinje cell circuitry contribute to neuronal dysfunction in ATXN1[82Q] mice. J Neurosci 31:12778-12789.

5. Barrera I, Flores-Méndez M, Hernández-Kelly LC, Cid L, Huerta M, Zinker S, López-Bayghen E, Aguilera J, Ortega A. (2010) Glutamate regulates eEF1A phosphorylation and ribosomal transit time in Bergmann glial cells. Neurochem Int 57:795-803.

6. Barski JJ, Dethleffsen K, Meyer M. (2000) Cre recombinase expression in cerebellar Purkinje cells. Genesis 28:93-98.

7. Belachew S, Aguirre AA, Wang H, Vautier F, Yuan X, Anderson S, Kirby M, Gallo V. (2002) Cyclin-dependent kinase-2 controls oligodendrocyte progenitor cell cycle progression and is downregulated in adult oligodendrocyte progenitors. J Neurosci 22:8553-8562.

8. Bellamy TC. (2006) Interactions between Purkinje neurons and Bergmann glia. Cerebellum 5:116-126.

9. Benomar A, Krols L, Stevanin G, Cancel G, LeGuern E, David G, Ouhabi H, Martin JJ, Durr A, Zaim A, et al. (1995) The gene for autosomal dominant cerebellar ataxia with pigmentary macular dystrophy maps to chromosome 3p12-p21.1. Nat Genet 10:84-88.

10. Besnard F, Brenner M, Nakatani Y, Chao R, Purohit HJ, Freese E. (1991) Multiple interacting sites regulate astrocyte-specific transcription of the human gene for glial fibrillary acidic protein. J Biol Chem 266:18877-18883.

11. Brasnjo G and Otis TS. (2001) Neuronal glutamate transporters control activation of postsynaptic metabotropic glutamate receptors and influence cerebellar long-term depression. Neuron 31:607-616.

12. Burnashev N, Khodorova A, Jonas P, Helm PJ, Wisden W, Monyer H, Seeburg PH,

Sakmann B. (1992) Calcium-permeable AMPA-kainate receptors in fusiform cerebellar glial cells. Science 256:1566-1570.

13. Cahoy JD, Emery B, Kaushal A, Foo LC, Zamanian JL, Christopherson KS, Xing Y, Lubischer JL, Krieg PA, Krupenko SA, Thompson WJ, Barres BA (2008) A transcriptome database for astrocytes, neurons, and oligodendrocytes: a new resource for understanding brain development and function. J Neurosci 28:264-278.

14. Carrascosa C, Torres-Aleman I, Lopez-Lopez C, Carro E, Espejo L, Torrado S, Torrado JJ. (2004) Microspheres containing insulin-like growth factor I for treatment of chronic neurodegeneration. Biomaterials 25:707-714.

15. Cerminara NL, Rawson JA, Apps R. (2010) Electrophysiological characterization of the cerebellum in the arterially perfused hindbrain and upper body of the rat. Cerebellum 9:218-231.

16. Chakrabarti L, Zahra R, Jackson SM, Kazemi-Esfarjani P, Sopher BL, Mason AG, Toneff T, Ryu S, Shaffer S, Kansy JW, Eng J, Merrihew G, MacCoss MJ, Murphy A, Goodlett DR, Hook V, Bennett CL, Pallanck LJ, La Spada AR. (2010) Mitochondrial dysfunction in NnaD mutant flies and Purkinje cell degeneration mice reveals a role for Nna proteins in neuronal bioenergetics. Neuron 66:835-847.

17. Chen H, Dzitoyeva S, Manev H. (2010) 5-Lipoxygenase in mouse cerebellar Purkinje cells. Neuroscience 171:383-389.

18. Chou AH, Chen CY, Chen SY, Chen WJ, Chen YL, Weng YS, Wang HL. (2010) Polyglutamine-expanded ataxin-7 causes cerebellar dysfunction by inducing transcriptional dysregulation. Neurochem Int 56:329-339.

19. Chung SH, Calafiore M, Plane JM, Pleasure DE, Deng W. (2011) Apoptosis inducing factor deficiency causes reduced mitofusion 1 expression and patterned Purkinje cell degeneration. Neurobiol Dis 41:445-457.

20. Clark HB, Burright EN, Yunis WS, Larson S, Wilcox C, Hartman B, Matilla A, Zoghbi HY, Orr HT. (1997) Purkinje cell expression of a mutant allele of SCA1 in transgenic mice leads to disparate effects on motor behaviors, followed by a progressive cerebellar dysfunction and histological alterations. J Neurosci 17:7385-7395.

21. Clement AM, Nguyen MD, Roberts EA, Garcia ML, Boillée S, Rule M, McMahon AP, Doucette W, Siwek D, Ferrante RJ, Brown RH Jr, Julien JP, Goldstein LS, Cleveland DW. (2003) Wild-type nonneuronal cells extend survival of SOD1 mutant motor neurons in ALS mice. Science 302:113-117.

22. Cui W, Allen ND, Skynner M, Gusterson B, Clark AJ. (2001) Inducible ablation of astrocytes shows that these cells are required for neuronal survival in the adult brain. Glia 34:272-282.

23. Custer SK, Garden GA, Gill N, Rueb U, Libby RT, Schultz C, Guyenet SJ, Deller T, Westrum LE, Sopher BL, La Spada AR. (2006) Bergmann glia expression of polyglutamine - expanded ataxin-7 produces neurodegeneration by impairing glutamate transport. Nat Neurosci 9:1302-1311.

24. David G, Abbas N, Stevanin G, Durr A, Yvert G, Cancel G, Weber C, Imbert G, Saudou F, Antoniou E, et al. (1997) Cloning of the SCA7 gene reveals a highly unstable CAG repeat expansion. Nat Genet 17:65-70.

25. David G, Durr A, Stevanin G, Cancel G, Abbas N, Benomar A, Belal S, Lebre AS, Abada-Bendib M, Grid D, et al. (1998) Molecular and clinical correlations in autosomal dominant cerebellar ataxia with progressive macular dystrophy (SCA7). Hum Mol Genet 7:165-170.

26. Dixon KJ and Sherrard RM. (2006) Brain-derived neurotrophic factor induces post-lesion transcommissural growth of olivary axons that develop normal climbing fibers on mature Purkinje cells. Exp Neurol 202:44-56.

27. Donald S, Humby T, Fyfe I, Segonds-Pichon A, Walker SA, Andrews SR, Coadwell WJ, Emson P, Wilkinson LS, Welch HC. (2008) P-Rex2 regulates Purkinje cell dendrite morphology and motor coordination. Proc Natl Acad Sci U S A 105:4483-4488.

28. Duvick L, Barnes J, Ebner B, Agrawal S, Andresen M, Lim J, Giesler GJ, Zoghbi HY, Orr HT. (2010) SCA1-like disease in mice expressing wild-type ataxin-1 with a serine to aspartic acid replacement at residue 776. Neuron 67:929-935.

29. Eiraku M, Tohgo A, Ono K, Kaneko M, Fujishima K, Hirano T, Kengaku M. (2005) DNER acts as a neuron-specific Notch ligand during Bergmann glial development. Nat Neurosci 8:873-880.

30. Enevoldson TP, Sanders MD, Harding AE. (1994) Autosomal dominant cerebellar ataxia with pigmentary macular dystrophy: A clinical and genetic study of eight families. Brain 117:445-460.

31. Euler P, Friedrich B, Ziegler R, Kuhn A, Lindenberg KS, Weiller C, Zucker B. (2012) Gene expression analysis on a single cell level in Purkinje cells of Huntington's disease transgenic mice. Neurosci Lett 517:7-12.

32. Fernandez AM, Gonzalez de la Vega AG, Planas B, Torres-Aleman I. (1999) Neuroprotective actions of peripherally administered insulin-like growth factor I in the injured olivo-cerebellar pathway. Eur J Neurosci 11:2019-2030.

33. Foo LC, Allen NJ, Bushong EA, Ventura PB, Chung WS, Zhou L, Cahoy JD, Daneman R, Zong H, Ellisman MH, Barres BA. (2011) Development of a method for the purification and culture of rodent astrocytes. Neuron 71:799-811.

34. Frank MG, Wieseler-Frank JL, Watkins LR, Maier SF. (2006) Rapid isolation of highly enriched and quiescent microglia from adult rat hippocampus: immunophenotypic and functional characteristics. J Neurosci Methods 151:121-130.

35. Fremeau RT Jr, Troyer MD, Pahner I, Nygaard GO, Tran CH, Reimer RJ, Bellocchio EE, Fortin D, Storm-Mathisen J, Edwards RH. (2001) The expression of vesicular glutamate transporters defines two classes of excitatory synapse. Neuron 31:247-260.

36. Furrer SA, Mohanachandran MS, Waldherr SM, Chang C, Damian VA, Sopher BL, Garden GA, La Spada AR. (2011) Spinocerebellar ataxia type 7 cerebellar disease requires the coordinated action of mutant ataxin-7 in neurons and glia, and displays non-cell-autonomous bergmann glia degeneration. J Neurosci 31:16269-16278.

37. Gamboa C, Ortega A. (2002) Insulin-like growth factor-1 increases activity and surface levels of the GLAST subtype of glutamate transporter. Neurochem Int 40:397-403.

38. Garcia-Segura LM, Rodriguez JR, Torres-Aleman I. (1997) Localization of the insulin-like growth factor I receptor in the cerebellum and hypothalamus of adult rats: an electron microscopic study. J Neurocytol 26:479-490.

39. Garden GA, Libby RT, Fu YH, Kinoshita Y, Huang J, Possin DE, Smith AC, Martinez RA, Fine GC, Grote SK, Ware CB, Einum DD, Morrison RS, Ptacek LJ, Sopher BL, La Spada AR. (2002) Polyglutamine-expanded ataxin-7 promotes non -cell-autonomous purkinje cell degeneration and displays proteolytic cleavage in ataxic transgenic mice. J Neurosci 22:4897-4905.

40. Garden GA and La Spada AR. (2008) Molecular pathogenesis and cellular pathology of spinocerebellar ataxia type 7 neurodegeneration. Cerebellum 7:138-149.

41. Gatchel JR, Watase K, Thaller C, Carson JP, Jafar-Nejad P, Shaw C, Zu T, Orr HT, Zoghbi HY. (2008) The insulin-like growth factor pathway is altered in spinocerebellar ataxia type 1 and type 7. Proc Natl Acad Sci U S A 105:1291-1296.

42. Giunti P, Stevanin G, Worth PF, David G, Brice A, Wood NW. (1999) Molecular and clinical study of 18 families with ADCA type II: Evidence for genetic heterogeneity and de novo mutation. Am J Hum Genet 64:1594-1603.

43. Gouw LG, Digre KB, Harris CP, Haines JH, Ptacek LJ. (1994). Autosomal dominant cerebellar ataxia with retinal degeneration: Clinical, neuropathologic, and genetic analysis of a large kindred. Neurology 44:1441-1447.

44. Guo JU, Ma DK, Mo H, Ball MP, Jang MH, Bonaguidi MA, Balazer JA, Eaves HL, Xie B, Ford E, Zhang K, Ming GL, Gao Y, Song H. (2011) Neuronal activity modifies the DNA methylation landscape in the adult brain. Nat Neurosci 14:1345-1351.

45. Gurney ME, Pu H, Chiu AY, Dal Canto MC, Polchow CY, Alexander DD, Caliendo J, Hentati A, Kwon YW, Deng HX, et al. (1994) Motor neuron degeneration in mice that express a human Cu,Zn superoxide dismutase mutation. Science 264:1772-1775.

46. Guyenet SJ, Furrer SA, Damian VM, Baughan TD, La Spada AR, Garden GA (2010) A simple composite phenotype scoring system for evaluating mouse models of cerebellar ataxia. J Vis Exp pii:1787.

47. Hamilton SR, Chatrian GE, Mills RP, Kalina RE, Bird TD. (1990) Cone dysfunction in a subgroup of patients with autosomal dominant cerebellar ataxia. Arch Ophthalmol 108:551-556.

48. Hanrieder J, Wicher G, Bergquist J, Andersson M, Fex-Svenningsen A. (2011) MALDI mass spectrometry based molecular phenotyping of CNS glial cells for prediction in mammalian brain tissue. Anal Bioanal Chem 401:135-147.

49. Hayashi S and McMahon AP. (2002) Efficient recombination in diverse tissues by a tamoxifen-inducible form of Cre: a tool for temporally regulated gene activation/inactivation in the mouse. Dev Biol 244:305-318.

50. Helmlinger D, Abou-Sleymane G, Yvert G, Rousseau S, Weber C, Trottier Y, Mandel JL, Devys D. (2004a) Disease progression despite early loss of polyglutamine protein expression in SCA7 mouse model. J Neurosci 24:1881-1887.

51. Helmlinger D, Hardy S, Sasorith S, Klein F, Robert F, Weber C, Miguet L, Potier N, Van-Dorsselaer A, Wurtz JM, et al. (2004b) Ataxin-7 is a subunit of GCN5 histone acetyltransferase-containing complexes. Hum Mol Genet 13:1257-1265.

52. Helmlinger D, Hardy S, Abou-Sleymane G, Eberlin A, Bowman AB, Gansmüller A, Picaud S, Zoghbi HY, Trottier Y, Tora L, Devys D. (2006) Glutamine-expanded ataxin-7 alters TFTC/STAGA recruitment and chromatin structure leading to photoreceptor dysfunction. PLoS Biol 4:e67.

53. Hirai H, Pang Z, Bao D, Miyazaki T, Li L, Miura E, Parris J, Rong Y, Watanabe M, Yuzaki M, Morgan JI. (2005) Cbln1 is essential for synaptic integrity and plasticity in the cerebellum. Nat Neurosci 8:1534-1541.

54. Hollmann M, Hartley M, Heinemann S. (1991) Ca2+ permeability of KA-AMPA--gated glutamate receptor channels depends on subunit composition. Science 252:851-853.

55. Holmberg M, Johansson J, Forsgren L, Heijbel J, Sandgren O, Holmgren G. (1995) Localization of autosomal dominant cerebellar ataxia associated with retinal degeneration and anticipation to chromosome 3p12-p21.1. Hum Mol Genet 4:1441-1445.

56. Huang H, Bordey A. (2004) Glial glutamate transporters limit spillover activation of presynaptic NMDA receptors and influence synaptic inhibition of Purkinje neurons. J

Neurosci 24:5659-5669.

57. Iino M, Goto K, Kakegawa W, Okado H, Sudo M, Ishiuchi S, Miwa A, Takayasu Y, Saito I, Tsuzuki K, Ozawa S. (2001) Glia-synapse interaction through Ca2+-permeable AMPA receptors in Bergmann glia. Science 292:926-929.

58. Ilieva H, Polymenidou M, Cleveland DW. (2009) Non-cell autonomous toxicity in neurodegenerative disorders: ALS and beyond. J Cell Biol 187:761-772.

59. Ingram MAC, Orr HT, Clark B. (2012) Genetically engineered mouse models of the trinucleotide-repeat spinocerebellar ataxias. Brain Res Bull 88:33-42.

60. Ipser JC, Syal S, Bentley J, Adnams CM, Steyn B, Stein DJ (2012) 1H-MRS in autism spectrum disorders: a systematic meta-analysis. Metab Brain Dis.

61. James R, Searcy JL, Le Bihan T, Martin SF, Gliddon CM, Povey J, Deighton RF, Kerr LE, McCulloch J, Horsburgh K. (2012) Proteomic analysis of mitochondria in APOE transgenic mice and in response to an ischemic challenge. J Cereb Blood Flow Metab 32:164-176.

62. Jung H and Holt CE. (2010) Local translation of mRNAs in neural development. Wiley Interdiscip Rev RNA 2:153-165.

63. Jungblut M, Tiveron MC, Barral S, Abrahamsen B, Knobel S, Pennartz S, Schmitz J, Perraut M, Pfrieger FW, Stoffel W, Cremer H, Bosio A. (2012) Isolation and characterization of living primary astroglial cells using the new GLAST-specific monoclonal antibody ACSA-1. Glia 60:894-907.

64. Kang HJ, Kawasawa YI, Cheng F, Zhu Y, Xu X, Li M, Sousa AM, Pletikos M, Meyer KA, Sedmak G, Guennel T, et al. (2011) Spatio-temporal transcriptome of the human brain. Nature 478:483-489.

65. Kashiwabuchi N, Ikeda K, Araki K, Hirano T, Shibuki K, Takayama C, Inoue Y, Kutsuwada T, Yagi T, Kang Y, Aizawa S, Mishina M. (1995) Impairment of motor coordination, Purkinje cell synapse formation, and cerebellar long-term depression in GluRδ2 mutant mice. Cell 81:245-252.

66. Kramer JM, Kochinke K, Oortveld MA, Marks H, Kramer D, de Jong EK, Asztalos Z, Westwood JT, Stunnenberg HG, Sokolowski MB, Keleman K, Zhou H, van Bokhoven H, Schenck A. (2011) Epigenetic regulation of learning and memory by Drosophila EHMT/G9a. PLoS Biol 9:e1000569.

67. Kurihara H, Hashimoto K, Kano M, Takayama C, Sakimura K, Mishina M, Inoue Y, Watanabe M. (1997) Impaired parallel fiber – Purkinje cell synapse stabilization during cerebellar development of mutant mice lacking the glutamate receptor δ2 subunit. J Neurosci 17:9613-9623.

68. La Spada AR, Fu Y, Sopher BL, Libby RT, Wang X, Li LY, Einum DD, Huang J, Possin DE, Smith AC, Martinez RA, Koszdin KL, Treuting PM, Ware CB, Hurley JB, Ptacek LJ, Chen S. (2001) Polyglutamine-expanded ataxin-7 antagonizes CRX function and induces cone-rod dystrophy in a mouse model of SCA7. Neuron 31:913-927.

69. Li C, Han L, Ma CW, Lai SK, Lai CH, Shum DK, Chan YS. (2012) Maturation profile of inferior olivary neurons expressing ionotropic glutamate receptors in rats: role in coding linear accelerations. Brain Struct Funct.

70. Lichter-Konecki U, Mangin JM, Gordish-Dressman H, Hoffman EP, Gallo V. (2008) Gene expression profiling of astrocytes from hyperammonemic mice reveals altered pathways for water and potassium homeostasis in vivo. Glia 56:365-377.

71. Lino MM, Schneider C, Caroni P. (2002) Accumulation of SOD1 mutants in postnatal motoneurons does not cause motoneuron pathology or motoneuron disease. J Neurosci 22:4825-4832.

72. Liu JL, Wang HL, Zhang LF, Xu YF, Deng W, Zhu H, Qin C. (2011) Metabonomics study of brain-specific human S100B transgenic mice by using high-performance liquid chromatography coupled with quadrupole time of flight mass spectrometry. Biol Pharm Bull 34:871-876.

73. Llinás R, Mühlethaler M. (1988) An electrophysiological study of the in vitro, perfused brain stem-cerebellum of adult guinea-pig. J Physiol 404:215-240.

74. López-Bayghen E, Rosas S, Castelán F, Ortega A. (2007) Cerebellar Bergmann glia: an important model to study neuron-glia interactions. Neuron Glia Biol 3:155-167.

75. Malatesta P, Hartfuss E, Gotz M. (2000) Isolation of radial glial cells by fluorescent-activated cell sorting reveals a neuronal lineage. Development 127:5253-5263.

76. Marko K, Kohidi T, Hadinger N, Jelitai M, Mezo G, Madarasz E (2011) Isolation of radial glia-like neural stem cells from fetal and adult mouse forebrain via selective adhesion to a novel adhesive peptide-conjugate. PLoS One 6:e28538.

77. Márquez-Ruiz J and Cheron G. (2012) Sensory stimulation-dependent plasticity in the cerebellar cortex of alert mice. PLoS One 7:e36184.

78. Martin J, Van Regemorter N, Del-Favero J, Lofgren A, Van Broeckhoven C. (1999) Spinocerebellar ataxia type 7 (SCA7): Correlations between phenotype and genotype in one large Belgian family. J Neurol Sci 168:37-46.

79. Martin JJ, Van Regemorter N, Krols L, Brucher JM, de Barsy T, Szliwowski H, Evrard P, Ceuterick C, Tassignon MJ, Smet-Dieleman H, et al. (1994) On an autosomal dominant form of retinal-cerebellar degeneration: An autopsy study of five patients in one family.

Acta Neuropathol 88:277-286.

80. Martinez E, Palhan VB, Tjernberg A, Lymar ES, Gamper AM, Kundu TK, Chait BT, Roeder RG. (2001) Human STAGA complex is a chromatin-acetylating transcription coactivator that interacts with pre-mRNA splicing and DNA damage-binding factors in vivo. Mol Cell Bio 21:6782-6795.

81. McMahon SJ, Pray-Grant MG, Schieltz D, Yates JR 3rd, Grant PA. (2005) Polyglutamine-expanded spinocerebellar ataxia-7 protein disrupts normal SAGA and SLIK histone acetyltransferase activity. Proc Natl Acad Sci U S A 102:8478-8482.

82. Merienne K, Friedman J, Akimoto M, Abou-Sleymane G, Weber C, Swaroop A, Trottier Y. (2007) Preventing polyglutamine-induced activation of c-Jun delays neuronal dysfunction in a mouse model of SCA7 retinopathy. Neurobiol Dis 25:571-581.

83. Michalik A, Martin JJ, Van Broeckhoven C. (2004) Spinocerebellar ataxia type 7 associated with pigmentary retinal dystrophy. Eur J Hum Genet 12:2-15.

84. Miyashiro K, Dichter M, Eberwine J. (1994) On the nature and differential distribution of mRNAs in hippocampal neurites: implications for neuronal functioning. Proc Natl Acad Sci U S A 91:10800-10804.

85. Moccia R, Chen D, Lyles V, Kapuya E, E Y, Kalachikov S, Spahn CM, Frank J, Kandel ER, Barad M, Martin KC. (2003) An unbiased cDNA library prepared from isolated Aplysia sensory neuron processes is enriched for cytoskeletal and translational mRNAs. J Neurosci 23:9409-9417.

86. Mookerjee S, Papanikolaou T, Guyenet SJ, Sampath V, Lin A, Vitelli C, DeGiacomo F, Sopher BL, Chen SF, La Spada AR, Ellerby LM. (2009) Posttranslational modification of ataxin-7 at lysine 257 prevents autophagy-mediated turnover of an N-terminal caspase-7 cleavage fragment. J Neurosci 48:15134-15144.

87. Mount HT, Dean DO, Alberch J, Dreyfus CF, Black IB. (1995) Glial cell line-derived neurotrophic factor promotes the survival and morphologic differentiation of Purkinje cells. Proc Natl Acad Sci U S A 92:9092-9096.

88. Müller T, Kettenmann H. (1995) Physiology of Bergmann glial cells. Int Rev Neurobiol 38:341-359.

89. Nieto-Bona MP, Garcia-Segura LM, Torres-Aleman I. (1993) Orthograde transport and release of insulin-like growth factor I from the inferior olive to the cerebellum. J Neurosci Res 36:520-527.

90. Nieto-Bona MP, Busiguina S, Torres-Aleman I. (1995) Insulin-like growth factor I is an afferent trophic signal that modulates calbindin-28kD in adult Purkinje cells. J Neurosci Res 42:371-376.

91. Novak A, Guo C, Yang W, Nagy A, Lobe CG. (2000) Z/EG, a double reporter mouse line that expresses enhanced green fluorescent protein upon Cre-mediated excision. Genesis 28:147-155.

92. Orr HT and Zoghbi HY. (2007) Trinucleotide repeat disorders. Annu Rev Neurosci 30:575-621.

93. Otis TS, Wu YC, Trussell LO. (1996) Delayed clearance of transmitter and the role of glutamate transporters at synapses with multiple release sites. J Neurosci 16:1634-1644.

94. Ottersen OP, Zhang N, Walberg F. (1992) Metabolic compartmentation of glutamate and glutamine: morphological evidence obtained by quantitative immunocytochemistry in rat cerebellum. Neuroscience 46:519-534.

95. Palhan VB, Chen S, Peng GH, Tjernberg A, Gamper AM, Fan Y, Chait BT, La Spada AR, Roeder RG. (2005) Polyglutamine-expanded ataxin-7 inhibits STAGA histone acetyltransferase activity to produce retinal degeneration. Proc Natl Acad Sci U S A 102:8472-8477.

96. Pinto L, Mader MT, Irmler M, Gentilini M, Santoni F, Drechsel D, Blum R, Stahl R, Bulfone A, Malatesta P, Beckers J, Gotz M. (2008) Prospective isolation of functionally distinct radial glial subtypes--lineage and transcriptome analysis. Mol Cell Neurosci 38:15-42.

97. Poblete-Naredo I, Guillem AM, Juárez C, Zepeda RC, Ramírez L, Caba M, Hernández-Kelly LC, Aguilera J, López-Bayghen E, Ortega A. (2011) Brain-derived neurotrophic factor and its receptors in Bergmann glia cells. Neurochem Int 59:1133-1144.

98. Poirier MA, Li H, Macosko J, Cai S, Amzel M, Ross CA. (2002) Huntingtin spheroids and protofibrils as precursors in polyglutamine fibrilization. J Biol Chem 277:41032-41037.

99. Pramatarova A, Laganière J, Roussel J, Brisebois K, Rouleau GA. (2001) Neuron-specific expression of mutant superoxide dismutase 1 in transgenic mice does not lead to motor impairment. J Neurosci 21:3369-3374.

100. Reichelt W, Knöpfel T. (2002) Glutamate uptake controls expression of a slow postsynaptic current mediated by mGluRs in cerebellar Purkinje cells. J Neurophysiol 87:1974-1980.

101. Reitman ZJ, Jin G, Karoly ED, Spasojevic I, Yang J, Kinzler KW, He Y, Bigner DD, Vogelstein B, Yan H. (2011) Profiling the effects of isocitrate dehydrogenase 1 and 2 mutations on the cellular metabolome. Proc Natl Acad Sci U S A 108:3270-3275.

102. Rekling JC, Jensen KH, Jahnsen H. (2012) Spontaneous cluster activity in the inferior

olivary nucleus in brainstem slices from postnatal mice. J Physiol 590 (Pt 7):1547-1562.

103. Rosen DR, Siddique T, Patterson D, Figlewicz DA, Sapp P, Hentati A, Donaldson D, Goto J, O'Regan JP, Deng HX, et al. (1993) Mutations in Cu/Zn superoxide dismutase gene are associated with familial amyotrophic lateral sclerosis. Nature 362:59-62.

104. Rothstein JD, Martin L, Levey AI, Dykes-Hoberg M, Jin L, Wu D, Nash N, Kuncl RW. (1994) Localization of neuronal and glial glutamate transporters. Neuron 13:713-725.

105. Rozen,S. and Skaletsky,H.J. (1998) Primer 3. Version 4. http://www.broadinstitute.org/genome_software/other/primer3.html.

106. Scholefield J and Wood MJ. (2010) Therapeutic gene silencing strategies for polyglutamine disorders. Trends Genet 26:29-38.

107. Schwartz PM, Levy RL, Borghesani PR, Segal RA. (1998) Cerebellar pathology in BDNF -/- mice: the classic view of neurotrophins is changing. Mol Psychiatry 3:116-120.

108. Sherrard RM and Bower AJ. (2001) BDNF and NT3 extend the critical period for developmental climbing fibre plasticity. Neuroreport 12:2871-2874.

109. Slemmer JE, De Zeeuw CI, Weber JT. (2005) Don't get too excited: mechanisms of glutamate-mediated Purkinje cell death. Prog Brain Res 148:367-390.

110. Springer JE, Mu X, Bergmann LW, Trojanowski JQ. (1994) Expression of GDNF mRNA in rat and human nervous tissue. Exp Neurol 127:167-170.

111. Strom AL, Forsgren L, Holmberg M. (2005) A role for both wild-type and expanded ataxin-7 in transcriptional regulation. Neurobiol Dis 20:646-655.

112. Sun W, Lee S, Zhabotynsky V, Zou F, Wright FA, Crowley JJ, Yun Z, Buus RJ, Miller DR, Wang J, McMillan L, Pardo-Manuel de Villena F, Sullivan PF (2012) Transcriptome atlases of mouse brain reveals differential expression across brain regions and genetic backgrounds. G3 (Bethesda) 2:203-211.

113. Sutton MA and Schuman EM. (2006) Dendritic protein synthesis, synaptic plasticity, and memory. Cell 127:49-58.

114. Takahashi M, Sarantis M, Attwell D. (1996) Postsynaptic glutamate uptake in rat cerebellar Purkinje cells. J Physiol 497 (Pt 2):523-530.

115. To KW, Adamian M, Jakobiec FA, Berson EL. (1993) Olivopontocerebellar atrophy with retinal degeneration. An electroretinographic and histopathologic investigation. Ophthalmology 100:15-23.

116. Tolbert DL and Clark BR. (2000) Olivocerebellar projections modify hereditary Purkinje

cell degeneration. Neuroscience 101:417-433.

117. Tolbert DL, Bradley MW, Tolod EG, Torres-Aleman I, Clark BR. (2001) Chronic intraventricular infusion of glial cell line-derived neurotrophic factor (GDNF) rescues some cerebellar Purkinje cells from heredodegeneration. Exp Neurol 170:375-379.

118. Tolbert DL and Clark BR. (2003) GDNF and IGF-1 trophic factors delay hereditary Purkinje cell degeneration and the progression of gait ataxia. Exp Neurol 183:205-219.

119. Tomomura M, Rice DS, Morgan JI, Yuzaki M. (2001) Purification of Purkinje cells by fluorescence-activated cell sorting from transgenic mice that express green fluorescent protein. Eur J Neurosci 14:57-63.

120. Tsai MC, Tanaka K, Overstreet-Wadiche L, Wadiche JI. (2012) Neuronal glutamate transporters regulate glial excitatory transmission. J Neurosci 32:1528-1535.

121. Tsunemi T, Ashe TD, Morrison BE, Soriano KR, Au J, Roque RA, Lazarowski ER, Damian VA, Masliah E, La Spada AR. (2012) PGC-1α Rescues Huntington's Disease Proteotoxicity by Preventing Oxidative Stress and Promoting TFEB Function. Sci Transl Med 4:142ra97.

122. Vig PJ, Hearst S, Shao Q, Lopez ME, Murphy HA 2nd, Safaya E. (2011) Glial S100B protein modulates mutant ataxin-1 aggregation and toxicity: TRTK12 peptide, a potential candidate for SCA1 therapy. Cerebellum 10:254-266.

123. Wacker JL, Zareie MH, Fong H, Sarikaya M, Muchowski PJ. (2004) Hsp70 and Hsp40 attenuate formation of spherical and annular polyglutamine oligomers by partitioning monomer. Nat Struct Mol Biol 11:1215-1222.

124. Wang HL, Chou AH, Lin AC, Chen SY, Weng YH, Yeh TH. (2010) Polyglutamine-expanded ataxin-7 upregulates Bax expression by activating p53 in cerebellar and inferior olivary neurons. Exp Neurol 224:486-494.

125. Wang F, Xu Q, Wang W, Takano T, Nedergaard M. (2012) Bergmann glia modulate cerebellar Purkinje cell bistability via Ca2+-dependent K+ uptake. Proc Natl Acad Sci U S A 109:7911-7916.

126. Willson ML, McElnea C, Mariani J, Lohof AM, Sherrard RM. (2008) BDNF increases homotypic olivocerebellar reinnervation and associated fine motor and cognitive skill. Brain 131 (Pt 4):1099-1112.

127. Xiang Z, Valenza M, Cui L, Leoni V, Jeong HK, Brilli E, Zhang J, Peng Q, Duan W, Reeves SA, Cattaneo E, Krainc D. (2011) Peroxisome-proliferator-activated receptor gamma coactivator 1 α contributes to dysmyelination in experimental models of Huntington's disease. J Neurosci 31:9544-9553.

128. Yamamoto A, Lucas JJ, Hen R. (2000) Reversal of neuropathology and motor dysfunction in a conditional model of Huntington's disease. Cell 101:57-66.

129. Yata K, Oikawa S, Sasaki R, Shindo A, Yang R, Murata M, Kanamaru K, Tomimoto H (2011) Astrocytic neuroprotection through induction of cytoprotective molecules; a proteomic analysis of mutant P301S tau-transgenic mouse. Brain Res 1410:12-23.

130. Yoo SY, Pennesi ME, Weeber EJ, Xu B, Atkinson R, Chen S, Armstrong DL, Wu SM, Sweatt JD, Zoghbi HY. (2003) SCA7 knockin mice model human SCA7 and reveal gradual accumulation of mutant ataxin-7 in neurons and abnormalities in short-term plasticity. Neuron 37:383-401.

131. Yvert G, Lindenberg KS, Picaud S, Landwehrmeyer GB, Sahel JA, Mandel JL. (2000) Expanded polyglutamines induce neurodegeneration and trans-neuronal alterations in cerebellum and retina of SCA7 transgenic mice. Hum Mol Genet 9:2491-2506.

132. Yvert G, Lindenberg KS, Devys D, Helmlinger D, Landwehrmeyer GB, Mandel JL. (2001) SCA7 mouse models show selective stabilization of mutant ataxin-7 and similar cellular responses in different neuronal cell types. Hum Mol Genet 10:1679-1692.

133. Zanjani H, Herrup K, Mariani J. (2004) Cell number in the inferior olive of nervous and leaner mutant mice. J Neurogenet 18:327-339.

134. Zanjani HS, McFarland R, Cavelier P, Blokhin A, Gautheron V, Levenes C, Bambrick LL, Mariani J, Vogel MW. (2009) Death and survival of heterozygous Lurcher Purkinje cells in vitro. Dev Neurobiol 69:505-517.

135. Zhuo L, Theis M, Alvarez-Maya I, Brenner M, Willecke K, Messing A. (2001) hGFAP-cre transgenic mice for manipulation of glial and neuronal function in vivo. Genesis 31:85-94.

136. Zoghbi HY and Orr HT. (2000) Glutamine repeats and neurodegeneration. Ann Rev Neurosci 23:217-247.

137. Zu T, Duvick LA, Kaytor MD, Berlinger MS, Zoghbi HY, Clark HB, Orr HT. (2004) Recovery from polyglutamine-induced neurodegeneration in conditional SCA1 transgenic mice. J Neurosci 24:8853-8861.

Stephanie A. Furrer

Department of Neurology
1959 NE Pacific St., Box 356465
Seattle, WA 98195
(206)616-8364
safurr@uw.edu

EDUCATION

UNIVERSITY OF WASHINGTON SEATTLE, WA
Ph.D. in Neurobiology & Behavior **Anticipated August 2012**
Doctoral thesis: Cerebellar degeneration and prevention of symptom progression in a mouse model of spinocerebellar ataxia type 7.

UNIVERSITY OF WISCONSIN MADISON, WI
B.S. in Molecular Biology **May 2006**
With Comprehensive Honors

AWARDS and HONORS

- Auditory Neuroscience Training Grant, 2012-2013
- Keystone Symposia travel scholarship, 2011
- American Society of Human Genetics Trainee Research Semifinalist Award, 2010
- University of Washington Graduate School Travel Award, 2010
- Institutional Training Grant for Neurobiology (GM07108-35), 2009-2012
- National Ataxia Foundation Ataxia Investigator's Meeting travel grant, 2008
- Achievement Rewards for College Scientists (ARCS) Fellowship, 2006-2009
- Pfizer/Connecticut Business & Industry Association (CBIA) Fellowship, 2005
- Hilldale Undergraduate Research Fellowship, 2005
- Phi Eta Sigma, 2004
- Dean's List, 2002 – 2005

RESEARCH EXPERIENCE

UNIVERSITY OF WASHINGTON SEATTLE, WA
LABORATORIES OF DRS. ALBERT LA SPADA AND GWENN GARDEN
Graduate Student **June 2007 – Present**
Investigated the pathogenesis of spinocerebellar ataxia type 7.

PFIZER GLOBAL RESEARCH & DESIGN GROTON, CT
DISCOVERY CANCER BIOLOGY GROUP
Primary Research Intern **May 2006 – August 2006**
Investigated a genetic pathway involved in the initiation of tumor metastasis.

UNIVERSITY OF WISCONSIN MADISON, WI
DEPARTMENT OF ANATOMY; LAB OF DR. GRACE BOEKHOFF-FALK
Undergraduate Research Assistant **March 2004 – May 2006**
Investigated the role of the gene *distal-less* in the origination and migration of glial cells in the *Drosophila* peripheral nervous system.

TEACHING EXPERIENCE

UNIVERSITY OF WASHINGTON SEATTLE, WA
TA in Neurobiology 301: Intro to Cellular & Molecular Neurobiology **Winter 2008**

UNIVERISTY OF WISCONSIN MADISON, WI
Student Athlete Tutor **Fall 2005**

PUBLICATIONS

Furrer SA, Waldherr SM, Mohanachandran MS, Baughan TD, Nguyen KT, Sopher BL, Damian VM, Garden GA, La Spada AR. (*Submitted*). Excision of SCA7 transgene expression in a conditional mouse model restores motor function and prevents cerebellar synaptic reorganization.

Furrer SA, Mohanachandran MS, Waldherr SM, Chang C, Sopher BL, Damian VM, Garden GA, La Spada AR. (2011). Spinocerebellar ataxia type 7 cerebellar disease requires the coordinated action of mutant ataxin-7 in neurons and glia, and displays non-cell autonomous Bergmann glia degeneration. J Neurosci 31(45): 16269-16278.

Guyenet SJ, **Furrer SA**, Damian VM, Baughan TD, La Spada AR, Garden GA. (2010). A simple composite phenotype scoring system for evaluating mouse models of cerebellar ataxia. J Vis Exp. pii:1787.

PRESENTATIONS

Furrer SA, Waldherr SM, Mohanachandran MS, Sopher BL, La Spada AR, Garden GA. (2011). Inducible Cre mediated excision of polyglutamine-expanded ataxin-7 after disease onset prevents symptom progression in PrP-floxed-SCA7-92Q BAC mice. Nanosymposium presentation at the annual Society for Neuroscience meeting. November 12-16, 2011. Washington, D.C.

Furrer SA, Chang C, Sopher BL, Damian VM, Ashe T, Garden GA, La Spada AR. (2010). Cerebellar neurodegeneration in SCA7 requires the expression of polyglutamine-expanded ataxin-7 in both neurons and glia. Platform presentation at the 60th annual meeting of the American Society of Human Genetics. November 2-6, 2010. Washington, D.C.

POSTER PRESENTATIONS

Furrer SA and Garden GA. (2011). Therapeutic intervention after symptom onset halts further symptom progression in a mouse model of neurodegeneration. ARCS annual luncheon. October 10, 2011. Sheraton Hotel, Seattle, WA.

Furrer SA, Waldherr SM, Mohanachandran MS, Chang C, Sopher BL, La Spada AR, Garden GA. (2011). Spinocerebellar ataxia type 7 transgenic mouse phenotype is reversible following symptom-onset. Keystone Symposium on Neurodegenerative Diseases: The Molecular and Cellular Basis for Neurodegeneration. February 21-26, 2011. Taos, NM.

Furrer SA, Chang C, Sopher BL, La Spada AR, Garden GA. (2010). Bergmann glia modulate pathogenesis in a transgenic murine model of Spinocerebellar ataxia type 7. Cold Spring Harbor Laboratory Meeting on Glia in Health and Disease. July 22-26, 2010. Cold Spring Harbor, NY.

Furrer SA and Garden GA. (2010). Defining the optimal time for therapeutic intervention in a mouse model of Spinocerebellar ataxia type 7. ARCS spring student showcase. April 12, 2010. University of Washington, Seattle, WA.

Furrer SA, Garden GA, La Spada AR. (2009). Bergmann glia as a therapeutic target for Spinocerebellar ataxia type 7: genetic and pharmacological approaches. Gordon Research Conference on Glia Biology. March 15-19, 2009. Ventura, CA.

Furrer SA and La Spada AR. (2008). Glutamate transporter modulators as a potential therapy for Spinocerebellar ataxia type 7. ARCS spring student showcase. April 14, 2008. University of Washington, Seattle, WA.

UNIVERSITY/COMMUNITY SERVICES

Neurobiology and Behavior Community Outreach **2007 – Present**

- Secretary (2007 – 2012.)
- Membership Liaison (2007 – Present).

Neurobiology and Behavior PhD Program Admissions Committee **2009 – 2012**

LABORATORY SKILLS

- Transgenic mouse models, Cre-loxP system
- Assessment of motor behavior in mice
- Genotype analysis utilizing PCR
- Immunofluorescent techniques (free-floating or frozen tissue sections)
    - Fix, collect, section mouse brains
    - Image collection and analysis using a fluorescent microscope and Slidebook 5.0
- Cell culture, primary cells and immortal cell lines
- Western blot protein analysis
- RNA isolation and analysis using real-time RT-PCR
- Fluorescent Activated Cell Sorting (FACS)
- Microsoft Excel and Graphpad Prism 4.0

OTHER INTERESTS

- Concert band, clarinet
- Volleyball
- Softball